The charnockite-anorthosite suite of rocks exposed in central Dronning Maud Land, East Antarctica: a study on fluid-rock interactions, and post-entrapment change of metamorphic fluid inclusions

Die charnockitischen und anorthositischen Gesteinsserien im zentralen Dronning Maud Land: Fluid-Gesteins-Wechselwirkungen und die Veränderung metamorpher Fluid-Einschlüsse nach ihrer Bildung

Bärbel Kleinefeld

Geologie der Polargebiete
Fachbereich Geowissenschaften
Universität Bremen
Postfach 330440
28334 Bremen

Table of contents

Abstract

The study area of central Dronning Maud Land, East Antarctica is a typical example of a granulite facies Precambrian terrane that was exposed to substantial polymetamorphism during the late Neoproterozoic/early Palaeozoic. Fluid inclusion studies from typical representatives of the charnockite-anorthosite suite of rocks, associated gneisses and syenitic intrusives give new constraints on both peak metamorphic conditions and post-peak metamorphic processes during retrograde uplift. Detailed petrographical studies were supported by Electron Microprobe techniques and combined with microthermometry and Raman spectrometry data.

Three distinct fluid phases, either consisting of $CO_2\pm N_2$, H_2O-salt or $CO_2\pm N_2\pm H_2O$-salt were differentiated. All fluid inclusion types are hosted by plagioclase, quartz and garnet and display textural relationships indicative for a primary (metamorphic or magmatic) origin. The $CO_2\pm N_2$ fluid is most abundant, and it is assumed that it played an important role during metamorphic charnockite formation and anorthosite emplacement. However, evidence of post-entrapment change reveals that a large number of inclusions were subjected to profound reequilibration processes that resulted in a modification of original fluid properties, often accompanied by the partial to complete loss of an aqueous component.

An important indicator for the residual character of some $CO_2\pm N_2$ fluid inclusions was the frequent observation of sheet silicate and carbonate microcrystals that were produced by a micro-chemical reaction of an originally CO_2-$H_2O\pm N_2$ fluid with its plagioclase host. These observations from the anorthosite complex were used to model the fluid-host interaction with consideration of different original fluid compositions. Compared to an actual fluid inclusion it is obvious, that volume estimations of solid phases can be used as a starting point to reverse the retrograde reaction and recalculate the compositional and volumetrical properties of the original fluid. Isochores for an unmodified inclusion can thus be reconstructed, leading to a more realistic estimation of P-T conditions during earlier metamorphic stages or fluid capturing.

Although $CO_2\pm N_2$ inclusions detected within the anorthosite body and associated shear zones reveal a large range in densities, isochoric calculations for the highest density inclusions are in accordance with independent P-T data for near peak-metamorphic conditions. This again illustrates that metamorphic minerals (plagioclase and garnet) are able to preserve the original metamorphic fluid, as substantial reequilibration processes do not take place uniformly within single crystals. A detailed fluid inclusion study can thus provide valuable constraints on the P-T conditions acting during different stages of fluid entrapment and reequilibration.

A selection of representative isochores from the different basement lithologies have

been correlated with P-T constraints based on mineral-equilibria data available from other studies. The gradual decrease in fluid densities best fits a clockwise P-T path and mineral-fluid equilibration during near isothermal decompression is postulated for the post-peak-metamorphic and retrograde development of the rocks exposed in central Dronning Maud Land.

Zusammenfassung

Das Arbeitsgebiet im zentralen Dronning Maud Land (Ostantarktis) ist ein typisches Beispiel für einen granulitfaziellen präkambrischen Terran, der während des späten Neoproterozoikums/frühen Paläozoikums durch intensive Polymetamorphose überprägt wurde. Untersuchungen von Fluid-Einschlüssen repräsentativ ausgewählter Gesteine der Charnockit-Anorthosit-Folge, der assoziierten Gneise und der syenitischen Intrusiva liefern neue Hinweise sowohl auf die *peak*-metamorphen Bedingungen als auch auf die *post-peak*-metamorphen Prozesse, die während des retrograden Aufstiegpfades stattfanden. Detaillierte petrographische Studien wurden durch Elektronenstrahl-Mikrosonden-Untersuchungen ergänzt und mit mikrothermometrischen und Raman spektrometrischen Analysemethoden kombiniert.

Drei unterschiedliche fluide Phasen konnten identifiziert werden, die entweder aus $CO_2\pm N_2$, H_2O-Salz oder einem komplexen $CO_2\pm N_2\pm H_2O$-Salz Gemisch bestehen. Die Wirtsminerale für alle Einschlusstypen sind Plagioklas, Quarz und Granat. Die Einschlüsse zeigen eine texturelle Anordnung, die für einen primären (primär metamorphen oder magmatischen) Ursprung charakteristisch ist. Am weitesten verbreitet sind $CO_2\pm N_2$ Einschlüsse, die während der Enstehung metamorpher Charnockite und der Intrusion des Anorthositkörpers eine vermutlich wichtige Rolle einnahmen. Anzeichen für eine Veränderung der Einschlüsse nach ihrer Entstehung weisen jedoch darauf hin, dass eine grosse Anzahl von Fluid-Einschlüssen umfangreichen Reequilibrierungsprozessen ausgesetzt waren. Diese führten zu einer Veränderung der ursprünglichen Fluid-Eigenschaften, die häufig mit einem partiellen oder vollständigen Verlust der wässrigen Anteile einhergingen. Ein wichtiges Anzeichen für den residualen Charakter einiger $CO_2\pm N_2$ Einschlüsse ist das häufige Auftreten von Schichtsilikaten sowie karbonatischen Mikrokristallen, die durch eine mikro-chemische Reaktion des umgebenden Wirtsminerals mit dem ursprünglich eingeschlossenen Fluid (CO_2-$H_2O\pm N_2$) entstanden sind. Diese Beobachtungen an Gesteinen des Anorthositkörpers wurden verwendet, um die wechselseitige Reaktion zwischen dem Fluid und dem umgebenden Wirtsmineral zu modellieren. Dabei wurden unterschiedliche ursprüngliche Fluid-Zusammesetzungen berücksichtigt. Im Vergleich mit tatsächlich vorkommenden Einschlüssen zeigt sich, dass Volumenabschätzungen der Festphase als Ausgangspunkt für eine rechnerische Umkehr der retrograden Reaktion genutzt werden können. Dies erlaubt die Berechnung der ursprünglichen Volumina und Zusammensetzungen von Fluid-Einschlüssen. Auf diese Weise können Isochoren für ursprüngliche und unveränderte Einschlüsse berechnet werde, was eine realistischere Abschätzung der P-T-Bedingungen während einer früh-metamorphen Phase oder dem Moment der

Einschlussbildung ermöglicht.

Obwohl die $CO_2 \pm N_2$ Einschlüsse des Anorthositkörpers und der mit ihm assoziierten Scherzonen einen weiten Dichtebereich abdecken, stimmen die Isochoren der dichtesten Einschlüsse mit aus unabhängigen Daten rekonstruierten P-T-Bedingungen nahe der *Peak*-Metamorphose überein. Dies wiederum zeigt, dass metamorphe Mineralphasen (Plagioklas und Granat) durchaus in der Lage sind, das ursprüngliche Fluid zu konservieren, da umfangreiche Reequilibrierungsprozesse innerhalb eines Kristalls nicht gleichmäßig ablaufen. Die detaillierte Untersuchung von Fluid-Einschlüssen kann daher wichtige Hinweise auf P-T-Bedingungen während unterschiedlicher Phasen der Einschluss-Bildung und -Reequilibrierung liefern.

Eine repräsentative Auswahl von Isochoren aus den verschiedenen lithologischen Einheiten des Grundgebirges wurde mit unabhängigen P-T-Daten aus publizierten Arbeiten korreliert. Die allmähliche Abnahme der Fluid-Dichten kann am besten mit einem im Uhrzeigersinn verlaufenden P-T-Pfad erklärt werden. Sie weist auf Mineral-Fluid-Equilibrierung unter Einfluss isothermer Druckentlastung während der retrograden Entwicklung der im zentralen Dronning Maud Land anstehenden Gesteine hin.

1. Introduction

1.1.   Fluid -rock interactions in deep-seated crustal rocks

In recent years, the origin, nature and role of the fluid phase involved in granulite formation has again become a vital subject of scientific interest. In most Precambrian terranes, continental crust consists of granulites, with a difference between a (relatively) more superficial part (felsic, metasedimentary granulites) and a more igneous, intrusive deeper part (Touret, 1995). Affiliated peak metamorphism is suggested to be triggered by a sudden temperature increase, most probably related to intrusions of mantle derived melts (magmatic underplating) (Touret, 1995). Rocks generated or modified under granulite facies conditions are water deficient, and metamorphism has taken place at temperatures that would be sufficient to cause melting in the presence of water. The apparent dryness is reflected in the anhydrous mineralogy. Orthopyroxene-bearing members of the charnockite - anorthosite suite of rocks (*cf.* chapter 2) are abundant. Sheet silicates and amphiboles are absent or are present only as minor components. This implies that metamorphism has either occurred under fluid absent conditions, or the fluid must have been of other than predominantly aqueous composition. The absence or subordinate occurence of free H_2O and dominance of $CO_2 \pm N_2 \pm CH_4$ bearing fluids in granulitic lithologies has been demonstrated by several fluid inclusion studies from various granulite terranes worldwide (*e.g.* Raith *et al.*, 1990; Santosh & Yoshida, 1992).

Prograde or peak-metamorphic inclusions have been shown to be preserved in varying metamorphic minerals that have undergone a metamorphic cycle (Blom, 1988; Vry & Brown, 1991; Bakker & Mamtani, 2000). Nevertheless, the assumption that CO_2-rich fluids even of high density always reflect peak metamorphic conditions has been questioned, and shown to be misleading (*e.g.* Lamb et al., 1987; Lamb; 1990). Furthermore, fluid inclusions detected in metamorphic rocks frequently reveal densities, which are incompatible with P-T constraints derived from solid phase equilibria (*e.g.* Swanenberg, 1980; Sterner & Bodnar, 1989; Phillipot & Selverstone, 1991). That inclusions undergo varying compositional and density changes during metamorphic history has been demonstrated by several findings in nature and experiment (*e.g.* Sterner & Bodnar, 1989; Hall & Sterner, 1993; Bakker & Jansen, 1994). Küster & Stöckhert (1997) even presumed, that quartz is unable to preserve primary (metamorphic) inclusions that were captured above 300°C. It is thus very likely that fluid inclusions that formed during peak-metamorphic granulite facies conditions have experienced multiple retrograde modifications, including complete or partial decrepitation (failure by fracturing), stretching (failure by plastic creep), diffusion, or

reactions of the fluid with its mineral host (so-called "back-reactions" in Heinrich & Gottschalk, 1995). Additionally, the retrograde fluid evolution is characterised by a complicated regime of large and small scale fluid migration and influx, combined with fluid mixing and/or buffering. One example for large scale fluid migration is the pervasive influx or channelling of a carbonic fluid along shear zones, which some workers suggest to be responsible for "incipient" charnockite formation (*e.g.* Srikantappa *et al.*, 1985; Hansen *et al.*, 1987). The free fluid phase might also be involved in ongoing alteration processes. Pineau *et al.* (1981) have described the formation of small carbonate particles at the emplacement of former inclusions through the reaction of a CO_2-rich fluid with an incoming H_2O-salt fluid. These "late" carbonates are suggested to be very abundant in many granulites (Touret, 1995). Aqueous fluids may also be involved in retrograde mineral reactions leading to the formation of hydrous phases (like sheet silicates) and remarkable variations in fluid salinities.

Potential host minerals react differently to the possible modification processes, and the mechanisms of local reequilibration are not systematic. As a result, the overall fluid movement was often not able to homogenise the fluid composition, not even in hand specimen scale (Touret, 1995), and samples may comprise a large variation in fluid compositions and densities.

It can be stated that fluid-rock interactions (involving modification of fluid inclusions and the interaction of an enclosed fluid with its mineral host) are abundant during granulite formation. The majority of fluid inclusions detected within granulite terranes are in fact characterised by the dominance of a CO_2-rich and nearly complete absence of an H_2O-bearing component. However, this does not necessarily imply, that the current fluid is identical with the fluid active during metamorphic reactions. In order to derive any useful data on former P-T conditions, fluid inclusion populations must be differentiated and related to specific stages of metamorphic history. Any possible mechanism of secondary change has to be taken into account during the evaluation and interpretation of derived data. A change in original fluid composition or density may specify reequilibration processes which are not yet completely understood, or give valuable information about particular reequilibration processes, which are known to occur only under certain conditions.

1.2.   Previous studies and scope of the thesis

Hitherto, fluid inclusion data of metamorphic charnockites and associated granulitic lithologies from East Antarctica are rare, and have only been reported from the Lützow-Holm Bay (LHB) region (Santosh & Yoshida, 1991, 1992). The authors show that the fluid imprint on gneiss and metamorphic charnockite assemblages is dominantly pure CO_2, and postulate an external, sub-lithospheric origin of the preserved fluid. Furthermore they combine fluid inclusion data with P-T-data derived from mineral phase equilibria and geochronologic information, and conclude that the LHB rocks followed a clockwise prograde and retrograde P-T-t-path.

The granulite facies basement complex exposed in the Petermannketten and the Otto-von-Gruber-Gebirge, central Dronning Maud Land, East Antarctica, comprises lithologies typical of Precambrian granulite terranes. In this study, basement gneisses that have obviously been subjected to metamorphic charnockitisation and subsequent leaching processes, massif-type anorthosites and associated shear zone samples, as well as anorogenic syenite and charnockite intrusives are investigated with regard to their modal and chemical mineral composition (using Electron Microprobe technique), and fluid content.

In a first step, the gneisses, anorthosites and shear zone samples are classified according to the recommendations of the IUGS subcommission for members of the charnockite-anorthosite suite of rocks. The main objective of this study is to examine the contemporary fluid content preserved in the different lithologies by microthermometry and Raman spectrometry. The data are evaluated in context of the nature of the fluid present during the early stage of granulitic metamorphism, charnockite formation and intrusion and deformation of the anorthosite body. It is illustrated that early-metamorphic fluids may be preserved in metamorphic minerals, although the influence of post-entrapment change is abundant and substantial. Derived density data are used to calculate isochores, which are correlated with independent P-T-data to give further constraints on the character of the retrograde P-T-path.

Based on the frequent observation of carbonate and sheet silicate microcrystals in carbonic fluid inclusions, further emphasis is put upon micro-chemical reaction processes between an enclosed CO_2-H_2O fluid and its mineral host during retrogression. It is assumed that a fluid that originally contained an aqueous phase may react with surrounding plagioclase under complete consumption of the aqueous phase, and the formation of carbonates and sheet silicates. A quantitative model is established to describe volumetric and compositional changes caused by the possible reactions. The model is applied to hypothetical and actual fluid inclusions. It is shown

that the combination of fluid inclusion data with thermodynamic modelling may provide crucial constraints on the volumetrical and compositional properties of the original fluid inclusion trapped during high-grade metamorphism. Isochores for an unmodified original inclusion can thus be reconstructed, leading to a more realistic estimation of P-T conditions during earlier metamorphic stages or fluid capturing.

The results are presented in two chapters devided on the basis of rock types (gneisses and anorthosites) and sample localities and (Petermannketten and Otto-von-Gruber-Gebirge). The detailed study using thermodynamic modelling techniques is presented in a separate chapter which consists of a manuscript that has been accepted for publication by the *Journal of Metamorphic Geology*.

2. The charnockite - anorthosite suite of rocks

2.1.   Classifying rocks of the charnockite series

Rocks of the charnockite series (Holland, 1900) or the charnockite- anorthosite suite of rocks (Goldschmidt, 1916) are widespread in Precambrian terranes. Often the entire range of compositions from granitic to anorthositic varieties occurs in close proximity. Charnockitic rocks can be igneous, meta-igneous or thoroughly metamorphic, and despite the fact that they often show signs of deformation and recrystallisation, they have been included in the classification scheme of igneous rocks (Streckeisen, 1976; Le Maitre, 1989). Chemically, they are defined as equivalent to plutonic rocks of QAPF fields 2-10, i.e. 0-100 vol% alkali-feldspar or plagioclase, and 0-60 vol% quartz component. The difference, though, lies in the mineralogical composition. Instead of, or in addition to biotite and hornblende, which are the typical major mafic minerals in calc-alcalic rocks, orthopyroxene or fayalite + quartz are present. Perthitic or antiperthitic development of feldspar is a further characteristic. Using the classification of the QAPF double triangle, perthite (*sensu stricto*) is counted as "A" (alkali feldspar), antiperthite as "P" (plagioclase) and mesoperthite as 50/50 A/P. Originally, the orthopyroxene had been specified as hypersthene (Fs_{30-50}) (*cf.* Isachsen, 1968; LeMaitre, 1989), but that no longer is an approved mineral name (*cf.* Morimoto, 1988). The presence of very fine-grained chlorite and calcite in brittle crystal fractures causes a "greasy-green" colouring of plagioclase, which in return is responsible for the typical "waxy grey-green" appearance of the rocks (Shelley, 1993).

The mineralogical difference described above reflects a variation in P_{H2O}-T conditions during rock formation and charnockitic rocks are characterised by low H_2O-activities in the fluid phase. Thereby, igneous charnockitic rocks represent CO_2-rich synmetamorphic intrusives while metamorphic varieties are products of dehydration reactions caused by the reduction of water-activity. The members of the charnockite series are the granulite-facies equivalent of calc-alcalic rocks, which normally contain mineral assemblages typical for the upper amphibolite facies (Isachsen, 1968; Shelley, 1993). Thus, the metamorphic varieties of the charnockitic rocks are also properly described as granulites, whereas igneous charnockitic rocks may be given more standard names (*e.g.* orthopyroxene granite). The nomenclature used in literature is confusing, as long as general and special terms are used mutually for the same rock types. The varying names that may be applied to members of the charnockitic rock suite are given in Table 2.1.

In the present study, samples were labelled according to the strict definition of the term "charnockite" (Holland, 1900; Streckeisen, 1976). Special terms were used when

available, and general terms applied, when no special terms exist (Table 2.1).

Table 2.1:   *Special and general names used for charnockitic rocks (after Le Maitre, 1989)*

QAPF field	General term	Special term
2	orthopyroxene alkali feldspar granite	alkali feldspar charnockite
3	orthopyroxene granite	3a: charnockite
		3b: farsundite
4	orthopyroxene granodiorite	opdalite or charno-enderbite
5	orthopyroxene tonalite	enderbite
6	orthopyroxene alkali feldspar syenite	--
7	orthopyroxene syenite	--
8	orthopyroxene monzonite	mangerite
9	monzonorite (orthopyroxene monzodiorite)	jotunite
10	norite (orthopyroxene diorite) or anorthosite if M (mafic minerals) < 10 vol%	--

2.2.   Massif-type anorthosites

One distinctive member of the charnockitic rock suite is the group of anorthosites or "plagioclasites". The cumulate rocks are defined to contain 90 vol% plagioclase with a compositional range of andesine to bytownite (An_{30-70}), and a focal point on An_{40-60}, but no albite, and < 10 vol% mafic minerals, preferably hornblende, pyroxene and olivine (Le Maitre, 1989). Ashwal (1993) differentiates between four major types of anorthosites: Archean anorthosites, Proterozoic massif-type anorthosites, anorthosites in layered intrusions and lunar anorthosites. Subordinate varieties are anorthosites of oceanic settings and anorthosite inclusions in igneous rocks. Massif-type anorthosite complexes can reach thousands of km^2 in areal extend, and are typically made up of nearly monomineralic coarse to very coarse grained anorthosites, leuconorites, leucogabbros, and leucotroctolites. Minor volumes of comagmatic norites, gabbros, troctolites, and Fe-Ti-oxide-rich rocks including massive ilmenite-magnetite ore-deposits also form part of the common anorthosite complexes. Additionally, most massifs contain small dikes or intrusions of Fe-, Ti-, and P-rich rocks, i.e. ferrodiorites or ferrogabbros. Spatially associated with nearly all massif-type anorthosites are rocks of broadly granitic composition, essentially other members of the charnockitic rock suite. Most commonly reported is an intrusive relationship, with the granitoid suite being younger than the associated anorthositic rocks. The reverse relationship is rare or absent, and it is well accepted that the chemically independent granitic melts generated from anatexis of the country rocks during intrusion of the main magma suite and probably mixed with variable amounts of highly fractionated anorthositic residual melt (*e.g.* De Waard, 1968a, b; Kolker & Lindsley, 1989; Ashwal, 1993; Emslie *et al.*, 1994 and references herein).

Despite many attempts to unravel the history of massif-type anorthosites, their

genesis has still remained unclear. Models concerning a typical tectonic environment, the origin and chemical composition of the parental magmas, the mode of emplacement (melt versus crystal mush) and depth of crystallisation are miscellaneous (*e.g.* Ashwal, 1993 and references herein; Schiellerup *et al.*, 2000; Krause *et al.*, 2001). So far, plate tectonic settings as different as Andean-type margins and continental rifts have been discussed as being characteristic for massif-type anorthosite genesis (*e.g.* Bruce *et al.*, 1989; McLelland, 1989; Ashwal, 1993 and references herein). A similar dissension subsists with regard to original magma derivation. At present, massif-type anorthosites are believed to have crystallised from either crustally contaminated mantle-derived mafic melts that have fractionated olivine and pyroxene at depth (Emslie, 1985; Ashwal, 1993) or primary aluminous gabbroic to jotunitic melts derived from the lower continental crust (Longhi *et al.*, 1999; Duchesne *et al.*, 1999; Schiellerup *et al.*, 2000). Concerning the mode of crystallisation, several authors favour emplacement of anorthosites as crystal-rich mush that formed in large, slowly cooling magma chambers before ascending into the upper crust as coalescending diapirs (*e.g.* Ashwal, 1993; Lafrance *et al.*, 1996).

Intrusion ages reported from massif-type anorthosites are concentrated upon the period between 1.8 and 0.9 Ga (Ashwal, 1993; Scoates, 2000). Data indicating a late-Proterozoic to early-Phanerozoic age of emplacement have so far only been reported from the Aïr ring complex, Niger (*e.g.* Demaiffe *et al.*, 1991 a, b) and from the Eckhörner and O.-v.-Gruber anorthosites , central Dronning Maud Land, East Antarctica (Mikhalsky *et al.*, 1997; Jacobs *et al.*, 1998).

2.3. "Incipient" or "arrested-type" charnockitisation

The main known types of charnockitic rocks comprise *(a)* magmatic charnockitic rocks associated with large massif-type anorthosites (for example O.-v.-Gruber anorthosite complex, Antarctica: *e.g.* Kämpf & Stackebrandt, 1985), *(b)* massive charnockites found in granulite terranes (for example Nilgiri Hills, India: *e.g.* Raith *et al.* 1990), *(c)* metamorphic charnocktisation in contact aureoles around intrusive enderbites (for example South Africa: *e.g.* van den Kerkhof & Grantham, 1999), and *(d)* abundant pervasive metamorphic charnockitisation along fractures and shear zones in gneissic complexes. The latter, also referred to as "arrested-type" or "incipient" charnockitisation, has first been described by Pichamuthu (1960) from Kabbaldurga, southern India, and several other locations throughout the southern Indian high-grade terrane and the adjacent Sri Lankan terrane have been reported thereafter (*cf.* Ravindra-Kumar *et al.*, 1985; Srikantappa *et al.*, 1985; Hansen *et al.*, 1987). As a typical feature observed in Precambrian gneiss complexes, incipient charnockitisation is also known from the northern hemisphere *e.g.* from Siberia and Finland (Perchuk *et al.*,

1989). However, no secured data on this type of charnockitisation have yet been reported from the East Antarctic craton as to be expected when considering the several findings on the other crustal segments of former East Gondwana (India, Sri Lanka) and their common geological history.

Meso- and macroscopically, the hornblende-, biotite- and/or quartzofeldspathic gneisses typically show grey-green patches and streaky zones where the original gneiss texture is blurred or completely erased by recrystallisation and grain-size coarsening. Mineralogical changes in these zones involve the partial to complete breakdown of hornblende, biotite and garnet and the neoblastesis of orthopyroxene (hypersthen). Despite the variable bulk chemistry, mineral composition and texture of the host gneisses, the charnockite is always a coarse-grained orthopyroxene-bearing rock with remarkably uniform granitic composition (Raith & Srikantappa, 1993), which hints at more or less pronounced element mobility and open-system behaviour during the dehydration process (*e.g.* Hansen *et al.*, 1987; Stähle *et al.*, 1987; Milisenda *et al.*, 1991). Because of this observation and the conspicuous intimate relationship between gneisses and "arrested-type" metamorphic charnockites, a fluid-controlled mechanism to explain this phenomena is widely favoured (*e.g.* Janardhan *et al.*, 1979; Newton *et al.*, 1980; Glassley, 1983; Stähle *et al.*, 1987; Raith *et al.*, 1989; Santosh *et al.*, 1990; Perchuk *et al.*, 2000).

Some workers have proposed a high grade CO_2-metasomatic process to be responsible for the spatially restricted decrease in H_2O-activity - a prerequisite assumed to be essential for *in situ* charnockitisation (*e.g.* Touret, 1971; Newton *et al.*, 1980; Glassley, 1983; Raith *et al.*, 1989 and references herein). According to them, CO_2-influx causes the expulsion or dilution of pore-fluids. Sufficient amounts of CO_2 are suggested to originate from *e.g.* degassing of crystallising underplated basaltic magma, decarbonation of subducted oceanic lithosphere or upper mantle, or sudden tapping and expulsion of 'fossil' reservoirs of 'internally' derived and buffered carbonic fluids trapped in deeper-crustal granulites. The idea of CO_2-influx is supported by the observation, that the majority of fluid inclusions hosted by incipient charnockites is CO_2-dominated. The infiltration and mobility of significant amounts of CO_2 require an environment structurally controlled by fracturing and shearing, and it has been shown that even diffuse patches and stringers and random distribution of patchy charnockites have developed along tectonically generated structures (*e.g.* Dobmeier & Raith, 2000).

However, the appeal of carbonic fluids as a mainspring in granulite metamorphism has been confined by their poor wetting ability relative to silicate mineral grain boundaries, inhibiting infiltration, and the low solubilities of silicate constituents in CO_2-rich fluids. Thereupon more recent studies have concentrated on the importance of alkali-mobility and the role of highly saline fluid phases ("brines") during granulite

facies metamorphism and charnockitisation processes (*e.g.* Perchuk & Gerya, 1992, 1993; Newton *et al.*, 1998). The role of potassium in the formation of some arrested charnockites has been demonstrated by Stähle *et al.* (1987). Perchuk & Gerya (1992, 1993) proposed, that the chemical potentials of CO_2, H_2O and K_2O in a metamorphic fluid govern the charnockitisation process during retrogression, and that high alkali activity allows orthopyroxene formation under H_2O-activities similar or even higher than that for the initial gneisses. Additionally, experimental studies have shown that concentrated supercritical brines have appropriate low H_2O-activities, high infiltration ability and high alkali mobility to foster charnockite formation (*e.g.* Shmulovich & Graham, 1996; Aranovich & Newton, 1998).

Perchuk *et al.* (2000) even found evidence of both fluid regimes described above, and they concluded that two immiscible fluids, i.e. an alkalic supercritical brine and almost pure CO_2 coexisted during incipient charnockite formation. According to them, the ongoing metasomatic process could also be responsible for partial melting, a feature often observed in conjunction with arrested-type charnockites. The abundance of pegmatites, quartzo-feldspathic veins and migmatites spatially associated with incipient charnockites has also been interpreted in terms of partial melting under H_2O-undersaturated conditions (*e.g.* Bhattacharya & Sen, 1986; Holness, 1993), which in turn provoked early workers to explain the formation of incipient charnockites by metamorphism of anhydrous lithologies (*e.g.* Lamb & Valley, 1984) or the extraction of partial hydrous melts (*e.g.* Fyfe, 1973; Waters, 1988; Burton & O'Nions, 1990).

In summary, most recent studies agree that the known domains of arrested-type charnockitisation formed by in situ dehydration processes during a late stage of tectonothermal history at a structurally controlled site (Dobmeier & Raith, 2000). Nevertheless, mechanisms conducting fluid movements during high-grade metamorphism and incipient charnockite formation, and the scale at which fluid-controlled processes operate (mm, m, km) have not been examined to a satisfying degree yet. Fluid fugacities can be controlled by several parameters *e.g.*, the internal buffering by metamorphic reactions (fluid-rock interaction), diffusion processes, immiscibility of complex fluid phases or wetting properties of mineral-fluid under given metamorphic conditions, largely determining the mobility of fluids of different compositions. Consequently, varying mechanisms are currently envisaged to account for arrested charnockitisation in different granulite terranes, either operating independently, in conjunction or mutual relationship. Thus, the debate about the models mentioned above is still controversial and more detailed investigations will have to be carried out before concluding explanations may be given.

3. Principles of fluid inclusion studies

3.1. Theoretical background - the ideal model

Fluid inclusions are present in nearly all rock types whether derived from the crust or the mantle. As they are almost ubiquitous in geologic samples their study is applicable to a variety of geologic questions. Most natural fluids (gases and liquids at high pressure) consist of molecular compounds of the system C-O-H-N-S + salt (with "salt" representing e.g. NaCl, $CaCl_2$, KCl and other chlorides). The "simple" species H_2O, CO_2, CH_4, N_2 and H_2S appear to be most stable in fluid inclusions. Brewster (1823) and Sorby (1858) were amongst the first to realise their potential for the understanding of geologic problems, and three main prerequisites for the model of ideal fluid inclusion behaviour can be ascribed to these early workers:

The host crystal of inclusions that formed under high P-T conditions is impermeable to any chemical changes

Because of the crystals' rigidity, external variations in stress are not transferred to the fluid and the compressibility and expansion of the host crystal are negligible over geologic P-T conditions

The host crystal is considered to transfer heat between the geologic surroundings and the fluid inclusion.

Based on these presumptions, the ideal model fluid inclusions are considered to be closed ("isoplethic") and constant volume ("isochoric") systems that remain in thermal equilibrium with their immediate environment. Consequently, once entrapped within a crystal, the fluid inclusion follows an isochoric and isoplethic path through P-T space where internal pressure is dependent on the imposed temperature (*cf.* Sorby, 1858; Roedder, 1984).

For the composition of the isopleth, the P-T conditions that prevail at the moment of entrapment from a homogeneous fluid phase dictate the bulk molar volume (density) of the fluid inclusion. If the inclusion remains an isoplethic-isochoric system, then no matter how many times it is heated or cooled, the P-T trajectory of the inclusion is locked on the isochore which passes through the point (in P-T space) of entrapment (Fig. 3.1). As the inclusion cools from its entrapment point the internal pressure drops and the isochore eventually intersects the miscibility boundary of the given system. At this point the homogeneous fluid separates into a liquid-like and a vapour-like phase, i.e. a bubble nucleates. As fluid isochores have positive P-T slopes, the temperature at which the bubble appears must be less than the entrapment temperature. The natural cooling path of the fluid may be reversed in the laboratory by heating above room temperature and observing the inclusion through a microscope (method of

microthermometry). Thus, the minimum formation temperature of the inclusion may be determined from the temperature of homogenisation (Th) of the bubble (i.e. the point at which the bubble disappears upon heating) (Fig. 3.1). Additionally, the mode of homogenisation i.e. homogenisation into the liquid phase (the bubble shrinks upon heating) or into the vapour phase (the bubble grows upon heating) indicates, whether the original homogeneous fluid was vapour-like or liquid-like (Fig. 3.1).
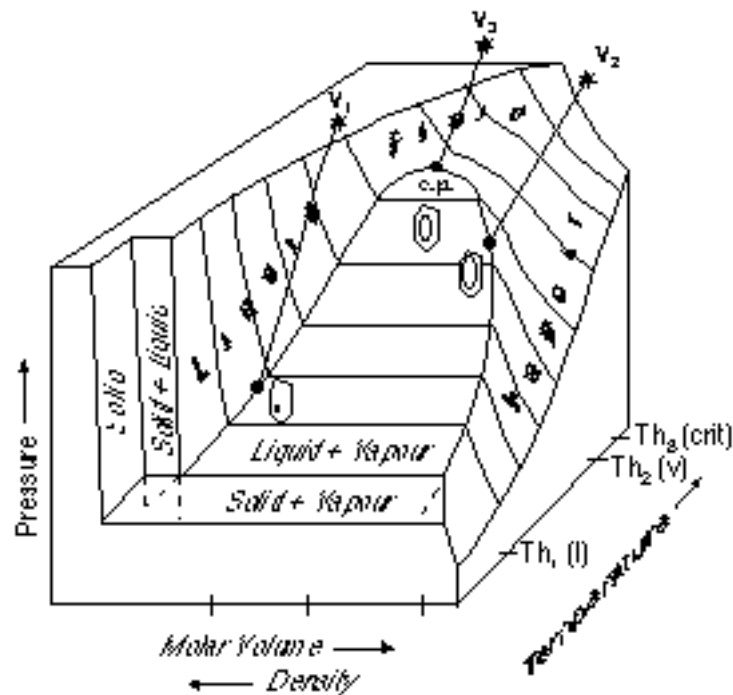
Fig. 3.1: *Schematic diagram of PVT properties in the unary CO_2 system., (modified after Burruss, 1981). Three pure CO_2 inclusions with different molar volume (V1-3) were trapped in the one phase region and "locked" to the associated isochore at the moment of trapping marked by the star. Upon cooling, phase separation occurs as soon as the isochore intersects the miscibility boundary (black dots). Proportions of the separated liquid and vapour phase are determined by the lever rule. Black dots also mark the PVT conditions at the moment of homogenisation (upon heating). Note that the molar volume determines the mode of homogenisation. Th (l), (v), or (crit). c.p. = critical point (31.1 °C for pure CO_2).*

As much as the temperature of homogenisation is characteristic of the molar volume of a fluid, the melting temperature (Tm) of the solid phases that formed through supercooling and freezing of the inclusion provides an indication of the composition of the captured fluid. In the H_2O-salt system, for example, the eutectic melting temperature is characteristic of the type of salt present, whereas the extent to which the melting point of ice is depressed provides an indication of the bulk salinity of the inclusions. In carbonic inclusions, the lowering of the triple point of pure CO_2 (-56.6°C) is symptomatic for the presence of additional gas species, such as N_2 or CH_4.

The phase behaviour described above (Th and Tm) is valid for simple unary or binary systems (*e.g.* pure CO_2 or H_2O-salt). The prevalent fluids identified in the study

area either belong to the system $CO_2 \pm N_2$ or H_2O-salt, but a more complex fluid, containing H_2O-$CO_2 \pm$salt, was detected as well. In H_2O-gas-salt-rich systems, further phase transitions, *e.g.* formation and melting of a gas hydrate (or clathrate) and/or partial homogenisation of a subsystem, can be observed during heating or cooling, which complicates the interpretation of microthermometrical data. For example, the presence of a CO_2-clathrate ($CO_2 \bullet 5.75\ H_2O$) at the moment of ice melting or partial homogenisation of the subsystem, has a crucial effect on the proper calculation of bulk fluid composition or molar volume, as it deprives small amounts of H_2O and CO_2 from the bulk system. Consequently, neglecting its appearance would result in incorrect estimates of salinities or densities of the remaining gaseous species. For more detailed descriptions of possible phase changes, fluid behaviour in more complex systems or the significance of clathrate refer to *e.g.* Diamond (1992, 2001) for CO_2-H_2O inclusions; Thiery *et al.* (1994) and van den Kerkhof (1988) for the system $CO_2 \pm CH_4 \pm N_2$; Bodnar (1993) for H_2O-NaCl fluid systems, and Collins (1979) and Bakker (1998) for gas hydrates in fluid inclusions.

Phase changes observed and abbreviations used in this study to describe the phase transitions are summarised in Table 3.1.

Table 3.1: Abbreviations used in this study to describe phase changes observed during microthermometrical measurements

abbreviation	explanation
Tme	temperature of eutectic melting in the H_2O-salt system
Tm (aq or CO_2)	temperature of final ice melting or of solid carbonic phase
Tm clath.	temperature of final clathrate melting
Th (CO_2 or tot)	temperature of homogenisation (of the carbonic phase or total homogenisation)
Th (l/v/crit)	mode of homogenisation (to the liquid/ vapour phase or critical)
NaCl*eq*	salinity calculated from Tm for the equivalent amount of NaCl in solution

3.2. Practical aspects of fluid inclusion studies

That the previously described ideal model only approximately reflects the actual facts found in nature is a matter of course. Care has to be taken when conducting a fluid inclusion study to avoid any misinterpretation of *e.g.* phase proportions or densities.

An important prerequisite to any fluid inclusion study is a detailed knowledge of the nature and texture of the host mineral, *e.g.* its formation conditions, possible signs of deformation, growth zonation or alteration. Additionally, varying fluid inclusion generations and assemblages should be differentiated on the base of distribution, number, phase proportions, size and shape. The properties of an inclusion assemblage

combined with data derived from microthermometry measurement (*e.g.* Th, Tm) form the smallest unit of geological information. Nearly every inclusion assemblage is characterised by a standard deviation (or better for small numbers: total range) in inclusion attributes. Thus, crucial conclusions can be drawn concerning the nature of the fluid at the time of entrapment (homogeneous versus heterogeneous fluid phase), and whether the inclusions have been altered and changed after trapping (*cf.* 3.2.1).

Formation of a fluid inclusion assemblage in the one-phase field, i.e. trapping of a homogeneous fluid, will result in inclusions with relatively similar microthermometric properties and uniform volumetric proportions at room temperature. This principle is also valid for all solid phases that precipitate from such a fluid during cooling (formation of *"daughter minerals" e.g.*, salt crystals or nahcolite).

Contrary to the features described above, trapping of a heterogeneous fluid phase i.e. trapping in a multi-phase field, results in variable microthermomeric properties and a mutable distribution of relative volumetric proportions of the included phases at room temperature. Reasons for heterogeneity of a natural fluid phase may be boiling, effervescence or immiscibility of the present fluid species (*e.g.*, water/hydrocarbon). This principle also applies to solid phases that were "accidentally-trapped" during inclusion formation.

The determination of densities -the key parameter for many geological interpretations- is only justified when both phase behaviour and composition of individual inclusions are known. The density is calculated by means of experimentally derived models (equations of state) using data obtained by the observation of phase transitions at controlled temperatures ("microthermometry"), and knowledge of the composition of gases, entrapped solids, and/or frozen fluids as gained by Raman spectrometry (*c.f.* chapters 4.5 to 4.6).

Many fluid inclusion studies aim at the calculation of isochores from inclusion densities. Isochores can be combined with independent pressure and/or temperature estimates for a better understanding of metamorphic conditions.

In summary, the main parameters that have to be respected when selecting representative densities (and isochores) for any interpretation of fluid inclusion work are:

the precise relationship between inclusions (host mineral) and metamorphic stage

the compositional complexity of fluid inclusions (inclusions with a similar fluid content must be chosen, as *e.g.*, the presence of reasonable amounts of N_2 in $CO_2 \pm N_2$ fluid inclusions can drastically lower the inclusion densities)

the possibility of post-entrapment modification

3.2.1. Irreversible post-entrapment change

The occurence of variable of microthermometric properties (Th, Tm, volume fractions), already described as indicator for trapping of a heterogeneous fluid, may also indicate volumetric or compositional modifications of fluid inclusions after their formation. Reversible change (phase separation upon cooling, precipitation of "*daughter minerals*") has already briefly been addressed in the previous paragraph. However, the influence of irreversible secondary change of fluid inclusions, though is widely spread in (granulitic) metamorphic environments. It is therefore considered in more detail.

Several possible mechanisms that alter fluid inclusions *e.g.*, brittle and/or plastic deformation of the host-crystal, or reaction of the fluid with the enclosing mineral, have been reported from nature and experiment up to now (*cf.* Sterner & Bodnar, 1989; Hall & Sterner, 1993; Bakker & Jansen, 1994; Küster & Stöckhert, 1997; Heinrich & Gottschalk, 1995).

Brittle failure either results in complete or partial explosion (**"*decrepitation*"**) or implosion of fluid inclusions. Microstructural evidence for brittle failure are highly irregular inclusion shapes, radial cracks that originate from the inclusion, and healed microfractures represented by halos of small inclusions (*e.g.* Roedder, 1984).

The effect of plastic deformation on the enclosing mineral is generally referred to as **"*stretching*"** or **"*reequilibration*"**. The microstructural record is less pronounced and unequivocal. Regular or roundish to negative inclusion shapes have been suggested to be indicative for stretching (*e.g.* Sterner & Bodnar, 1989).

Both modes of irreversible deformation are triggered by differential stress (the pressure difference between the internal fluid pressure and the confining pressure acting on the host mineral) that builds up, as soon as the metamorphic P-T path deviates significantly from the fluid isochore. They are controlled by parameters like the mechanical strength of the host mineral, initial inclusion shape and size, prevailing temperature, or strain rate (*e.g.* Küster & Stöckhert, 1997). Additionally, the compositional change is influenced by selective loss of H_2O or nitrogen, which diffuse and migrate more easily than CO_2 through any host mineral (Vityk & Bodnar, 1998; Audétat & Günther, 1999; Touret, 2001). Next to the microstructural record, a correlation of inclusion size with Th (and thus densities) may be indicative for the mode of failure and type of metamorphism. Large inclusions are more likely to undergo decrepitation and subsequent leakage than small inclusions due to their lower mechanical strength (*e.g.* Swanenberg, 1980; Bodnar *et al.*, 1989). Consequently, a positive correlation with Th, *e.g.*, the absence of large inclusions with high densities may hint at fluid loss due to overpressure, and thus (rapid) decompression during uplift. A negative correlation with inclusion size though, may indicate a phase of isobaric cooling, as inclusion size has to decrease without leakage in order to increase

the density (Touret, 2001).

In contrast to the formation of real *"daughter-phases"*, the occurrence of chemical reactions between the entrapped fluid and a reactive mineral host (e.g. feldspar, garnet, pyroxene) has been reported by only a few workers so far (*cf.* Andersen *et al.*, 1984; Heinrich & Gottschalk, 1995; Svensen *et al.*, 2001), and is not sufficiently well documented, yet. The reaction of parts of a complex fluid with the inclusion walls results in the generation of a residual (probably less complex) fluid and one to several solids, so called *"step-daughter"* phases (Svensen *et al.*, 1999). Depending on the phases and components involved, this may either result in an increase or decrease of inclusion volume and densities.

The magnitude of modification usually varies between individual inclusions in one assemblage of originally identical fluids, which leads to variable inclusion properties in a petrographic assemblage. Processes involved may interact, and do not follow a well-defined scheme. However, the alleged ambiguities of origin and subsequent change can even cause the obtained data to have greater significance, provided that the techniques used are adequate to resolve them.

3.3.   Nomenclature

The classification scheme most widely used for the description of fluid inclusions was proposed by Roedder (1984). Roedder (1984) differentiates on a genetical base between *"primary"* inclusions that formed during mineral growth and *"secondary"* inclusions that developed after the primary crystallisation of the host, *e.g.*, through entrapment during healing of microfractures. A zone of overlap of these two types are so called *"pseudosecondary"* inclusions that may form along crystal faces or fractures that develop during crystal growth. In most metamorphic rocks, though, the application of the terms "primary" and "secondary" might be difficult or even impossible. The total fluid content of such samples is a record of the several stages of rock evolution and many generations of fluid assemblages occur in close proximity.

The size of most fluid inclusions is expressed in the range of several microns, and their shape varies between highly irregular (often a result of decrepitation), irregular, rounded and negative crystal shape. Distribution of inclusions throughout a crystal is described as single or isolated, alongside trails or planes/clusters. The physical state of enclosed phases is either liquid-like (l), vapour or gas-like (v) or solid (s).

In practice it is often difficult to observe eutectic melting temperatures, which are characteristic of the type of salt present in H_2O-salt inclusions. Therefore it is generally accepted to recalculate salinities on the base of freezing point depression caused by an equivalent amount of NaCl in solution, and salinity then is given in wt% NaCl*eq* (Table 3.1).

4. Analytical methods and data evaluation

4.1. Polarisation microscopy

Detailed petrographic studies were carried out on thinsections (approx. 25 μm thick) of 25 samples using a Zeiss Axioplan petrographic microscope equipped with Zeiss 2.5X, 5X, 10X and 40X objective lenses, 10X oculars, and an Olympus DP 10 digital camera. If more than one thinsection was prepared of a single sample *e.g.*, to allow a more detailed analysis on veins or pegmatitic mobilisates, the different thinsections were labelled with an additional letter in alphabetical order. The magmatic rocks were classified and named on the base of the estimated mode mineral content (in volume percent), using the QAPF double triangle and following the IUGS recommendations (Le Maitre, 1989). Metamorphic rock species were classified and named according to the hierarchical system recommended by Shelley (1993). The guidelines for classifying members of the charnockitic rock suite have already been discussed and specified in chapter 2.1. All mineral abbreviations used are based on Bucher & Frey (1994).

4.2. Electron Microprobe analysis

Polished thinsections were covered with a thin layer of vapourised carbon, and used for representative analysis of 7 gneiss, and anorthosite mineral assemblages. Mineral analyses and garnet element mappings were carried out on a Cameca SX-50 electron microprobe at the Ruhr-Universität-Bochum, Germany. It is fitted with four wavelength-dispersive spectrometers (WDS) and one energy-dispersive spectrometer (EDS). Qualitative and quantitative element analyses wer performed on alkali-feldspar, plagioclase, pyroxene and garnet. Operating conditions were an acceleration voltage of 15 kV and a beam current of 15 nA. Counting times were 20 s on peak and 10 s on background. A focussed beam was applied to all phases except for micas which were analysed with a slightly defocussed beam. Natural and synthetic minerals and glasses were used as calibration standards. Calculation of concentrations given in weight percent of elements was performed by the built-in correction procedure. Weight percent of oxides, mineral formulas and endmembers were calculated as described in Spear (1993) and using Excel spreadsheets kindly provided by Dr. P. Appel (Christian-Albrechts-Universität Kiel, Germany).

The calculation of the mineral formulas of plagioclase and alkali-feldspars was carried out on the base of 8 oxygens, and of garnet on the base of 24 oxygens.

Very detailed electron microprobe analysis around single fluid inclusions hosted by plagioclase of a characteristical anorthosite sample were performed at the Montan Universität Leoben, Austria, using an upgraded ARL-SEMQ 30 microprobe equipped

with TAP, LiF and PET wavelength dispersive spectrometer crystals. Beam conditions were 20 kV and 15 nA. A plagioclase standard from the Leoben University was used for calibration. The Bastin correction was applied to the obtained data, and mineral formulas were calculated as described above.

4.3.   Microthermometry

Besides the petrographic examinations, the qualitative to semi-quantitative, non-destructive method of "microthermometry" is the most important analytical technique for characterising fluid inclusions. Its basic principle is the observation of various phase transitions under controlled conditions of heating and cooling. If the inclusions have simple compositions (less than 3 or 4 major components) then the microthermometric measurements allow the bulk composition and density of the inclusions to be calculated. If the inclusions are more complex, then the phase-transition temperatures provide useful constraints on the bulk composition and density, but additional analytical results must be combined to reach a more exact solution (*e.g.* Raman spectrometry).

Microthermometric measurements were carried out on fragments of doubly polished thicksections (ca. 100 *μ*m) using two different heating/freezing stages - a modified U.S. Geological Survey (U.S.G.S.) gas-flow stage at the Universität Bremen, Germany, and a Linkam MDS 600 stage at the Universität Leoben, Austria.

The modified U.S.G.S. gas-flow stage (FLUID INC., Denver, Colorado, U.S.A.) heats and cools samples over a temperature range of -196 °C to 700 °C, by passing preheated or chilled gas and/or liquid nitrogen directly over the specimen. The temperature is measured via a thermocouple element placed upon the wafer, and pressing it to the bottom window of the heating/cooling chamber. The stage is mounted on a Zeiss Standard-WL transmitted-light microscope, equipped with Leitz 4X, 10X and 32X long-working distance objective lenses, 10X oculars and a 12V/100V quartz-halogen light source.

The Linkam MDS 600 motor driven stage, combined with a TMS 93 temperature programmer and LNP 93/2 cooling system covers a temperature range of -196 °C to 600 °C. Heating/freezing experiments are controlled via a Pentium III 450 MHz computer with a Nokia 445Xpro monitor using the LinkSys software package. Held by a quartz crucible and sample carrier, a fragment of the specimen is placed upon a silver block equipped with heater and integral cooling chamber. A platinum resistor sensor is mounted near to the surface of the silver block and allows for an accurate and stable temperature signal. The stage is mounted on an Olympus BX 60 microscope (modified and supplied by FLUID INC.) outfitted for use with reflected and transmitted visible light, reflected UV light, and transmitted IR light, using 4X, 10X, 40X and 100X

Olympus long-working distance objective lenses for visible light and 10X oculars. Visible-light images are digitally acquired and viewed on the monitor using a JVC F553 3-ccd-chip video camera.

Both stages were calibrated and regularly monitored using synthetic fluid inclusion temperature standards provided by SYN FLINC, covering a temperature range from - 56.6 °C to 0.0 °C and 374.1 °C, the melting of pure CO_2, and the melting and homogenisation of pure H_2O, respectively. Additionally, the U.S.G.S. gas-flow stage was calibrated with an ice bath (0 °C) and liquid nitrogen (-196.8 °C). The accuracy of temperature measurements on either of the stages was determined to ± 0.2 °C at temperatures below 100 °C, and ± 0.4 °C at higher temperatures.

With respect to the size of sample wafers, their thickness, polishing quality and mineral content, heating rates were chosen and kept as a routine procedure in order to get best temperature reproducibilities for standard and sample measurements. When using the U.S.G.S. gas-flow stage, the location of the thermocouple relative to the inclusion(s) being measured was considered as well. At the beginning of every new experiment, samples were cooled close to liquid nitrogen temperature (-196 °C), and subsequently heated back to 32 °C very quickly (>50 °C/minute) to get a first impression of the fluid composition and to recognise even subtle phase changes *e.g.*, melting of very small amounts of carbon dioxide, initial melting near the eutectic or final ice melting of low salinity fluids. Knowing the approximate transition temperatures from the fast run, the experiments were repeated, stepping the temperature up in increments, and using progressively slower heating rates (50°/min, 10°/min and 5°C) from -120 °C until ca. 5 °C below the phase transition. Rates used for the exact determination of the temperature of phase changes were:

1°/min for CO_2 and H_2O melting and CO_2 homogenisation
2°/min for H_2O homogenisation
0.5°/min for sluggish reactions like recrystallisation or hydrate melting

The method of "cycling" (*c.f.* Roedder, 1984; Shepherd *et al.*, 1985; Goldstein & Reynolds, 1994) was applied to confirm *e.g.*, final clathrate melting or homogenisation temperatures in very small or dark fluid inclusions. Every phase change was measured at least two times to confirm the received data. For further descriptions of technical details concerning the stages or special techniques of measuring fluid inclusions with one of the stages mentioned above, refer to *e.g.* Roedder (1984), Shepherd *et al.*, (1985), or the stage reference manuals provided by Fluid Inc. and Linkam.

4.4.   Raman spectrometry

The application of Raman spectrometry on fluid inclusions allows the immediate qualitative and semi-quantitative measurement of individual phases in a non-destructive way. Especially the identification of small solid (crystalline) compounds like daughter minerals (carbonates, sulphates etc.), which are difficult to analyse by more traditional methods (*e.g.* electron microprobe) has been enhanced by this method.

A Dilor LABRAM confocal-Raman spectrometer combined with a frequency-doubled Nd-YAG laser (100 mW, 532.2 nm) and a Olympus BX 40 microscope with 50X and 100X objective lenses (Olympus) was used to identify fluid and solid phases in inclusions. Wavenumber measurements have an accuracy of 1.62 cm^{-1} at low $\Delta \nu$ (Raman shift around 0 cm^{-1}) and 1.1 cm^{-1} at high $\Delta \nu$ (around 3000 cm^{-1}). To analyse a homogeneous gas mixture and invisible small amounts of H_2O by Raman spectrometry, samples were held at controlled temperatures of +33 °C and -120 °C with a Linkam THMSG 600 heating-freezing stage. The objective lenses combined with a confocal optical arrangement enable a spatial resolution in the order of one cubic micrometre. Thus, the laser (100 mW frequency-doubled Nd-YAG with 532 nm wavelength i.e. a "green-laser") can be focussed on very small individual phases within multi-phase inclusions.

The interaction of the incident laser light with the molecular bonds in the target species scatters some of the incident light via the "Raman effect", emitting light with a frequency that is shifted from that of the laser, and that is characteristic of the vibrational mode and energy of the bond. A portion of the scattered light is collected through the microscope and focussed onto a diffraction grating. The grating selects the desired region of the Raman spectrum and reflects this onto a Peltier-cooled, matrix detector. The resulting spectrum (intensity versus Raman-shifted frequency) is displayed on a computer monitor for further processing and interpretation. The positions and intensities of Raman lines are slightly dependent on the density and especially on the physical state (gas or liquid). The implication for the accuracy of the quantitative Raman analysis is limited but measurements can be checked by the comparison with composition calculated or graphically estimated from microthermometrical data and available phase models (*cf.* chapter 3.6.). A more detailed description of the possible applications of Raman spectrometry on fluid inclusions can be found in *e.g.*, Dubessy *et al.* (1989) or Burke (2001).

4.5.   Bulk composition, molar volume and isochore calculations

Apart from a subordinate number of aqueous fluid inclusions, the majority of inclusions shows melting of a solid phase within a temperature range of –59.2 to –56.6 °C. Thus, the cavities were interpreted to contain a CO_2-dominated fluid. The lowering

of the triple point of pure CO_2 (-56.6 °C) by up to 2.6 °C is symptomatic of the presence of small quantities of additional gases such as CH_4 or N_2. However, nitrogen was the only additional gaseous species detected in CO_2-dominated inclusions by Raman analysis. The presence of N_2 could not always be confirmed by Raman spectrometry. In other cases the amount of N_2 detected by Raman spectrometry was lower than expected from graphic estimations where homogenisation and melting temperatures were transferred into volume-composition (VX) properties using the diagrams provided by Thiery *et al.* (1994). Vice versa, Raman spectrometric measurements sometimes proved the presence of accessory gases, where microthermometry had indicated a pure carbonic fluid phase.

Possible reasons for these discrepancies can be summarised as following:

The quality of Raman measurements is affected by many parameters *e.g.* the quality of wafer, inclusion size, shape and its position within the sample or its density (*cf.* Burke, 2001). No standards exist for the calibration of gas mixtures or the internal standard deviations of the Raman equipment. Although analytical conditions and methodology were tried to be optimised, it can not be completely excluded that one or another factor had a negative effect on the quality of the measurements, leading to less accurate results.

Due to the mineral colour (*e.g.* in garnet), the presence of many small solid or fluid inclusions that becloud single crystals (often the case in feldspar), or the darkish appearance of many CO_2-dominated inclusions, the quality of the observation of a phase transition may be limited. Consequently, the melting temperature measured by microthermometry does not correspond exactly to the actual content of the fluid inclusion although, the accuracy of the stages was determined to ± 0.2 °C for low temperature measurements and special techniques (*e.g.* cycling) had been applied.

The use of VX diagrams to graphically determine fluid compositions or molar volumes is afflicted with a relatively large error. The VX values incorporated in the published diagram for CO_2-N_2 fluid inclusions are based on an experimental reproduction of TPX-data. Deviations caused by inaccuracies may be sizeable especially in the critical region. For some inclusions, no data on composition or molar volume can be derived as no point of intersection exists for the curves of the melting- and homogenisation temperatures measured.

The deviation between compositional values derived from Raman analysis and those determined graphically may be as high as 7 mole % (*e.g.* incl. no. 2176-2-24). Albeit, the fact that the results attained by applying several methods do not always agree with each other, the error concerning the exact fluid composition lies within acceptable analytical limits. Particularly, if one considers the errors that occur during

molar volume/density and isochore calculations that result from the limited applicability of available equations of state.

Densities were calculated for all fluid inclusions whose composition could have been derived from either method, and thus guide values were obtained for inclusion assemblages. Nevertheless, to avoid possible miscalculations or misinterpretations, isochores were calculated only for representative fluid inclusions whose composition known from Raman microanalysis is in close accordance with results from graphic estimates.

The bulk compositions, molar volumes/densities and isochores of individual fluid inclusions were calculated from microthermometry data, Raman analysis and volume fraction estimates using the software packages *Fluids* (Bakker, in press) and *Clathrates* (Bakker, 1997). The programs provide several equations of state (EOS) for the calculations of PVTX properties of varying fluid systems. In consideration of the particular fluid system and the accuracy and limitations of the corresponding equations of state, the suitable equations were chosen for further calculations (see below). During all isochore computations the program took into account the compressibility and expansion of the hostmineral with the volumetric data for quartz taken from Hosieni *et al.* (1985) and from Berman (1988) for all other minerals. If the amount of N_2 detected by Raman spectrometry or graphic estimations did not exceed 2 mol%, fluid properties were calculated as being equivalent to pure CO_2. The error in molar volume calculations resulting from this assumption is by far smaller than liquid-vapour equilibrium calculations with published equations of state.

Pure CO_2

Molar volumes of pure CO_2 fluid inclusions were obtained from the homogenisation temperatures using the equation of Duschek *et al.* (1990), and isochore calculations are based on the equation of state of Span & Wagner (1996).

CO_2-N_2

VX properties of mixed CO_2-N_2 fluids were determined from homogenisation temperatures and Raman data according to the EOS of Thiery *et al.* (1994), based on the modelling of PTX-conditions by the Soave-Redlich-Kwong EOS (Soave, 1972) and molar volumes by the Lee-Kesler correlation (Lee & Kesler, 1975). Isochores were calculated applying the EOS of Duan *et al.* (1992, 1996).

H_2O-salt (NaCleq)

Fluid salinities (in wt% NaCl*eq*) were determined from final ice melting temperatures applying the data of Bodnar (1993). The EOS for bulk fluid density and isochore calculations given by Zhang & Frantz (1987) was used for further computations.

H_2O-CO_2±N_2±*salt*

Complex fluid systems containing mixtures of several gases (*e.g.* CO_2-CH_4-N_2), H_2O and salt are not yet accurately investigated by experimental studies. Consequently, data on solvus PVTX properties are not available and homogenisation temperatures can not be directly transformed into bulk molar volumes/densities but depend on estimation of volume fractions of the fluid phases present.

If clathrate melting in presence of a heterogeneous carbonic phase was observed in complex fluid systems, the program *Q2* from the software package *Clathrates* (Bakker, 1997) was used for the calculation of bulk fluid properties applying the EOS of Duan *et al*. (1992, 1996) and Thiery *et al*. (1994) (H_2O-CO_2-N_2-salt) or Duschek *et al*. (1990) (H_2O-CO_2-NaCl) in combination with volume fraction estimates. Isochores were calculated according to Bowers & Helgeson (1983) modified by Bakker (1999).

In salt free complex systems (H_2O-CO_2-N_2), volume fraction estimates were combined with volumetric properties calculated after Thiery *et al*. (1994) whereas isochores were calculated with the equation of state of Holloway (1977).

5. Geological setting

5.1. The position of central Dronning Maud Land in respect to Rodinia and Gondwana reconstruction

The geotectonic and metamorphic history of East Antarctica, and thus of Dronning Maud Land (DML), is closely related to the formation and fragmentation of Rodinia (McMenamin & McMenamin, 1990), an early Neoproterozoic supercontinent centred around Laurentia, and the subsequent amalgamation of Gondwana in late Neoproterozoic/early Palaeozoic times (*cf.* Bond *et al.*, 1984; Moores, 1991; Dalziel, 1991; Hoffmann, 1991).

As concluded from the correlation of palaeomagnetic data with relicts of Mesoproterozoic mobile belts preserved in the margins of Proterozoic continental nuclei, the assembly of Rodinia was connected with a phase of deformation and metamorphism caused by a collisional orogeny at ca. 1100-1000 Ma, also known as the "Grenville-age event". The exact position of individual Proterozoic cratons constituting Rodinia are still under debate (*cf.* Torsvik *et al.*, 1996; Pelechaty *et al.*, 1996; Weil *et al.*, 1998; Grunow, 1999; Meert, 2001), but it is in general agreed upon, that East Antarctica was facing the western margin of Laurentia (Moores, 1991).

Tectonic activities from ca. 750 Ma to ca. 550 Ma eventually led to the breakup of Rodinia and the consolidation of Gondwana (*cf.* Black & Liegeois, 1993; Rogers *et al.*, 1995a,b). The rifting and drifting of Rodinias continental elements probably began with the separation of East Gondwana as a coherent block, at ca. 750-730 Ma (Li & Powell, 1993; Powell *et al.*, 1993; Borg & DePaolo, 1994). The latest phase of diachronuous dispersal of Rodinia overlaps in time with early collision events between East Gondwana (Australia, India, East Antarctica) and West Gondwana cratons (South American and African cratons/shield areas), generally referred to as the "Pan-African event" (correlative to *e.g.* the Pan-Indian event, the Ross - or the Brasiliano orogeny). However, some authors have stated that parts of East Gondwana were not fully assembled until the latest Neoproterozoic to early Palaeozoic as indicated by the existence of Pan-African-age orogenic belts within East Antarctia, Australia, Madagascar and Sri Lanka (Shiraishi *et al.*, 1994; Grunow *et al.*, 1996). The final collision of East and West Gondwana at ca. 530 Ma resulted in the closing and consumption of the 'Mozambique Ocean' and the formation of the late Neoproterozoic/early Palaeozoic East African Orogen (EAO) (Stern, 1994) or the extended East African/Antarctic Orogen (EAAO) (Jacobs & Thomas., in press) (Fig. 5.1).

Antarctica, once forming the central part of Gondwana, today is pivotal for an improved reconstruction of the supercontinent. During the amalgamation of East and

West Gondwana, the study area of central Dronning Maud Land (cDML) was located next to the eastern margin of southern Africa (Fig. 5.1). Consequently, it shares distinct litho-chronological and tectonic characteristics with parts of the Mozambique Belt exposed in Mozambique, Madagascar, Sri Lanka and southern India.
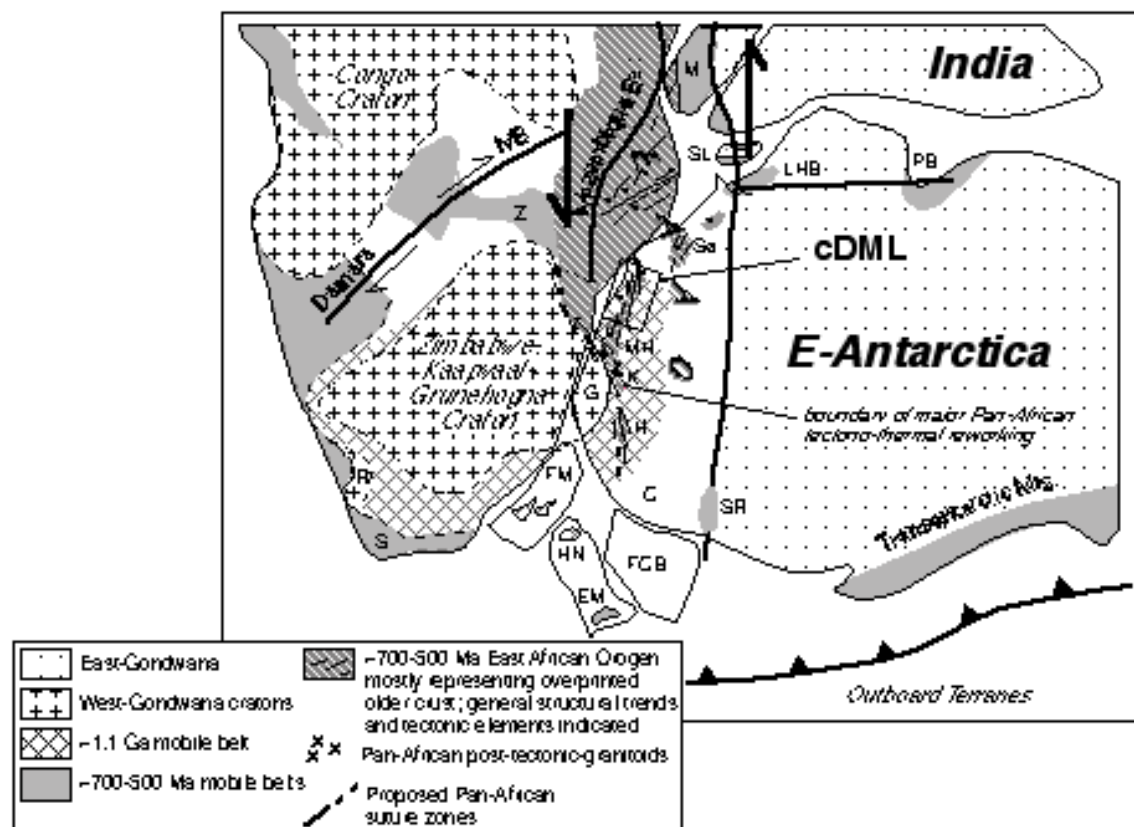
Fig. 5.1: *The position of cDML (marked by the rectangle) within the late Neoproterozoic/early Palaeozoic supercontinent Gondwana (reconstruction after Lawver & Scotese, 1987). C: Coates Land; EAAO: East African/Antarctic Orogen; EM: Ellsworth Mountains; FCB: Filchner crustal block; FM: Falkland Microplate; G: Grunehogna craton; H: Heimefrontfjella; HN: Haag Nunatak; K: Kirvanveggen; LHB: Lützow-Holm bay; M: Madagascar; MB: Mwembesi shear zone; MH: Mühlig-Hofmann-Gebirge; PB: Prydz Bay; R: Richtersveld craton; S: Saldania belt; SL: Sri Lanka; Sø: Sør Rondane; SR: Shackleton Range; Z: Zambesi belt; (modified after Jacobs & Thomas, in press).*

A Pan-African high-grade metamorphic overprint of earlier Grenville-age structures, a pre- to post-tectonic anorthositic and granitic (charnockitic) magmatic province and sinistral shear zones typical for most parts of the Mozambique Belt in Africa (*e.g.* Pinna *et al.*, 1993; Kröner, 1997) find their analogies in cDML (Jacobs *et al.*, 1998). Thus, DML and the region farther east, also termed the "East Antarctic mobile belt", are interpreted to represent the continuation of the Pan-African Mozambique Belt into Antarctica (Unrug, 1996; Dirks & Wilson, 1995; Jacobs *et al.*, 1998). Nevertheless, it has yet remained unclear where the Mozambique Suture between E- and W-

Gondwana projects into Antarctica and whether there is just one or more of them to be detected (Jacobs *et al.*, 1998). Shackleton (1996) suggests to locate the suture in Heimefrontfjella, western DML, while Grunow *et al.* (1996) and Wilson *et al.* (1997) argue for the Lützow-Holm Complex as an alternative location. The latter shows better correlation with data from Jacobs *et al.* (1995, 1998), who interpret the Pan-African-age tectonised part of Dronning Maud Land as a foreland thrust belt with the core and suture of the belt located farther to the east. However, due to the similar geotectonical situations found in DML and the Lützow-Holm Bay complex, pinpointing the exact position of the suture between East and West Gondwana in East Antarctica is still an outstanding problem. Hitherto, no clear answer has been given to the question whether DML originally was part of East or West Gondwana or if it even formed an individual microplate within the Mozambique Ocean (Jacobs *et al.*, 1998; Jacobs & Thomas, in press).

5.2.   Geography and geological evolution of central Dronning Maud Land

South of the Lazarev- and Riiser-Larsen-Sea, Dronning Maud Land encompasses the antarctic region between 20°W and 45°E. From its northern coastline to the south, the Nivlisen (Novolazarevskaya) and Lazarev ice shelve passes gradually over into a gentle foreland covered with thick inland ice sheets. At ca. 70°40'S and 11°-12°E, the ice sheet is interrupted by the Schirmacher Oase, the northernmost ice free spot and continental boundary of DML. Further south between 71°20'S and 72°20'S, a ca. 60 km wide steep and rugged mountain-ridge that runs subparallel to the coastline of East Antarctica for approximately 800 km protrudes the ice cover. This E-W trending mountain chain reaches from the Heimefrontfjella in the west to the Sør Rondane mountain complex in the east (Fig. 5.4). To the south, it is bordered by the Wegener inland ice which finds its continuation in the central antarctic ice cap. The study area of central Dronning Maud Land (cDML) lies between 8°E to 14°E, where the strongly accentuated relief (Fig. 5.2) reaches elevations of 3000 m and higher. CDML embraces the nearly N-S aligned mountain chains of Orvinfjella, comprising Drygalskiberge, Holtedahlfjella, Kurzegebirge, Dallmannberge, Småskeidrista and Conradgebirge, and of Wohlthatmassiv, including Alexander-von-Humboldt-Gebirge, Petermannketten and Otto-von-Gruber-Gebirge (Fig. 5.4). To the west cDML is flanked by the Mühlig-Hofmann-Gebirge, while to the east it continues into the Sør Rondane mountain complex.
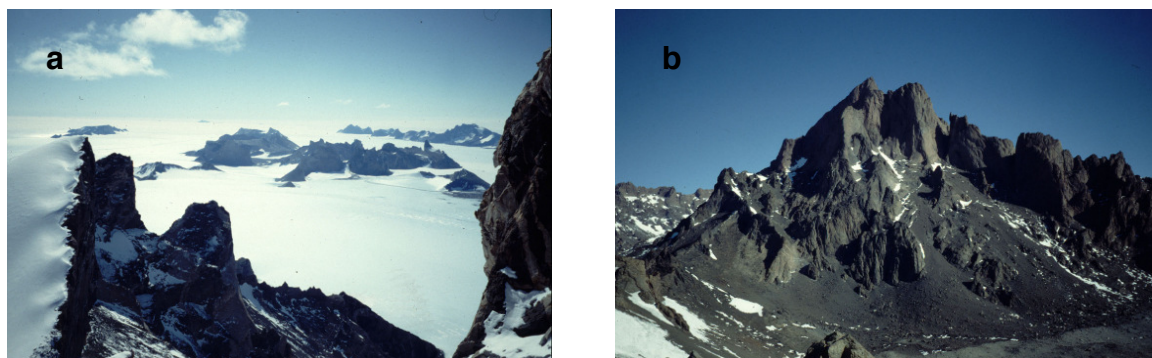
Fig. 5.2: *(a) The rugged morphology of the central Petermannketten; (b) The Otto-von-Gruber-Gebirge.*

Being situated at the margin of the East Antarctic craton, cDML has experienced at least two phases of major deformation and metamorphism: the "Grenville-age event" at ca. 1100 – 1000 Ma, which is only preserved in relics, and the younger and predominant "Pan-African event", that led to a strong pervasive overprint of the older structures. The various lithologic units cropping out in cDML can generally be described as a two-fold subdivision of metamorphic basement rocks versus syn-, late-, and/or post-kinematic intrusive bodies of felsic and mafic composition.

A thick supracrustal series of sedimentary and volcanic rocks, today forming the crystalline basement complex, was subjected to an extensive tectono-metamorphism at high- to medium-pressure granulite facies conditions (M_1 according to Bauer *et al.*, 1996). The metasedimentary units are composed of garnet-biotite±hornblende gneisses, garnet-sillimanite-cordierite–bearing metapelites, quartzites and calc-silicate boudins often associated with marble layers or lenses (Bauer *et al.*, 1996; Markl & Piazolo, 1998; Piazolo & Markl, 1999). The leucocrate paragneisses are mainly exposed in the A.-v.-Humboldt-Gebirge and Petermannketten, and often contain a network of dark-coloured to greenish hue or brown orthopyroxene-bearing patches and tubes crosscutting the gneissic foliation. This secondary charnockitisation pattern is locally interrupted by bleached zones around fractures and mylonite zones or undeformed pegmatite veins and felsic dykes (Paech, 1997) (Fig. 5.3).
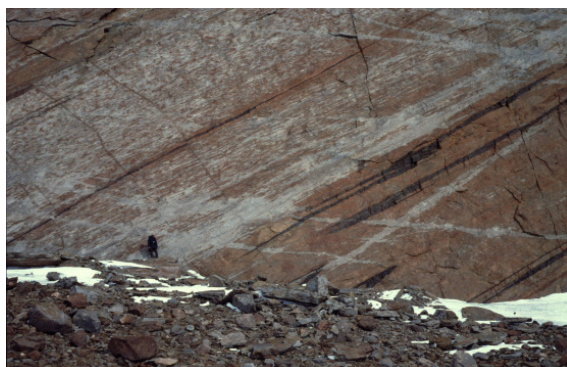

Fig. 5.3: *Field view of secondary charnockitisation pattern crosscut by light-grey bleached zones around fractures and foliation planes (central Petermannketten).*

30

The metavolcanic rocks are characterised by a layered sequence of fine-grained banded hornblende-bearing gneiss, plagiogneiss and amphibolites, hinting at a bimodal character of the original volcanic units, and intercalations of ultramafic lenses and metagabbros (Bauer *et al.*, 1996; Paech, 1997; Colombo & Talarico, in press). Magmatic zircons of these rocks gave crystallisation ages of ca. 1130 Ma and metamorphic zircon overgrowth at ca. 1080 Ma (Jacobs *et al.*, 1998). This early Grenville-age metamorphic event was associated with the syntectonic intrusion of granite sheets and plutons at ca. 1085 to 1075 Ma (Jacobs *et al.*, 1998), that were locally metamorphosed to garnet-bearing migmatic orthogneisses. Rare remnants of D1 deformation are S_1 planes parallel to the compositional layering and isoclinal, intrafolial and often rootless microfolds with variable orientations (Bauer *et al.*, 1996).

No further tectonothermal or magmatic imprint is recorded until ca. 600 Ma when anorogenic magmatism marked the onset of an extended period of late Neoproterozoic to lower Palaeozoic geodynamic activity. Subsequent high-grade tectonothermal overprint was caused by the collision of East and West Gondwana which is ascribed to the broader "Pan-African event". (*cf.* Black & Liegeois, 1993; Rogers *et al.*, 1995a,b). The intrusion of igneous rocks into the Grenville-age basement pre- and post-dates the geodynamic event.

In the Wohlthatmassiv, the magmatic activity started with the emplacement of a voluminous massif-type anorthosite complex (the O.-v.-Gruber–Anorthosite complex) associated with subordinate charnockites, ferrodiorites and norites (Kämpf & Stackebrandt, 1985; Jacobs *et al.*, 1998; Markl *et al.*, in press). The O.-v.-Gruber anorthosite complex crops out over approximately 250 km^2 and shows a relatively homogeneous plagioclase ± orthopyroxene ± clinopyroxene - magnetite - illmenite mineral assemblage. A common feature are layers and lenses of ultramafic composition, mainly composed of Fe-Ti oxides and orthopyroxene. The anorthosite complex is crosscut by ferrodioritic dykes, varying amounts of (leuco-) gabbros and (leuco-)norites and late Pan-African pegmatoids (Markl *et al.*, in press). Granitic plutons, anorthositic dykes, and rocks of the ferrodiorite suite also intruded in the area of the Petermanketten (Ravich & Kamenev, 1975; Parimoo *et al.*, 1988; Joshi *et al.*, 1991).

The margins of the anorthosite body were strongly deformed at ca. 580-550 Ma (Jacobs *et al.*, 1998). Deformation took place at medium-pressure granulite facies conditions of about 6.8 ± 0.5 kbar and 830 ± 20 °C, and is interpreted as representing the collisional stage, i.e. Pan- African I (Markl & Piazolo, 1998; D_2 in Bauer *et al.*, in press). Within the anorthosite body discrete mylonitic shear zones developed during this high grade event.

The main structural trend ascribed to the Pan African I (or D_2) deformational event is not homogenous throughout cDML. In the Wohlthatmassiv, tight B_2 fold axes are

preserved, but their original vergence is concealed by later refolding and rotation. Common features of the coeval metamorphism M_2 that can be observed within the metamorphic basement rocks include syntectonic migmatisation, dehydration melting of metapelites and expulsion of leucosomes (Bauer *et al.*, in press). The anorthosite body was affected by a foliation S_2 which bends gradually from E-W in the northern margins over NE-SW in the north-west to N-S at the western flank. In the eastern and central region no foliation is discernible, and undeformed magmatic textures and –layering are preserved. Thus, the anorthosite is interpreted as having behaved like a large delta-clast during deformation (Bauer *et al.*, in press; Markl *et al.*, in press).

A subsequent tectono-metamorphic event (Pan-African II; D_3/M_3 in Bauer *et al.*, in press) started with the syntectonic intrusion of granitoids and gabbros at approximately 530-515 Ma (Jacobs *et al.*, 1998; Bauer *et al.*, in press). Metamorphic conditions were at low–pressure granulite facies of 4 - 5 kbar and temperatures of about 640 ± 10 °C (Markl & Piazolo, 1998).

Extensional shearing (D_4) gave way for a second voluminous anorogenic anorthosite-charnockite cycle and the intrusion of post-tectonic syenite-batholiths at ca. 510 Ma (Mikhalsky *et al.*, 1997) that marked the final stage of Pan-African metamorphism. It was accompanied by a poorly developed and yet undated retrogression at pressures of approximately 2 - 5 kbar and 480 - 580 °C post-dating the voluminous intrusion of granitoids at 510 Ma (Markl & Piazolo, 1998; D_4 in Bauer *et al.*, in press).

Thermobarometric studies indicate a clockwise PT-path characterised by an isothermal decompression evolution for the early Pan-African I event, whereas the structures of the Pan-African II event are ascribed to a late-orogenic extensional collapse of the East African/Antarctic Orogen (Colombo & Talarico, in press.; Jacobs & Thomas, in press).

5.3.   Nomenclature of geographic sites in Dronning Maud Land

The naming of topographic features in central Dronning Maud Land has not been unitised yet. When selecting existing names for the use in this work, preference was given to the earliest approved or documented names, as recommended by the guidelines of the *"Composite Gazetteer of Antarctica"* (www.pnra.it/SCAR_GAZE), published by the *Scientific Committee on Antarctic Research (SCAR) - Working Group on Geodesy and Geographic Information*. According to SCAR recommendations, place names should be given in their original form and not in a translated version. In 1937, when Norway claimed the sector between 20°W and 45°E to secure its whaling activities, the region was named in honour of the Norwegian Queen Maud (1869-1938). Thus, the Norwegian term *Dronning Maud Land* is used throughout this study. On the other

hand, most geographic names that are in common use today can be traced back to the German Expedition led by A. Ritscher in 1938/39, during which the geography of Dronning Maud Land was systematically mapped with the help of aircraft and aerophotogrammetry. Consequently, German and Norwegian names are applied in hierarchical succession or according to their prevalence and acceptance throughout recent literature. English terms are applied, if no appropriate German or Norwegian names exist or if they are the ones most widely accepted.
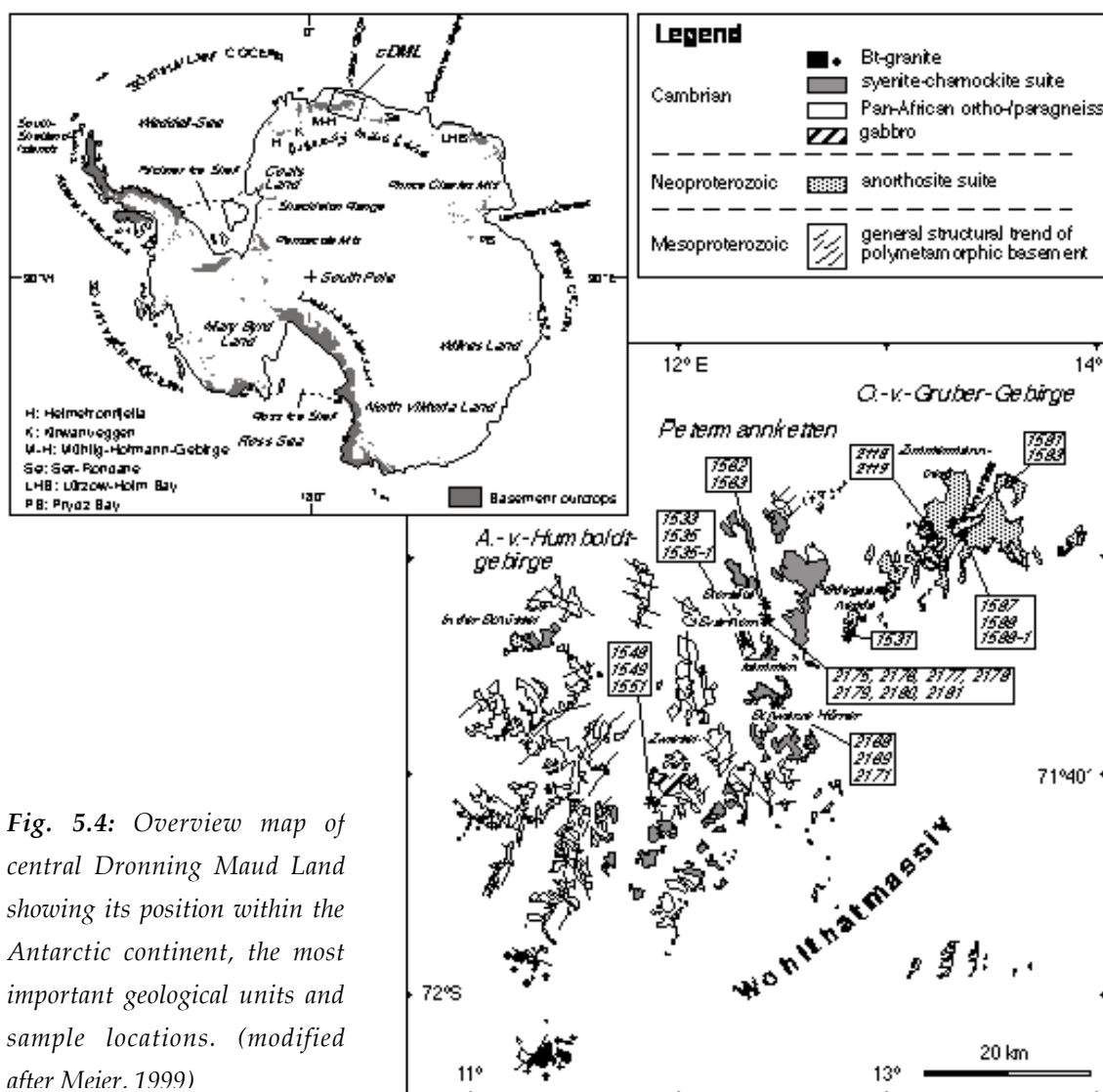

Fig. 5.4: Overview map of central Dronning Maud Land showing its position within the Antarctic continent, the most important geological units and sample locations. (modified after Meier, 1999)

6. The basement lithologies of the central Petermannketten - an example of secondary charnockitisation and leaching processes

The rocks studied and discussed in this chapter represent some of the major rock units exposed in the crystalline basement complex of cDML, as described in chapter 5.2. During the field campaign, varying surface colourings of corresponding rock units led to the assumption that the basement lithologies had been subjected to non-pervasive secondary charnockitisation, and fracture- and foliation controlled leaching processes. One intention of this study is to affirm or disprove this supposition, and to investigate in the character of the fluid phases potentially involved in the charnockitisation and/or leaching processes. Hence, analytical results were compared by means of different rock colouring, and as not all darkish rocks can be classified as charnockites s. str., the following presentation of data still relies on the primary, and generalising subdivision into "dark" and "light" rock types.

Table 6.1: *Locations and rock types of samples collected from the central Petermannketten. The colour attribute "dark" describes a greenish hue as characteristic of charnockites/secondary charnockitisation. "Light" refers to the leached or original rock colour.*

sample no.	locality	rock type	colour	latitude S	longitude E	altitude [m]
1533	Svarthornkammen	mangerite (gneissic)	dark	71°29.2'	12°27.3'	1540
1535	Svarthornkammen	granitic gneiss (migmatitic)	light	71°29.2'	12°27.3'	1340
1535-1	Svarthornkammen	granitic gneiss	dark	71°29.2'	12°27.3'	1340
1548	Zwieselhögda	granitic grt-gneiss	light	71°46.3'	12°00.8'	1760
1549	Zwieselhögda	qtz-alkali-fsp-syenite	light	71°46.3'	12°00.8'	1760
1551	Zwieselhögda	hbl-bearing granitic gneiss	light	71°46.3'	12°00.8'	1760
1562	Storsåta	granitic grt-gneiss	dark	71°27.1'	12°30.6'	1240
1563	Storsåta	granitic grt-gneiss	light	71°27.1'	12°30.6'	1240
2168	Schwarze Hörner	qtz-rich granitic gneiss	light	71°35.7'	12°33.4'	1660
2169	Schwarze Hörner	charnockite (massive)	dark	71°35.7'	12°33.4'	1660
2171	Schwarze Hörner	charnockite (massive)	dark	71°35.7'	12°33.4'	1660
2175	SE Storsåta	alkali-fsp-syenite	light	71°29.0'	12°31.1'	1400
2176	SE Storsåta	granitic grt-gneiss (migmatitic)	light	71°29.0'	12°31.1'	1400
2177	SE Storsåta	charno-enderbite (massive)	dark	71°29.0'	12°31.1'	1400
2178	SE Storsåta	granitic gneiss (migmatitic)	light	71°29.0'	12°31.1'	1400
2179	SE Storsåta	charnockite (migmatitic, 2179a)	dark	71°29.0'	12°31.1'	1400
		jotunite (massive, 2179c)				
2180	SE Storsåta	charno-enderbite (migmatitic)	dark	71°29.0'	12°31.1'	1400
2181	SE Storsåta	monzonitic grt-gneiss (migmatitic)	light	71°29.0'	12°31.1'	1400

6.1. Metamorphic charnockites and gneisses of the basement lithologies

6.1.1. Petrography of "dark" rock varieties (thinsections no. 1535-1, 1562, 2169, 2171, 2177, 2179a, 2179b, 2180)

Macroscopically, the fine to medium grained "dark" rock varieties are equigranular to inequigranular, and characterised by a distinct greenish to brownish colouring. Gneissic samples show a pronounced foliation. In some rocks, the foliation is interrupted and destroyed by coarse grained migmatitic zones, whereas massive varieties lack any preferred or distinctive texture.

The main mineral constituents of these samples (major and minor phases) are plagioclase, K-feldspar, quartz, green hornblende, biotite, garnet, orthopyroxene and clinopyroxene in varying amounts and phase proportions. Muscovite, black and dark red opaque phases, apatite, zircon, chlorite, monazite, tourmaline, titanite and calcite were identified as accessories. Note that not all samples contain all phases mentioned above (see Table 6.2).

Table 6.2: Modal compositions (in vol%) of "dark" varieties of gneissic samples from the basement lithologies of the Petermannketten. x ≤ 2 vol%. Thinsection 2179a represents the migmatitic part, and 2179c the massive part of sample 2179.

| sample no.	1535-1	1562	2169	2171	2177	2179a	2179c	2180
rock type	granitic gneiss	granitic grt-gneiss	charnockite	charnockite	charno-enderbite	charnockite	jotunite	charno-enderbite
plagioclase	30	35	7	20	30	25	40	40
K-feldspar	35	20	35	40	15	15	5	15
quartz	20	35	45	25	40	35	x	15
biotite	3	5	5		x	10	10	10
muscovite	x		x	x	x	x		x
garnet		3			5			7
green hornblende	6		x	7			15	
orthopyroxene			5	5	5	10	15	7
clinopyroxene				x			10	
opaque phase	x	x	x	x	x	x	x	x
apatite	x	x	x	x	x	x	x	
zircon	x	x		x	x	x		x
chlorite	x	x	x		x	x		
monazite	x							
titanite	x	x						
tourmaline	x							
calcite	x	x			x			
relictic phase	x	x		x			x	

Samples no. 1535-1 and 1562 that do not contain orthopyroxene, comprise a strongly altered relictic phase with yellow to brownish colouring, which could not be further identified by optical microscopy or electron microprobe analysis. Nevertheless, this phase was also observed in conjunction with orthopyroxene or relictic in migmatitic zones of sample 2179 (Fig. 6.1e, f). Therefore it is interpreted as being a product of pyroxene alteration.

The amount of *plagioclase* is lowest in charnockite sample no. 2169 (c. 7 vol%) and highest in samples 2179c and 2180 (c. 40 vol%) (Table 6.2). However, the characteristics of the anhedral to subhedral plagioclase grains are similar throughout all darkish rocks. Within a total range of c. 0.05 to 2.0 mm, they show an average grain size of c. 0.5 to 1 mm. Typically, plagioclases display polysynthetic twinning after albite- and/or pericline twin law in addition to commencing formation of dihedral angles and straight grain boundaries. Myrmekitic intergrowth with small, rod-like quartz grains is common (Fig. 6.1a). Secondary alteration to sericite and calcite is pervasive or restricted to intracrystalline microfractures.

Modal proportions of *K-feldspar* vary between c. 5 and 40 vol% and sizes of the anhedral to subhedral grains spread from 0.1 to 2.5 mm (seriate grain size distribution). One representative feature of K-feldspar grains is perthitic unmixing. Microcline-type albite and pericline twinning infrequently occurs. Diffuse and discontinuous crosshatched twinning further indicate the presence of microcline (Fig. 6.1b), that sometimes reveals vermicular intergrowth with adjacent quartz. Sporadic alteration to fine grained aggregates of sheet-silicates is restricted to intra-/ and intercrystalline fissures or grain boundaries.

Quartz, which is only an accessory phase in thinsection 2179c may take up c. 15 to 45 vol% with the highest value reached in sample no. 2169 (Table 6.2). Grain size distribution of anhedral to subhedral crystals is seriate to inequigranular, ranging from 0.1 to 7.2 mm. Generally, small grain sizes belong to (secondary) quartz that shows graphic or vermicular intergrowth with feldspar, biotite or garnet. The longest dimensions belong to disc-shaped quartz grains, which are flattened and aligned along foliation planes of gneissic samples (Fig. 6.1c). Next to the disc-shaped habit, quartzes exhibit further deformation features as extinction, bent deformation lamellae, and inter- and intracrystalline microfractures. Occasionally, the fissures are filled with fine grained network of muscovite, chlorite and biotite. Frequent indicators of dynamic recrystallisation and recovery are irregular grain boundaries, subgrain rotation and subgrain formation (Fig. 6.1c). Zones of completely statically recrystallised grain aggregates with polygonal fabric and grain sizes of c. 0.1 to 0.5 mm were also observed.

Biotite is present in all rocks either as major, minor or accessory component. In most samples, two different varieties have been identified.
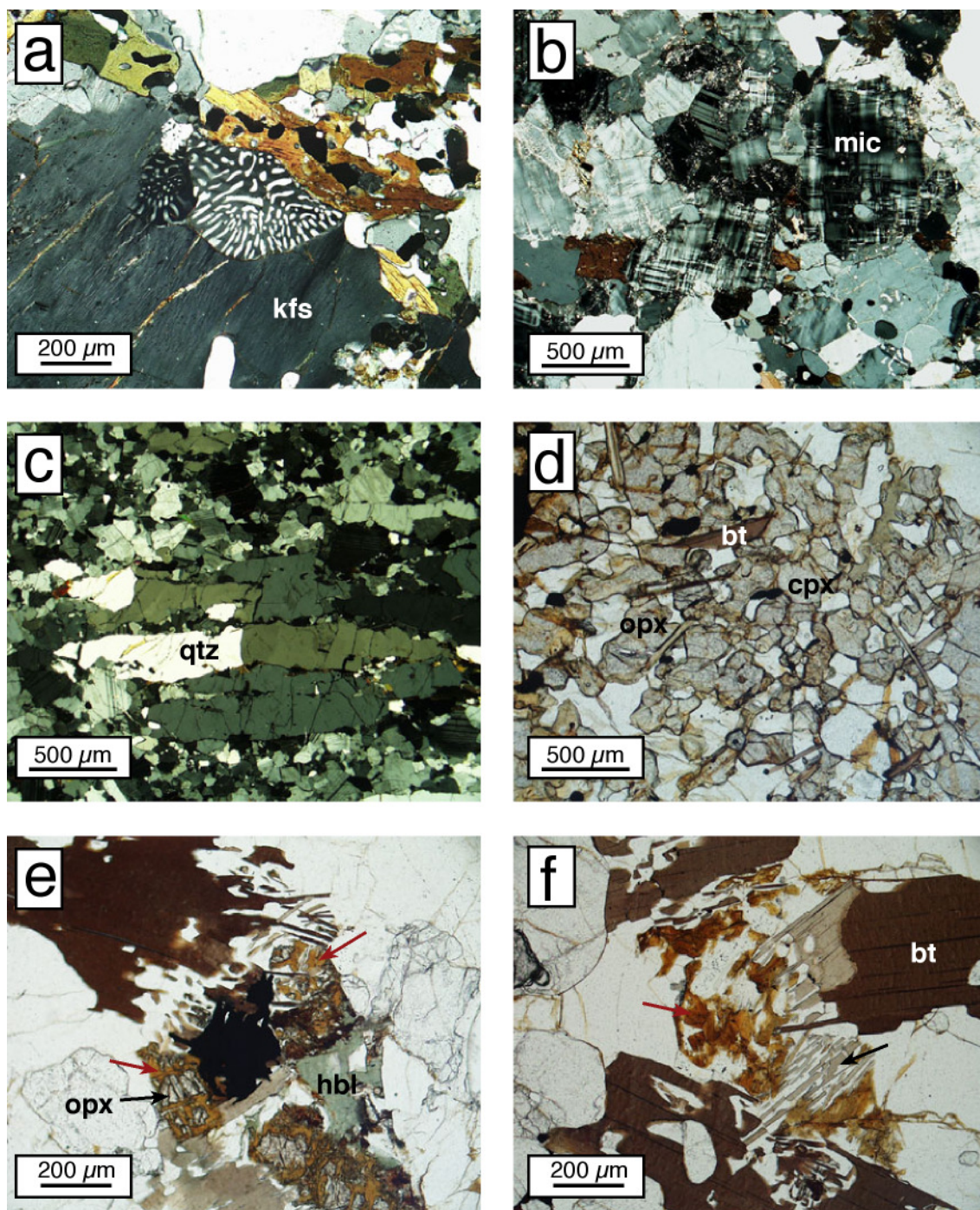
Fig. 6.1: *Microphotographs of characteristic mineral phases and textures of "dark" rock varieties: (a) myrmekitic growth of plagioclase and quartz into K-feldspar; (b) microcline with typical twinning; (c) disc-shaped quartz with differently orientated subgrains; (d) subhedral ortho- and clinopyroxene crystals and "primary" biotite flake; (e) alteration of orthopyroxene along rims and fractures resulting in the formation of a yellowish phase (red arrows), green hornblende, opaque phase and fringy biotite; (f) relictic phase without any relictic pyroxene, and biotite with vermicular quartz (arrow).*

One type of biotite is aligned along foliation planes or integrated in the fabric of massive samples. Pleochroitic colouring of the subhedral flakes is dark brown to light brown, and grain size is c. 0.3 to 1.0 mm (Fig. 6.1d). Inclusions of small rounded zircon grains are surrounded by black pleochroitic halos. The other, and assumedly secondary, type of mostly anhedral biotite may be larger, ranging from 0.2 to 2.0 mm in longest dimension. It displays similar pleochroitic colouring, but some grains also reveal pleochroism from dark to light green. The most characteristic attribute is its vermicular intergrowth with quartz, which results in a fringy appearance (Fig. 6.1e,f). Single grains generally overgrow the rocks' fabric, form rims around pyroxene or occur paragenetically with or as solid inclusion in in garnet or green hornblende. Around the strongly altered relictic phase of samples no. 1562 and 1535-1, biotite also appears in conjunction with calcite. It is not always possible to clearly differentiate both biotite varieties in respect to volume percentage estimation, as the second type may reveal epitaxical overgrowth on early grains.

Orthopyroxene (i.e. hypersthene), the mineral phase essential for classifying rocks in respect of the charnockitic rock suite, was detected in all thinsections except for samples no. 1562 and 1535-1. Orthopyroxene crystals are euhedral to subhedral, and range from c. 0.05 to 2.0 mm in size. Their pleochroitic colour changes between pale green to pale yellowish (Fig. 6.1d). Most minerals exhibit varying states of alteration along mineral cleavage planes, microfractures or grain margins. Alteration results in formation of brownish opaque phase, a network of unspecified yellow microcrystals or different sheet-silicates, green hornblende and secondary biotite (Fig. 6.1e). Biotite (early type), black opaque phase, quartz and feldspar occur as solid inclusions in orthopyroxene. *Clinopyroxene* was identified by means of weak pleochroism (light green and light red), and high birefringence. The euhedral to subhedral crystals are between c. 0.05 and 0.5 mm in size. Large grains are sometimes surrounded by a narrow rim of orthopyroxene.

Samples no. 1562, 2177 and 2180 contain subhedral *garnet* blasts that range from c. 0.1 to 4.0 mm in size. The blasts sometimes reveal open microfractures, and varying numbers and combinations of solid inclusions, which were identified as quartz, black opaque phase and biotite (early and late type).

Green hornblende is an accessory phase in sample no. 2169 and a major constituent in samples no. 1535-1, 2171, and 2179. The mineral grains are anhedral to subhedral, 0.2 to 0.8 mm in size. They reveal a strong pleochroism of light to dark green. Mineral cleavage planes are visible in sections cut perpendicular to the c-axis. In general green hornblende has formed as mantle around pyroxene. It has also developed along fractures and cleavage planes of pyroxene, or intergrown with biotite. Rarely, green hornblende displays beginning of calcitisation and sericitisation.
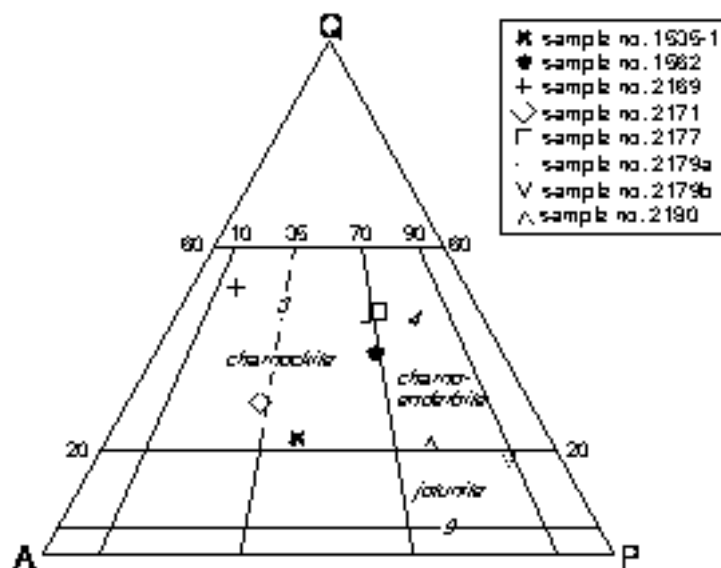
Fig. 6.2: *Classification of "dark" (charnockitic) rocks in the QAP triangle according to Le Maitre (1989) following the recommendations of the IUGS subcommission for the classification of charnockitic rocks. Modal compositions of plagioclase, K-feldspar and quartz are given in Table 6.2. With respect to the definition of the members of the charnockitic rock series (c.f. chapter 2.1), only samples no. 2169, 2171 and 2179a can be classified as charnockite s.str. The names of orthopyroxene bearing samples are given in the figure. Samples no. 1535-1 and 1562 do not contain orthopyroxene any more and are therefore classified as granitic gneiss and granitic grt-gneiss, respectively, although they show the typical charnockite colouring and contain a relictic phase that indicates former orthopyroxene occurance. Numbers in italics indicate the QAPF field number after Le Maitre (1989).*

6.1.2. Petrography of "light" rock varieties (thinsections no. 1535, 1548, 1551, 1563, 2168, 2176, 2178, 2181)

The group of "light" rock varieties comprises gneisses with fine layers of white, light and dark-grey minerals. Some samples exhibit migmatitic zones, garnet blasts, or roundish aggregates of green hornblende and biotite that overgrow the gneissic foliation. Macroscopically, the rocks are predominantly inequigranular, fine to medium grained.

Major and minor mineral phases distinguished during optical microscopy are plagioclase, K-feldspar, quartz, hornblende, garnet and biotite. Accessories observed are muscovite, chlorite, black and brownish opaque phases, apatite, zircon, calcite, rutile, monazite, and titanite.

Anhedral to subhedral *plagioclase* crystals range around 0.1 to 1.6 mm in size. They often reveal polysynthetic twinning after albite and pericline twin law, and myrmekitic intergrowth with quartz. Some grains display extinction, subgrains and/or irregular grain boundaries. Rarely, antiperthitic unmixing can be observed. Sericitisation of plagioclase grains occurs along fissures or restricted to single twin lamellae.

Table 6.3: *Modal compositions (vol%) of "light" varieties of gneiss and migmatite samples from the basement lithologies of the Petermannketten. x ≤ 2 vol%.*

sample no.	1535	1548	1551	1563	2168	2176	2178	2181
rock type	granitic gneiss	granitic grt-gneiss	hbl-bearing granitic gneiss	granitic grt-gneiss	qtz-rich granitic gneiss	granitic grt-gneiss	granitic gneiss	monzonitic grt-gneiss
plagioclase	25	20	20	25	7	25	20	40
K-feldspar	40	20	25	25	20	25	30	30
quartz	25	40	40	40	50	35	35	10
biotite	7	7	5	x	10	x	x	10
muscovite	x			x	x		x	x
garnet		7		5	5	5		4
green hornblende			7				x	
opaque phase	x	x	x	x	x	x	x	x
apatite	x	x	x	x	x	x		
zircon	x	x	x	x	x	x	x	x
chlorite		x	x	x		x		x
monazite				x				
calcite				x				
rutile		x		x	x			
titanite				x				
relictic phase		x		x	x	x		x

K-feldspar shows seriate grain size distribution, generally ranging from c. 0.05 to 1.5 mm, but grain sizes up to c. 30.0 mm are also present in migmatitic samples. The subhedral to anhedral grains commonly reveal perthitic unmixing and discontinuous crosshatched twinning as it is typical for microcline (Fig. 6.3a). Abundant microstructures caused by deformation and/or recovery include irregular grain boundaries (Fig. 6.3a), extinction, and subgrain formation. Fine grained recrystallised K-feldspar aggregates or thin twin lamellae are a subordinate feature. Straight grain boundaries and dihedral angles have preferably formed in contact with quartz and biotite. Evidence of brittle fracturing is given by the presence of inter- and intracrystalline fissures and microfractures. Regularly, they are filled with fine grained aggregates of muscovite, calcite and/or chlorite.

Quartz generally displays bimodal grain size distribution, ranging from c. 0.8 to 8.8 mm. In strongly foliated gneisses, large anhedral quartz crystals are disc-shaped and flattened parallel to the foliation planes (Fig. 6.3a). They show interlobate grain boundaries, undulous extinction and subgrain formation. The texture and habit of small quartz grains of these samples indicate dynamic and sometimes static recrystallisation, the latter leading to the formation of polygonal fabric, a lack of undulous extinction, and interfacial angles of approximately 120°. In migmatitic samples, grain size distribution is similar (c. 0.4 bis 6.4 mm), but the large crystals are anhedral old grains that do not show any preferred orientation.
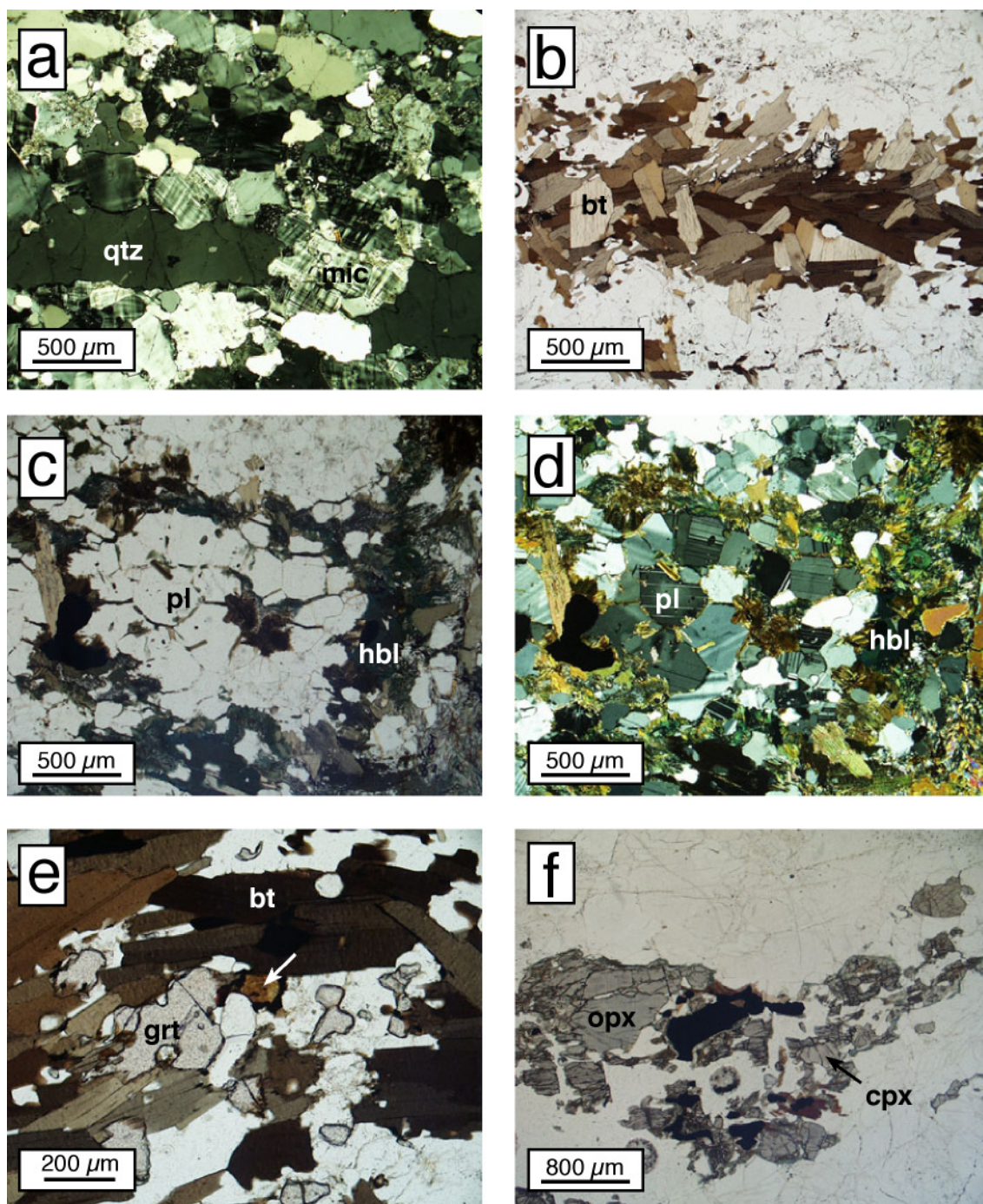
Fig. 6.3: *Microphotographs of "light" coloured samples of the basement lithologies: (a) disc-shaped quartz and microcline with irregular grain boundaries; (b) flaky (primary) biotite aligned within gneissic foliation; (c) green hornblende in circular arrangement around plagioclase; (d) the same display detail as in (c), but with crossed polars; (e) garnet, biotite, and relictic yellow phase (arrow); (f) orthopyroxene and clinopyroxene of mangerite sample no. 1533 (synkinematic intrusion, cf. chapter 6.2).*

Larger quartzes are sometimes crossed by open microfractures. Intergrown with plagioclase, rod like quartz in myrmekitic zones displays grain sizes of c. 0.1 to 0.4 mm. Similar grain sizes are typical for quartz that occurs as solid inclusion in, or graphic texture with, garnet or biotite.

All samples contain *biotite* at least as accessory phase, but mostly present as minor or major constituent. The anhedral to subhedral grains vary in size between c. 0.04 and 2.0 mm, and two varieties can be distinguished in some samples. One type of biotite is flaky and integrated into the rocks' fabric. It displays pleochroitic colours of light to dark brown (Fig. 6.3b). A second kind displays pleochroitic colours of light yellowish to dark brown and conspicuous vermicular intergrowth with rod like quartz, which results in a fringy appearance. In some samples, biotite also reveals pleochroism of light and dark green, or a change of colour from brownish to greenish towards crystal margins. The fringy biotite is less abundant. If garnet is present, both minerals occur paragenetically, often together with a relictic yellowish phase (Fig. 6.3e).
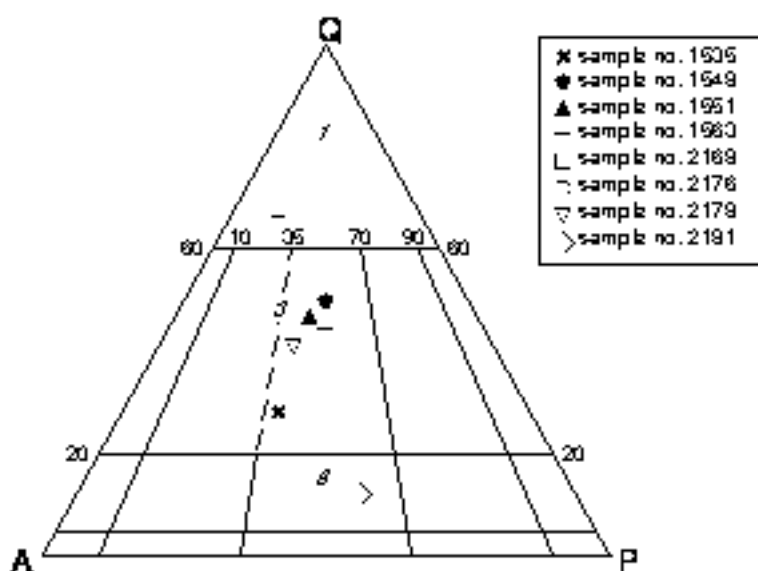
Fig. 6.4: For a better comparison with the darkish (partly charnockitic) samples, light gneisses are also plotted in the QAP-triangle. The modal composition and conspicuous mineral components were included into the name when classifying the rocks under investigation (e.g. qtz-rich granitic gneiss), cf. Table 6.1.

Anhedral to euhedral *garnet* blasts overgrow the gneissic foliation and range from c. 0.2 and 4.0 mm in size. The grains are often intergrown with biotite, some display spongy cellular relationship with quartz, or solid inclusions of opaque phases, K-feldspar, plagioclase or sheet silicates. Single garnets are crossed by open fractures, which may be filled with sheet silicates.

Only sample 1551 contains *green hornblende*, which is anhedral to euhedral, varying in size from 0.1 to 0.4 mm. Together with fine biotite flakes, the crystals are arranged in circles around aggregates of polygonal plagioclase (Fig. 6.3c, d).

6.1.3. Fluid inclusion studies (thicksections no. 1535, 1535-1, 1562, 1563, 2176, 2177, 2178, 2179a, 2179c, 2180, 2181)

Not all samples described in the previous chapter were suitable for microthermometry analysis, and hence, the most characteristic and promising ones were selected for further investigations. Within both groups of rocks ("dark" and "light" varieties) three different fluid phases containing either $CO_2 \pm N_2$, H_2O-salt or H_2O-$CO_2 \pm N_2$-salt, have been identified. Fluid inclusions are predominantly hosted by quartz and subordinately by plagioclase and garnet.

$CO_2 \pm N_2$- bearing inclusions

The fluid phase that is most abundant throughout the dark and light varieties of (migmatitic) gneisses is CO_2-rich with minor and varying amounts of nitrogen. When hosted by *quartz*, these inclusions range between 3.5 to 45.0 μm in size. They are mostly arranged in intracrystalline clusters and trails but single inclusions do also occur. Inclusion shapes are highly irregular or elongated (Fig. 6.6a), but predominantly roundish to negative crystal shape (Fig. 6.6b). Melting temperatures of solid CO_2 after supercooling to -120°C and reheating to room temperature is -58.3 to -56.6 °C (light rock types) and -58.4 to -56.6 °C (dark rocks) (Fig. 6.5a, b). Homogenisation temperatures range between 10.9 and 30.7 °C (light rocks) and 7.5 to 29.9 °C (dark rocks) and homogenisation either occurs to the liquid or to the vapour phase (Fig. 6.5a,b). Some rare inclusions also reveal fading of the miniscus of the bubble which indicates critical homogenisation. Densities calculated from homogenisation temperatures range between 0.17 and 0.84 gcm^{-3} for light rock varieties and 0.37 to 0.82 gcm^{-3} for dark rock varieties.

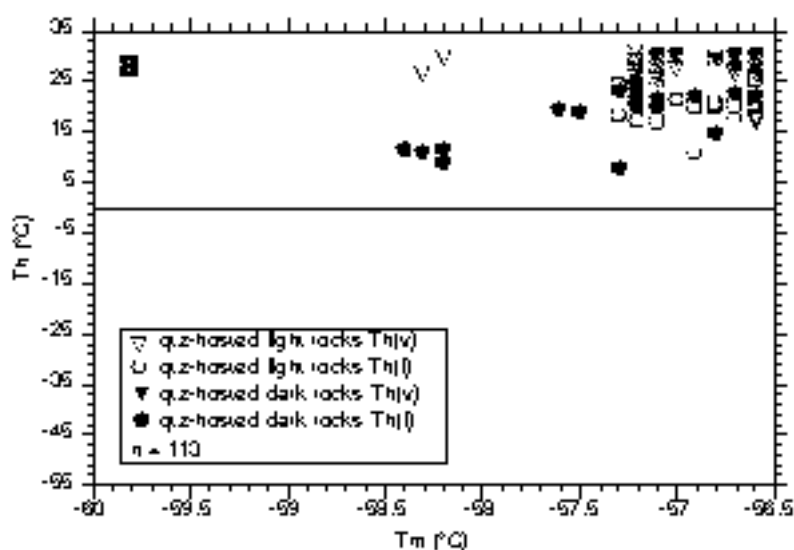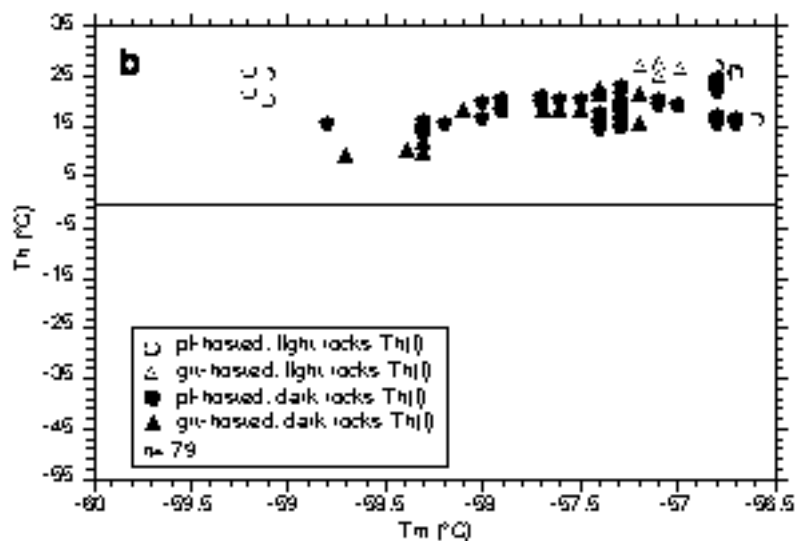**Fig. 6.5a:** *Homogenisation and melting temperatures of qtz-hosted $CO_2 \pm N_2$ inclusions of "dark" and "light" rock types. Homogenisation is either to the vapour or the liquid phase. Note that no characteristic regularity in Th or Tm of darkish and light rock varieties can be derived.*

Fig. 6.5b: *Homogenisation and melting temperatures of plagioclase and garnet-hosted $CO_2 \pm N_2$ inclusions of "dark" and "light" rock types. Homogenisation is always to the liquid phase. Dark rocks display a large range of Tm, whereas Tm of grt- and pl-hosted inclusions in the light rocks plot in clusters.*

The amount of N_2 detected by Raman microspectrometry or estimated from the melting point depression of CO_2 ranges between 0 and 10 mol% (in light rocks) and 0 to 16 mol% in dark rock varieties. Some of the quartz hosted fluid inclusions contain solid phases which were identified by Raman microspectrometry to be either nahcolite ($NaHCO_3$) or siderite ($FeCO_3$) (Fig. 6.7a).

$CO_2 \pm N_2$ inclusions hosted by *feldspar* crystals of light and dark rock varieties are predominantly arranged on intracrystalline clusters and trails and single fluid inclusions only occur in a subordinate number. The preponderant inclusion shape is elongated to square or negative crystal shape (Fig. 6.6c), and inclusion sizes range between 5.0 and 32.0 μm. Feldspar hosted fluid inclusions are more abundant in the darkish samples. The melting temperature of CO_2 after freezing is -59.2 to -56.6 °C and -58.8 to -56.7 °C in the light and dark samples, respectively (Fig. 6.6 b). Homogenisation of these fluids is always into the liquid phase within the limits of 16.0 and 26.7 °C (light rocks) and 13.0 and 23.9 °C (dark samples).

As Raman spectrometry and graphic estimations have revealed, the entrapped fluid contains up to 18 mol% N_2 in the darkish rock varieties and max. 3 mol% in the light samples. Enclosed microcrystals were identified with Raman microspectrometry to be calcite, Mg-calcite, dolomite, pyrophyllite and/or paragonite/muscovite (di-octahedral mica). Densities calculated from microthermometry and Raman spectrometry data range between 0.60 and 0.81 gcm^{-3} in light rocks, and between 0.47 and 0.81 gcm^{-3} in dark rocks.
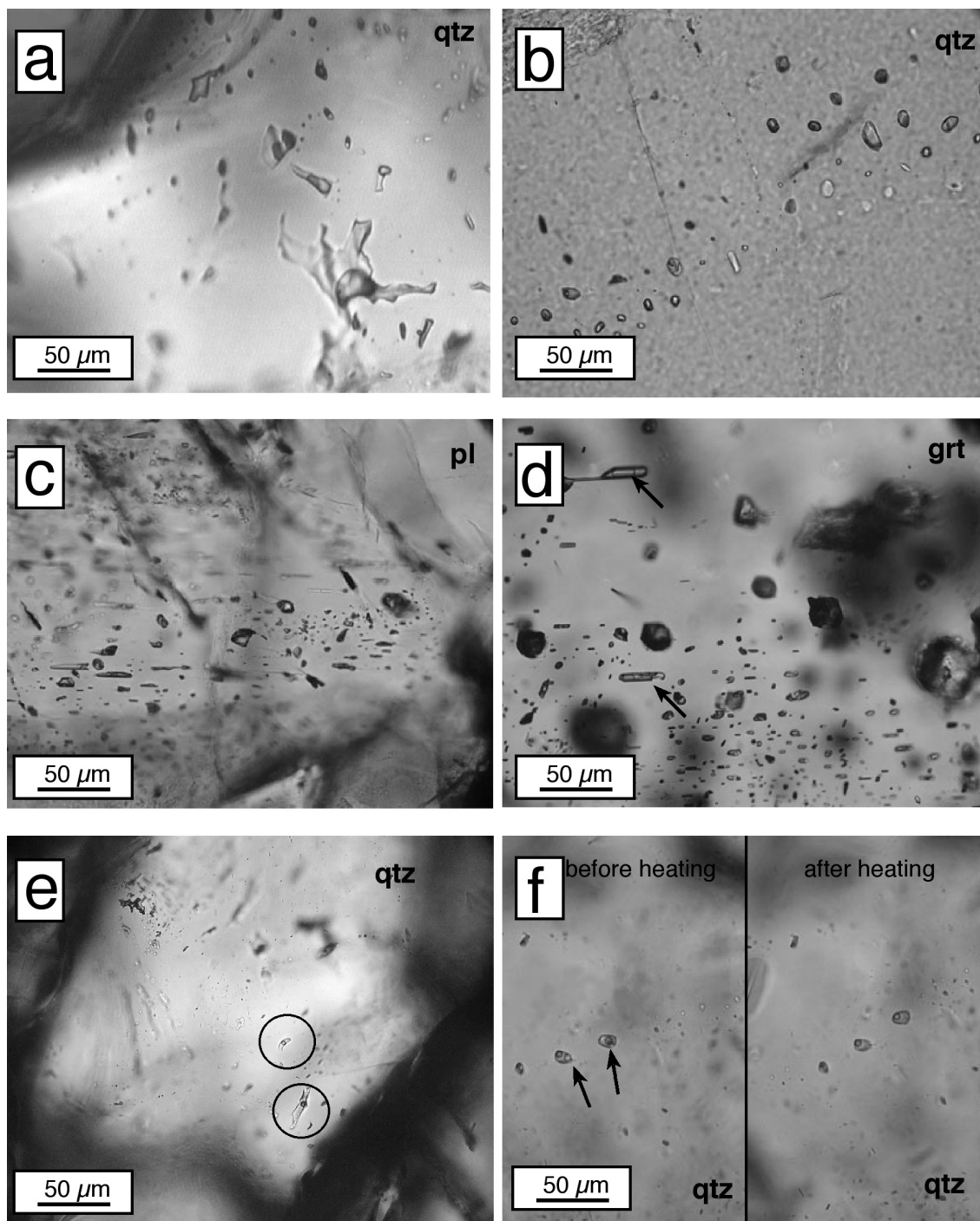
Fig. 6.6: Microphotographs of characteristic fluid inclusion types detected in quartz, plagioclase and/or garnet of "light" and "dark" rock types. (a) $CO_2\pm N_2$ inclusions with elongated and highly irregular shapes hosted by quartz; (b) Quartz-hosted $CO_2\pm N_2$ inclusions with roundish to negative crystal shape; (c) plagioclase hosted cluster of elongated $CO_2\pm N_2$ inclusions; (d) rare elongated $CO_2\pm N_2$ inclusions hosted by garnet; upper arrow points at a vapour bubble, lower arrow points at solid inclusions of carbonates and micas; (e) rare H_2O-salt inclusions hosted by quartz with irregular shape and small vapour bubble; (f) roundish H_2O-CO_2-salt inclusions with nahcolite daughter crystals (arrows at left) that dissolved during the heating cycle (right).
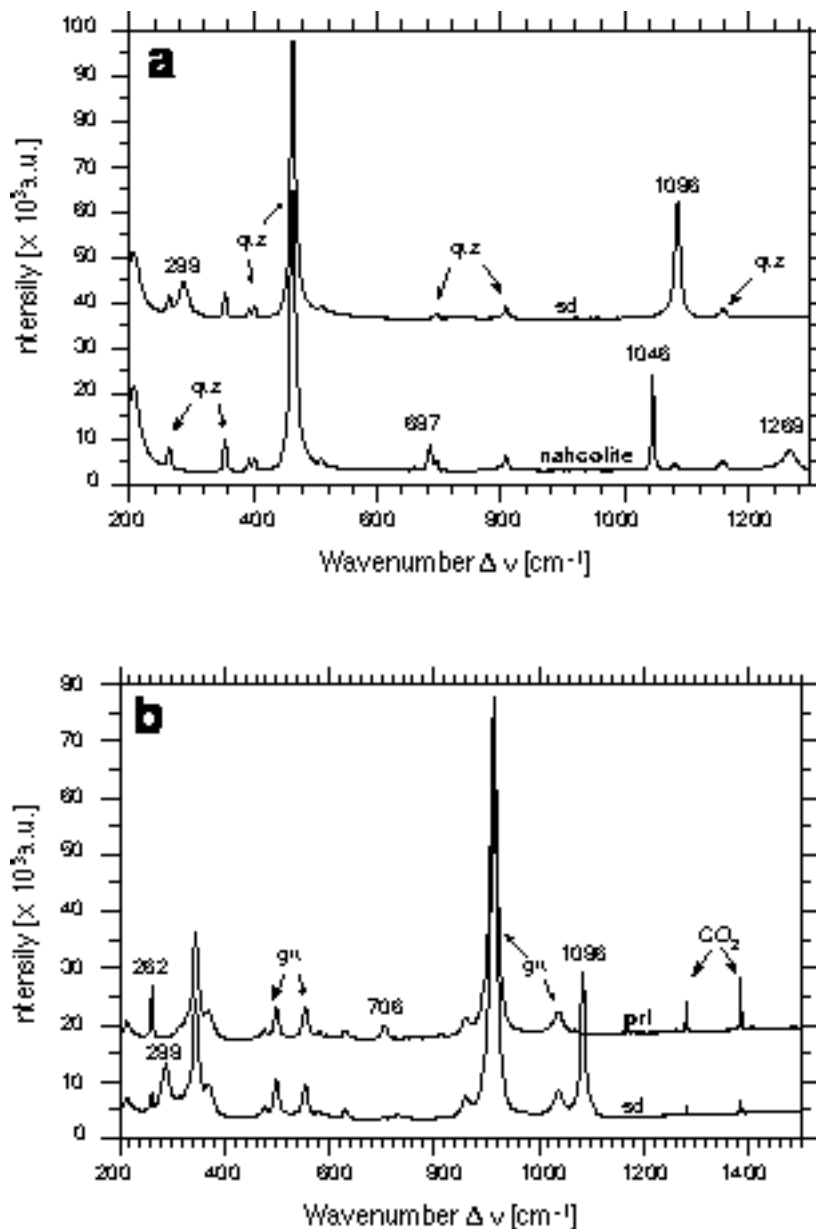
Fig. 6.7: *(a) Raman spectra of siderite and nahcolite microcrystals detected within $CO_2\pm N_2$ inclusions hosted by quartz, and (b) Raman spectra of siderite and pyrophyllite microcrystals detected in garnet-hosted $CO_2\pm N_2$ inclusions of "light" and "dark" rock types. Representative peaks of enclosed solids are labelled with the correlating wavenumber, and peaks of the hostminerals and prevailing fluid are marked with arrows .*

Garnet crystals rarely contain fluid inclusions large enough to be examined by microthermometry. The inclusions are elongated to roundish and arranged in intracrystalline planar arrays and trails (Fig. 6.6d). Single inclusions sometimes occur. The common size ranges from 3.0 to 15.0 μm, but may as well reach up to 40.0 μm. At room temperature, the inclusions are often darkish and the volume fraction of the vapour bubble in two-phase inclusions is c. 30 - 70 vol%. Melting of the solid CO_2-rich

phase occurs at -57.2 to -56.6 °C in inclusions found in light coloured gneisses and between -58.7 and -57. 2 °C in dark basement rocks. Homogenisation is always into the liquid phase at temperatures ranging from 24.8 to 26.9 °C and 8.8 to 22.4°C in light and dark rock types, respectively (Fig. 6.5b). The amount of nitrogen detected by Raman spectrometry does not exceed 7 mol% in inclusions found in the light rocks, whereas graphically estimated amounts in dark gneiss (sample no. 1562) reach as high as 21 mol%. Microcrystals enclosed in these inclusions (Fig. 6.6d) were identified as being either calcite, siderite, Ca/Mg-calcite, pyrophyllite or paragonite/muscovite in varying volume fractions and combinations (Fig. 6.7b).

H_2O-salt- bearing inclusions

Quartz is the only mineral that contains a low saline aqueous fluid. This type of fluid inclusions is rare, but more abundant in the light rock varieties. Inclusion shape is mostly irregular and elongated and rounded inclusions rarely occur (Fig. 6.6e). Inclusions are arranged on intracrystalline planes and trails, but single inclusions can be detected as well. Inclusion size ranges from 3.0 to 40.0 *μm* and 6.0 to 45.0 *μm* in light and dark rocks, respectively. At room temperature, the inclusions contain a liquid and a vapour phase, the latter occupying about 5 to 50 vol% of the total fill. After supercooling to -120°C, melting of the solid aqueous phase during reheating to room temperature occurs at minimum temperature of -3.5 °C in light rocks and -2.0 °C in dark samples (Fig. 6.8a, b). The melting temperatures correspond to a salinity of 5.71 and 3.34 wt% NaCl*eq*, respectively. Eutectic melting was only hardly visible in all inclusions under investigation, and thus appropriate data are scarce. In darkish rocks, eutectic melting was observed at -35.5 and -31.2 °C which hints at H_2O-NaCl-$MgCl_2$ as being the actual salt system. In light rock varieties, eutectic melting was observed at -29.3, -26.4, and -21.1 °C, of which the latter clearly indicates the presence of NaCl in solution.

Homogenisation usually occurred into the liquid phase, with Th ranging between 127.9 °C and 370.2 °C in light rocks and 140.0 to 363.0 °C in darkish samples (Fig. 6.8a, b). A few inclusions decrepitated before fluid homogenisation. Densities calculated from homogenisation temperatures vary between 0.51 and 0.96 gcm^{-3} (light rocks) and 0.52 and 0.94 gcm^{-3} (dark rocks), indicating a molar volume of 35.87 and 19.05 cm^{3}mol^{-1} and 34.59 and 19.27 cm^{3}mol^{-1}, respectively. Aqueous inclusions were inspected for traces of gaseous components like CO_2, N_2 or CH_4 with Raman spectrometry, but no indications of any of these gases were found. Small birefringent crystals enclosed in quartz hosted aqueous inclusions of the light rock types were identified as siderite.
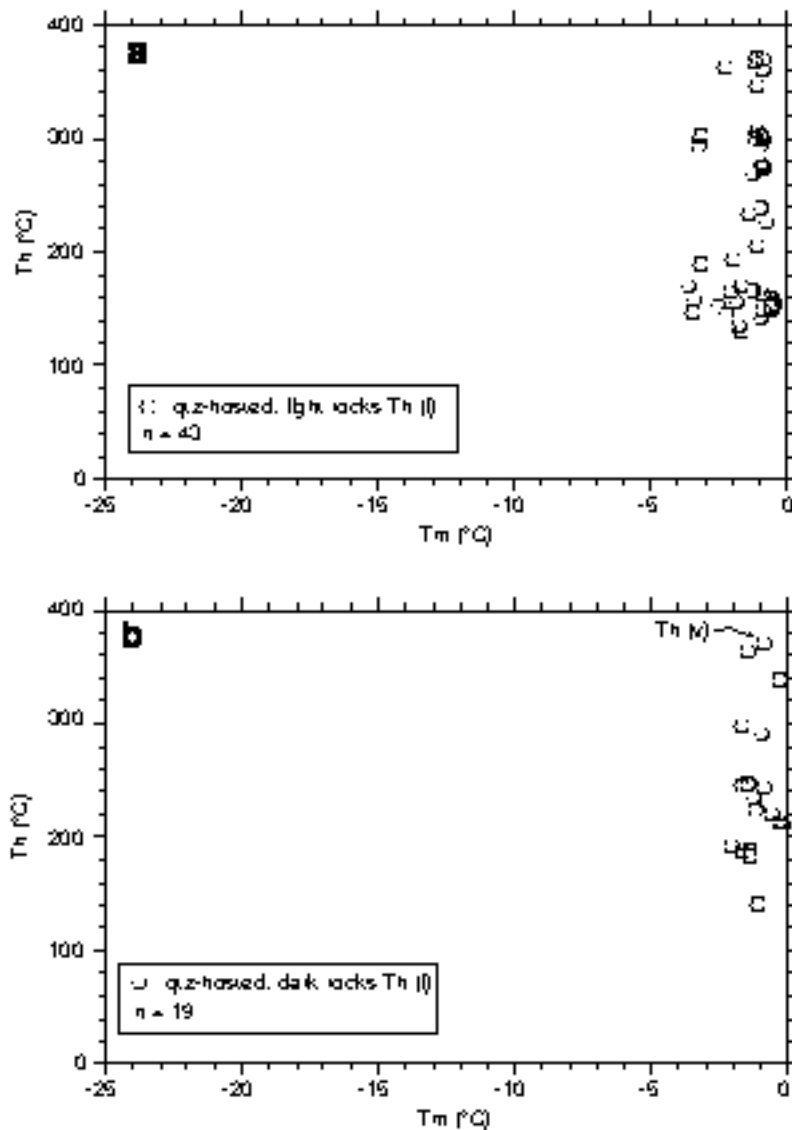
Fig. 6.8: *Homogenisation and final ice melting temperatures of quartz-hosted H_2O-salt inclusions from light and dark rock varieties.*

H_2O-$CO_2 \pm N_2$-salt bearing inclusions

Accept for one inclusion hosted by *garnet* (sample no. 1563), rare inclusions containing the complex H_2O-$CO_2 \pm N_2$-salt fluid mixture are hosted by *quartz* of both - dark and light - rock varieties. This type of irregular to roundish inclusions is arranged in intracrystalline clusters or trails in direct vicinity or at intersections of fluid assemblages containing H_2O-salt and $CO_2 \pm N_2$. Observed inclusion size ranges from 6.0 to 30.0 μm. The presence of a carbonic phase in this predominantly aqueous inclusions was either confirmed by direct observation of melting of a CO_2-rich phase at -58.3 to -56.6 °C, the observation of clathrate melting (Tm clath.) between 3.0 and 14.5 °C, or Raman spectrometric investigation. Additionally, Raman analysis yield N_2 contents of 3 to 15 mol%, and 3 to 14 mol% in some quartz-hosted inclusions of light and dark

rocks, respectively. Total homogenisation of the enclosed fluid phase was rarely observed at 147.7 to 382.0 °C, and decrepitation of these inclusions was common. The salinity of the aqueous phase was calculated from clathrate melting temperatures to vary between 0.87 and 6.74 wt% NaCl*eq*. Bulk fluid properties were calculated for those inclusions, where homogenisation of the carbonic phase occurred after final clathrate melting and densities range between 0.73 and 0.98 gcm^{-1} in light rocks and 0.52 and 0.98 gcm^{-3} in dark rocks. An additional characteristic feature of this inclusion type is the presence of birefringent microcrystals, which occur in uniform volume fraction and were identified as nahcolite by Raman spectrometry. These nahcolite crystals dissolved during heating until homogenisation temperature was reached (Fig. 6.6f), and are thus interpreted to be real daughter minerals.

6.1.4. Mineral chemistry of feldspars, pyroxenes and garnets of samples no. 1562, 1563, 2168, 2169, and 2181

The chemical compositions of individual feldspars, orthopyroxenes and garnets of some "light" and "dark" samples were calculated from Electron Microprobe analyses.

A selection of the results of feldspar analyses and endmember calculations from the basement rocks are illustrated in Fig. 6.9. The variation in the plagioclase and K-feldspar composition of all samples, and within single samples is small. It ranges between $An_{63}Ab_{36}Or_1$ and $An_{71}Ab_{28}Or_1$ for plagioclases, and between $An_{19.5}Ab_{0.5}Or_{80}$ and $An_8Ab_0Or_{92}$ for K-feldspars. Additionally, no significant differences in feldspar compositions of dark and light rock types can be detected (*cf.* samples no. 1562 and 1563, Fig. 6.9). The sometimes assumed iron incorporation into feldspars during the formation of charnockitic rocks, which is thought to be responsible for the greenish colouring, was not be approved.

The only data on pyroxene chemistry are available from sample no. 2169. The graphic representation of the orthopyroxene compositions in the Di-Hd-En-Fs quadrilateral shows a range of $En_{20}Fs_{72}Wo_2$ to $En_{28}Fs_{80}Wo_4$. Thus orthopyroxenes are labelled as ferrosilites according to the approved classification scheme of Morimoto (1998).
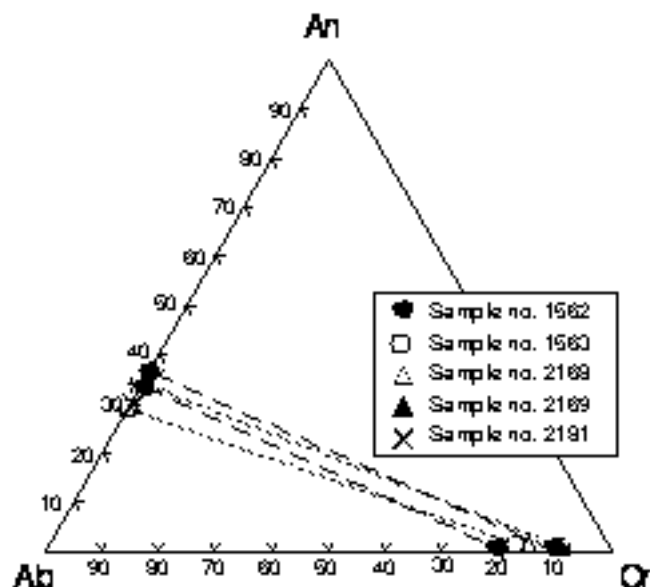
Fig. 6.9: *The maximum variation in plagioclase and K-feldspar composition (in mol%) is illustrated for samples no. 1562 and 1563. (filled and open circles). Only K-feldspar analyses exist of samples no. 2168 and 2169 (filled and open triangle), whereas for sample no. 2181 only plagioclase analyses are available (crosses).*
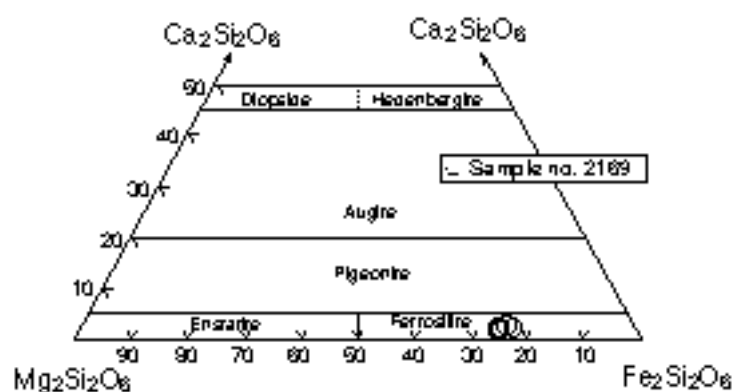
Fig. 6.10: *Orthopyroxene compositions (in mol%) of single crystals from sample no. 2169 ("dark" rock variety).*

Most garnets hosted by gneissic samples are relatively low in grossular component, and range between $Alm_{75}Grs_5Prp_{19}Sps_1$ and $Alm_{84}Grs_5Prp_{10}Sps_1$ in composition. Only garnets of sample 2168 reveal additional low values of pyrope component ($Alm_{86}Grs_5Prp_3Sps_6$) (Fig. 6.11a). The slight shift of Mg- and Fe-content that can be derived from the representation of the data in the Alm-Grs-Prp system (Fig. 6.11.a) reflects a compositional variation from rim to core within single garnet grains. Magnesium and iron behave antagonistically (Fig. 6.11c, d). A diffusional enrichment in almandine component, corresponding with a depletion in pyrope component occurs along the marginal contact of garnet with biotite. This behaviour is typical for

50

retrograde reequilibration processes. The detailed analyses ("XMaps") also exhibit a growth zonation of garnet with enrichment of the grossular component in the crystal core (Fig. 6.11b). The decrease of calcium from the core to the rim, connected with a nearly constant magnesium content (Fig. 6.11d) hints at a retrograde path influenced by isothermic decompression (Martignole & Nantel, 1982). An exhumation model related to this type of isothermic unloading can be explained with an uplift subsequent to magmatic underplating in continent/continent collision zones. A similar model has already been stated for the Shackleton Range (Olesch, 1991).
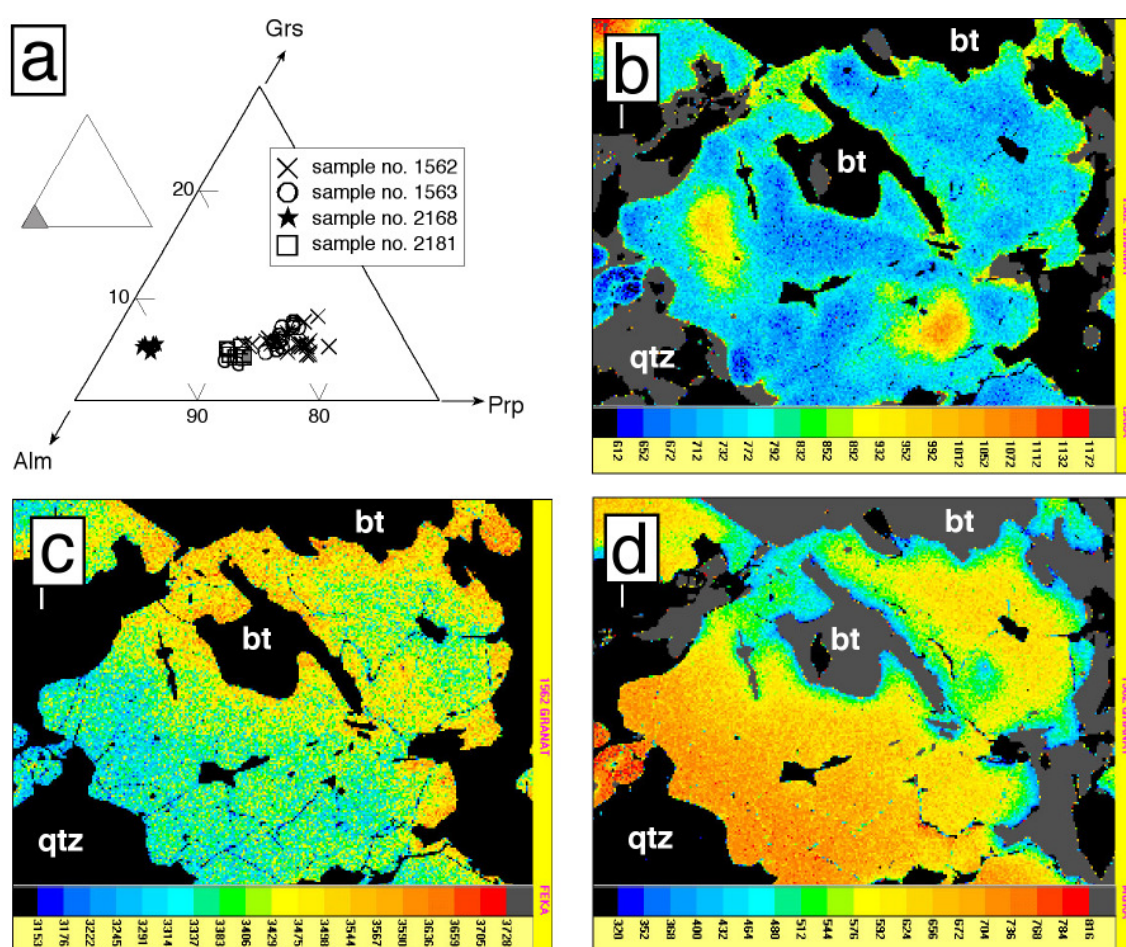
Fig. 6.11: *Composition of garnets hosted by grt-gneisses from central Petermannketten plottet in the Alm-Grs-Sps-triangle, and element distribution maps (Fe, Mg and Ca) of one garnet from sample no. 1562.*

51

6.2.   Syn- and postkinematic intrusions

6.2.1. Petrography (thinsections no. 1533, 1549, 2175)

Samples described in the following paragraph are representatives of syn- and postmetamorphic plutonic bodies that intruded into the basement lithologies (see chapter 5.2).

Macroscopically, the light-grey alkali-feldspar syenite and quartz-alkali-feldspar syenite (samples no. 2175 and 1549) are coarse grained, seriate to inequigranular with granitic-type texture. Euhedral K-feldspar phenocrysts may reach up to c. 20.0 mm in size. Major and minor mineral components are K-feldspar, plagioclase, quartz, biotite, and green hornblende. Accessory phases include muscovite, black and dark red opaque phases, apatite, zircon, rutile and titanite.

Microscopically, grain size of euhedral to subhedral *K-feldspar* ranges between c. 0.1 and 20.0 mm. Some crystals display perthitic unmixing, and microcline phenocrysts show twinning after Carlsbad twin law. Fractured crystals may be altered to sericite and calcite along fissures. K-feldspar is often invaded by myrmekite, and contains solid inclusions of quartz, biotite, hornblende, apatite, plagioclase and/or opaque phases.

Euhedral to anhedral *plagioclase* varies between c. 0.08 to 4.0 mm in size. Fine polysynthetic twinning after albite and pericline twin law is common and myrmekitic intergrowth with quartz occurs. Growth lines and pervasive sericitisation restricted to crystal cores indicate magmatic zoning. Additional sericitisation has developed along intracrystalline fractures.

Anhedral *quartz* varies from 0.1 to 6.0 mm in size and fills interstices between subhedral feldspars. It displays fissures, undulous extinction, subgrains and is vermicularly intergrown with, or included in, K-feldspar or biotite.

The common grain size of subhedral *biotite* crystals is c. 0.4 to 2.4 mm and pleochroitic colouring changes from yellowish to dark brown. Mineral phases overgrown by single biotite crystals are apatite, quartz, opaque phase and zircon, the latter being surrounded by black pleochroitic halos. Crystal margins show opacitisation and some grains are intergrown with either green hornblende or quartz.

Table 6.4: *Modal compositions (in vol%) of different younger plutonic rocks that intruded into the metamorphic basement lithologies described in chapter 5.2. x ≤ 2 vol%.*

sample no.	1533	1549	2175
rock type	mangerite (gneissic)	qtz-alkali-feldspar-syenite	alkali-feldspar-syenite
plagioclase	40	10	10
K-feldspar	50	60	70
quartz	6	20	7
biotite	x	5	5
muscovite		x	x
green hornblende	x	3	
orthopyroxene	3		
clinopyroxene	3		
opaque	x	x	x
apatite	x	x	x
zircon		x	x
chlorite	x		
rutile	x		x
titanite	x	x	x

Sample no. 1533 contains orthopyroxene and is therefore classified within the charnockite suite of rocks. Its texture is not unequivocal magmatic or metamorphic. This is characteristic of meta-igneous charnockitic rocks, as they typically form under high-pressures, and igneous textures are inevitably modified in some way.

The medium grained greenish sample macroscopically displays bimodal grain size distribution, and preferred orientation of large deformed feldspar and pyroxene crystals. K-feldspar, plagioclase and quartz were identified as main mineral compounds, whereas orthopyroxene and clinopyroxene are minor phases. The group of accessories comprises muscovite, opaque phase, apatite, rutile, titanite, zircon and chlorite.

Elongated subhedral *K-feldspar* grains show preferred orientation, and may be up to 10.0 mm in length. However, the most crystals range in size from c. 0.05 to 0.8 mm. They are often fractured and exhibit irregular grain boundaries, subgrains, and undulous extinction. Anhedral to subhedral *plagioclases* are in the range of 0.1 to 0.5 mm and thus more evenly grained. They display the same deformation features as the K-feldspars. Additionally, polysynthetic twinning and straight grain boundaries that sometimes form dihedral angles of 120° can be detected.

Anhedral *ortho-* and *clinopyroxene* crystals are aligned within the foliation, and vary in size from c. 0.05 to 0.5 mm (Fig. 6.6f). Orthopyroxene shows pleochroitc colours of light green and light red. The grains are fractured and mantled by green hornblende

and biotite. The latter also occurs as fracture-filling. Clinopyroxene reveals light green colours and very weak pleochroism. Fracturing and mantling by hornblende or biotite are less strongly developed.

Quartz nearly exclusively occurs as myrmekitic intergrowth with plagioclase in K-feldspar.

6.2.2. Fluid inclusion studies (thicksections no. 1533 & 2175)

The only type of fluid inclusions detected in the mangerite sample no. 1533 contains pure CO_2 and is hosted by *plagioclase*. The inclusions uniformly reveal negative crystal shapes and sizes ranging between 6.0 and 15.0 *µ*m. They are arranged on intracrystalline clusters and trails and the volume fraction of the vapour bubble present at room temperature is 40 to 50 vol%. Melting of the solid carbonic phase consistently appears at -56.6 °C and homogenisation into the liquid phase occurs between 16.9 and 26.6 °C (Fig. 6.12). Calculated densities lie in the range of 0.68 to 0.80 gcm^{-3}.

The majority of fluid inclusions observed in *quartzes* of the syenite intrusion (sample no. 2175) are arranged on intracrystalline planar arrays and trails, and are characterised by nearly perfect negative crystal shape with sizes that range between 3.0 and 60.0 *µ*m. A subordinate number of inclusions reveal similar arrangement but irregular and elongated forms. During microthermometry measurements, the only phase transitions observed were melting of a pure carbonic phase at c. -56.6 °C, and homogenisation of this fluid at temperatures between 16.3 and 28.4 °C (Fig. 6.12). In inclusions with negative crystal shape, homogenisation occurs into the liquid phase. Irregular inclusions generally display critical behaviour or homogenisation into the vapour phase. Investigation with Raman spectrometry has proved though, that the fluid also contains small amounts of H_2O, and minor amounts of N_2. Solid phases enclosed were identified as being accidentally trapped crystals of calcite, rutile and opaque phases. Densities calculated for this inclusions range between 0.21 to 0.81 gcm^{-3}. Bulk fluid properties of inclusions that had been proved to contain H_2O were calculated taking into account a maximum value of 15 vol% "hidden" H_2O (*cf.* Roedder, 1984). The resulting densities are in a similar range of 0.40 and 0.84 gcm^{-3}.

Feldspar crystals rarely contain single, dark fluid inclusions with highly irregular to negative crystal shapes. Melting temperatures of -56.6 °C indicate the presence of a pure carbonic phase, which was confirmed by Raman spectrometry. Homogenisation of these inclusions was at 27.9 and 28.5 °C into the liquid phase, which corresponds to calculated densities of 0.64 and 0.66 gcm^{-3} (68.42 and 66.92 cm^{3}mol^{-1}).
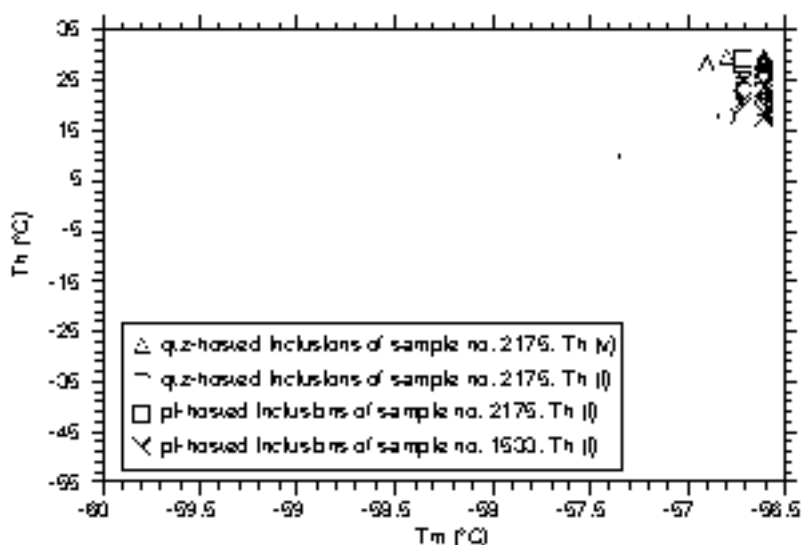

Fig. 6.12: *Homogenisation and melting temperatures of the carbonic phase of quartz and plagioclase hosted inclusions of the syenite and plagioclase-hosted inclusions of the mangerite samples.*

6.3. Summary and Discussion - metamorphic charnockitisation and successive leaching

The most dominant metamorphic features present in the basement lithologies of cDML today can most probably be traced back to the broader "Pan-African" event caused by the collision of East and West Gondwana (M2 & M3; *cf.* chapter 5). High-pressure granulite facies conditions (6.8±0.5 kbar, 830±20 °C) have been suggested for the first stage of Pan African metamorphism (Pan African I, M2), followed by a low-pressure granulitic event (Pan African II, M3; 4-5 kbar, 640±10 °C), and amphibolite facies retrogression (*cf.* chapter 5).

In progressive metamorphism the transition from amphibolite to garnulite facies is marked by a replacement of hydrous phases (*e.g.* biotite reacts to form orthopyroxene and K-feldspar plus water) and expulsion of the resulting aqueous phase. Dehydration processes and the presence of a fluid regime largely controlled by the absence of high water activities have been stated to be responsible for *in situ* charnockitisation (*cf.* chapter 2).

Massive and migmatitic gneisses of the metamorphic basement lithologies that crop

out in the central Petermannketten, cDML, show a patchy, non-pervasive greenish hue, sometimes associated with grain coarsening. The darkish lithologies are in turn crisscrossed by a fracture- and foliation controlled network of light coloured rocks (Fig. 5.3). The field hypothesis that the darkish colouring is linked to metamorphic charnockite formation, and that these charnockitic rocks were again subjected to leaching processes, has been verified by thorough petrographic studies.

The presence of orthopyroxene is crucial for a classification within the charnockite-anorthosite suite of rocks (*cf.* chapter 2), and the majority of "darkish" samples does indeed contain orthopyroxene (identified as being ferrosilite in sample 2169). Two of the samples displaying the conspicuous colour, and some of the light rock varieties contain a yellowish relictic phase that has also been found in conjunction with commencing orthopyroxene alteration (Fig. 6.1e,f; 6.3e). Hence it is concluded that the samples which at presence give evidence of the relictic phase did also contain orthopyroxene at some stage of their geological evolution. This implies that the formation of the charnockitic mineral assemblage in paragneiss was followed by processes that resulted in partial to complete orthopyroxene breakdown, locally accompanied by thorough leaching of the previously greenish rocks. In light-grey rocks that do not contain a relictic phase leaching processes may either have been more severe, or orthopyroxene did not form during granulitic metamorphism.

Retrograde destabilisation of the anhydrous phase assemblage is indicated by orthopyroxene alteration to form amphibole, biotite and garnet. The secondary biotite variation displays a distinct fringy appearance and vermicular intergrowth with quartz. Detailed microprobe analyses have revealed that single garnet crystals exhibit zonation characteristic of retrograde reequilibration processes, presumably connected to a phase of isothermal decompression (*cf.* chapter 3.2.1).

Besides the presence or absence of orthopyroxene, no further conspicuous difference in mineralogical composition of charnockitic and gneissic samples do occur. Furthermore, no valuable correlation can be drawn between the modal composition and the state of alteration in light and dark rocks (Table 6.2 & 6.3). Light samples reveal slightly stronger feldspar alteration to calcite and sericite than the darkish rocks, but the overall distribution of phases indicative for retrograde reaction (biotite, hornblende) can not be stated to be more abundant in the light rocks.

The observed retrograde mineral assemblage, locally restricted migmatitisation and the structurally controlled leaching, give clear evidence of the presence of an free aqueous phase during retrogression. For peak metamorphic conditions Colombo & Talarico (in press) on the base of mineral equilibria studies suggest that metamorphism was largely controlled by very low water activities.

Fluid inclusion studies have shown, that the majority of inclusions hosted by either quartz, plagioclase or garnet displayed phase transitions characteristic of a $CO_2 \pm N_2$ ("dry") fluid. The most $CO_2 \pm N_2$ inclusions suitable for microthermometry investigations were detected in quartz. All inclusions are arranged on intracrystalline trails or planes and thus textural evidence of early metamorphic (primary) origin is given. Carbonic inclusions from all host minerals predominantly exhibit roundish or negative crystal shapes indicating post-entrapment modification influenced by reequilibration processes. Some inclusions also contain microsolids identified as carbonates or sheet silicates. If detected in plagioclase-hosted inclusions, they most probably result from chemical interactions of the fluid with the surrounding mineral under consumption of the aqueous phase (*cf.* chapter 8). Nahcolite crystals in quartz, may either be an accidentally trapped phase or a real daughter phase of an H_2O-$CO_2 \pm N_2$-salt fluid, whose aqueous phase proportion has been lost during reequilibration (see below). The nitrogen content is generally in the range of 2 - 5 mol%. Taken all together, light rocks display a slight tendency towards lower N_2 contents, whereas darkish rocks show a larger variation of N_2 composition, especially in garnet and plagioclase hosted inclusions (Fig. 6.5a,b). All homogenisation temperatures plot in a narrow range between 7.5 and 30.7 °C. Homogenisation into the vapour phase only occurs in quartz hosted inclusions, and was less frequently observed in charnockitic samples (Fig. 6.13). Corresponding densities are homogeneous as well. In quartz-hosted inclusions (Th(l) or Th(v)) they lie between 0.17 to 0.84 gcm^{-3}. When hosted by plagioclase they are in a range from 0.47 to 0.83 gcm^{-3}, and densities of garnet-hosted inclusions vary from 0.44 to 0.75 gcm^{-3}.
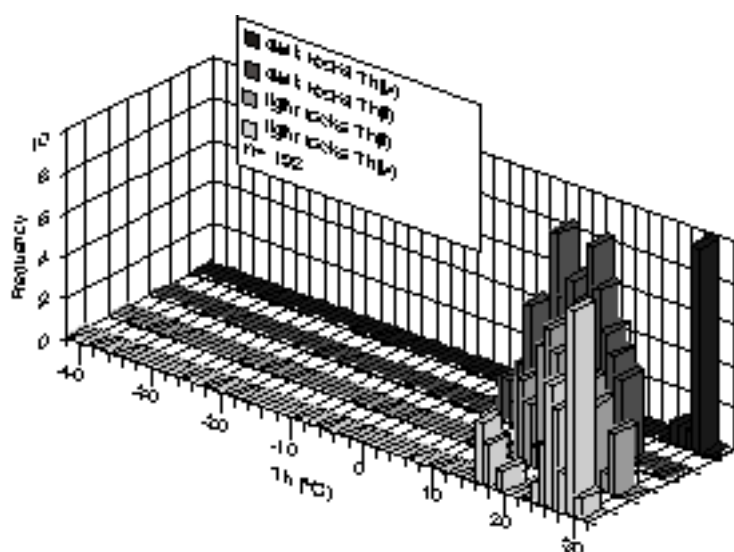
Fig. 6. 13: *All homogenisation temperatures measured in CO_2-N_2 inclusions hosted by quartz, garnet and plagioclase of light and darkish samples.*

A closer look at the available density values (and isochores, Fig. 6.16) reveals that high densities ($\geq$ 1 gcm^{-3}) as expected to result from granulite facies metamorphism have not been preserved during the retrograde stage. Even inclusions hosted by mechanically stable garnet do not reflect peak metamorphic conditions and the overall observation can be best explained with a modification of inclusions after their entrapment, resulting in fluid loss and/or volume change. A diagram depicting the relationship between inclusion size and homogenisation temperature (independent from the host mineral) reveals that no correlation exists between homogenisation temperatures and inclusion size. A positive correlation would in general indicate preferential decrepitation of larger inclusions due to internal overpressure and fluid loss. The even scatter of Th and inclusion size between 10 and 30°C and 5.0 to 20 μm (Fig 6.14.), though supports the earlier presumption that post-entrapment change was largely controlled by ductile deformation processes.

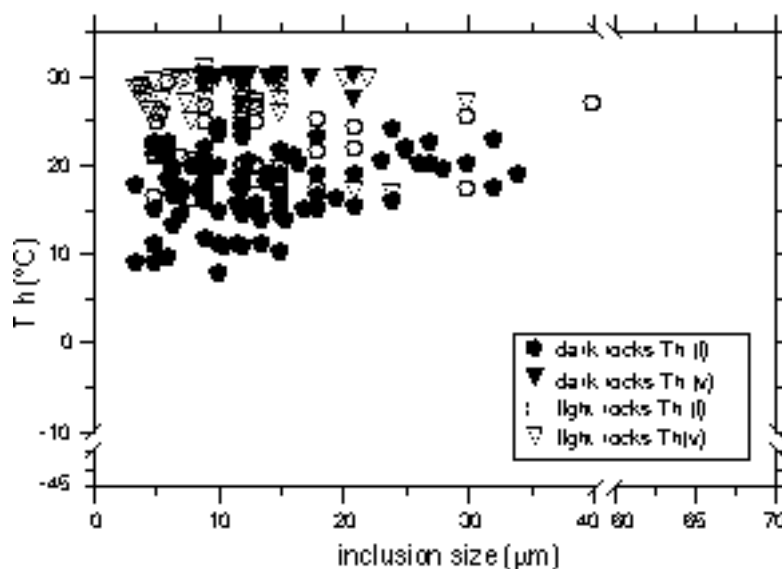**Fig. 6.14:** *Relationship between homogenisation temperatures and inclusion size of $CO_2 \pm N_2$ inclusions.*

Irregular to roundish H_2O-salt inclusions are only found in quartz and their textural arrangement on intracrystalline clusters and trails also implies early metamorphic (primary) formation. A comparison of aqueous inclusions detected in dark and light rock varieties shows that the inclusions do not differ with regard to their final ice melting temperatures, i.e. their salt content (max 5.71 wt% NaCleq), nor to their wide spread of Th. Density calculations exhibit the same similarity, as they vary between 0.54 and 0.96 gcm^{-3} in light rocks, and 0.52 and 0.94 gcm^{-3} in darkish samples. As in the CO_2-N_2 inclusions, a correlation of Th with inclusion sizes reveals a random distribution of depicted values (Fig. 6.15).
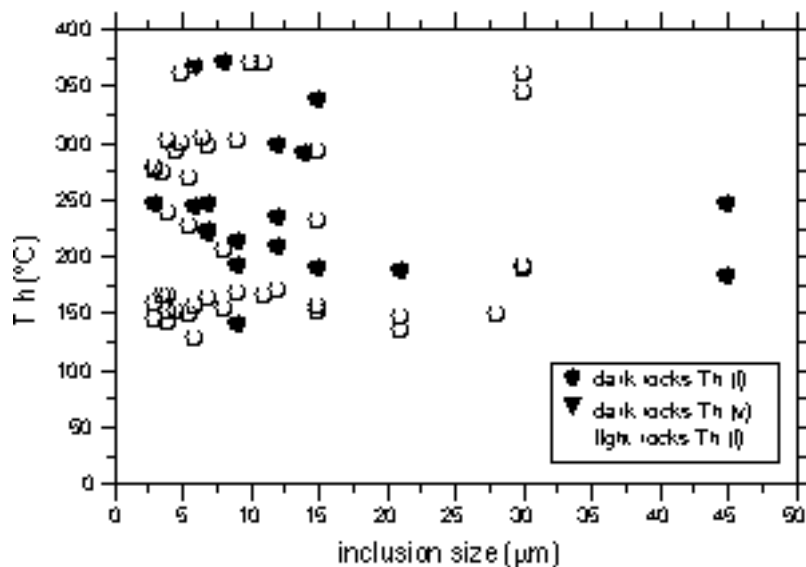
Fig. 6.16 *Correlation of inclusion size and homogenisation temperatures of quartz-hosted H_2O-salt inclusions from dark and light rock varieties.*

The origin and coexistence of aqueous and carbonic inclusions in granulite facies rocks has been described in earlier studies. For metasedimentary lithologies Touret (1995) states the prevalence of a prograde fluid of aqueous composition, which is essentially found as remnant of early brines with modified salinities and densities. At peak metamorphic granulite facies conditions, the influence of carbonic fluids becomes more important. Possible origins of the CO_2-dominated fluid regime include metamorphic reactions in carbonatic sediments, selective H_2O dissolution in silica melts, or the influx of magmatic CO_2 transported by deep-seated intrusions.

The third type of H_2O-CO_2±N_2-salt inclusions has rarely been detected in quartz of dark and light rocks, and only once hosted by garnet of a light coloured gneiss. Texturally they reveal the same primary (metamorphic) character as do the CO_2±N_2 and H_2O-salt inclusions. Their rare occurrence and close spatial relationship to inclusions of the aqueous and carbonic type implies, that they most probably formed by fluid mixing during mineral reequilibration/recrystallisation. Previously formed inclusions might e.g., be tapped and a homogeneous or heterogeneous fluid mixture may be resealed in a newly formed inclusion. That nahcolite formed as a real daughter phase (Fig. 6.6f) has important constraints on the nature of the aqueous phase present in these inclusions. Andersen *et al.* (1989) have suggested that nahcolite precipitates as real daughter mineral from a concentrated, highly alkaline aqueous inclusion with a high HCO_3^- content or an excess of CO_2. Even though the salinities of H_2O-salt inclusions and of H_2O-CO_2±N_2-salt inclusions do not exceed maximum values of 6.74 wt% NaCleq, these rare findings suggest that high alkaline brines have at least locally occurred. This again is in accordance with recent studies on granulitic metamorphism

that stress the importance of alkali-mobility and the role of highly saline fluid phases ("brines") during charnockitisation processes (*cf.* chapter 2).

None of the investigated samples shows any evidence of a late fluid phase responsible for the fracture and foliation controlled leaching. The presumably aqueous fluid seems to have been completely consumed during retrograde mineral reactions (*e.g.,* resulting in sericitisation of plagioclase). Thus no further conclusions on the nature of the leaching fluid can be drawn. The actual fluid content of post-tectonic syenite and mangerite intrusions, which possibly might have been accompanied by large scale fluid infiltration, does not allow detailed implications as well, although it has been proved that some of the generally CO_2-dominated inclusions do contain a maximum of 10 vol% H_2O.

The thorough influence of reequilibration processes that acted on the metamorphic fluid inclusions is also reflected by the position of isochores calculated from inclusion densities. Independent of fluid content, rock type (light or dark) or host mineral, none of the analysed inclusions reflects densities that could be correlated with the Pan-African event.
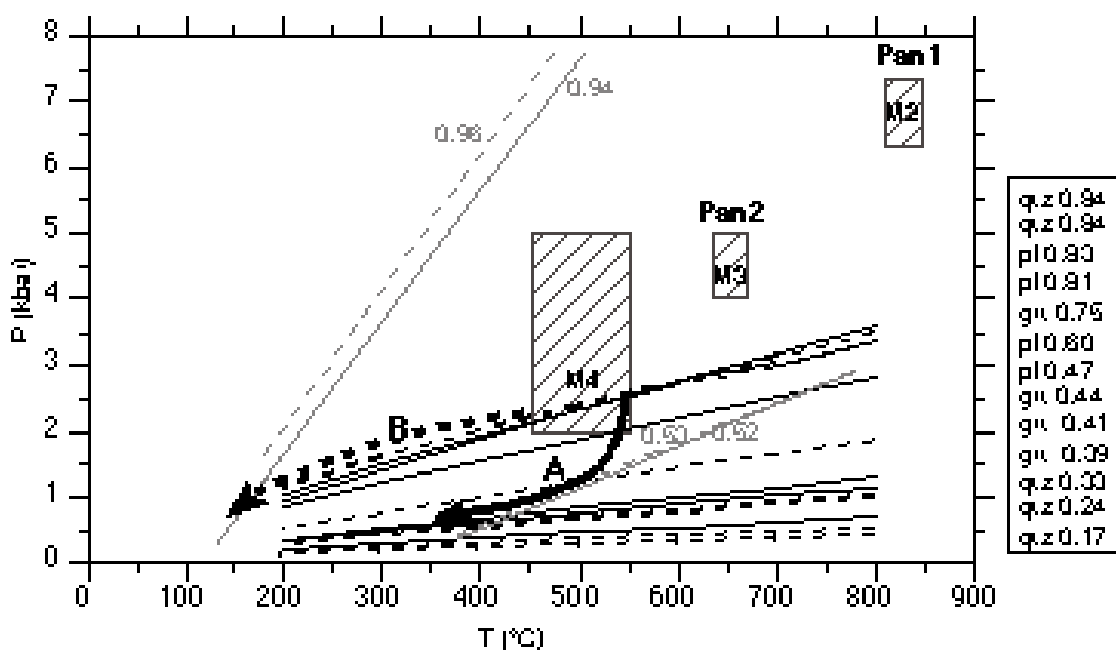
Fig. 6.16: *P-T diagram with isochores of minimum and maximum density values of H_2O-salt (grey lines with numbers indicating densities) and $CO_2 \pm N_2$ (black lines) inclusions. Solid lines depict inclusions hosted by dark rocks and dashed lines those measured in light rocks. The nature of the host mineral and densities in gcm^{-3} are indicated in the legend in the same order as the isochores. **M2**, **M3**, **M4** and grey boxes depict P-T constraints on Pan African I and II (**Pan1**, **Pan2**) metamorphism according to Markl & Piazolo (1998). Two possible P-T paths (**A**, **B**) resulting from correlation of fluid data with **M4** conditions are indicated. See text for explanation.*

All inclusions reequilibrated under retrograde conditions and highest density isochores intersect independently estimated M4 conditions at the low pressure range (c. 2.5 kbar, 550 °C). Maximum densities of aqueous inclusions hosted by quartz could be explained with volume loss under preservation of the original fluid content, which is generally interpreted to indicate a retrogression under isobaric cooling. A resulting P-T path (**B**, in Fig. 6.16) though would not be in good agreement with P-T conditions indicated by the isochores of carbonic inclusions. Minimum and average density isochores of aqueous inclusions, however, correlate with the gradual decrease in fluid densities of reequilibrated $CO_2\pm N_2$ inclusions. This indicates that retrogression of the metamorphic basement lithologies of the central Petermannketten most probably started with a phase of near isothermal uplift, followed by a stage of gradual cooling and decompression as depicted by path **A** in Fig. 6.16.

7. The Otto-von-Gruber-Gebirge - fluid content of a massif-type anorthosite complex

The rocks under investigation in this chapter were collected close to the former centre of the O.-v.-Gruber anorthosite body, where deformation features are less strongly developed than in its marginal parts. The hand specimen include five anorthosites (1581, 1583, 1587, 1588-1A, 2118), and two samples from mylonitic shear zones that have developed within the anorthosite body (1588, 1588-1B, 2119).

Table 7.1: Locations and rock types collected from the O.-v.-Gruber anorthosite complex. The attributes "dark" and "light" refer to macroscopic colouring as observed in the field.

sample no.	locality	rock type	colour	latitude S	longitude E	altitude [m]
1581	Zimmermannberg	anorthosite	dark	71°20.5'	13°23.8'	800
1583	Zimmermannberg	anorthosite	light	71°20.5'	13°23.8'	820
1587	SE Untersee	anorthosite with pegmatite (tonalitic)	light	71°21.2'	13°25.6'	700
1588	SE Untersee	mylonitic shear zone (norite)	dark	71°21.2'	13°25.6'	700
1588-1A/B	SE Untersee	anorthosite with shear plane (tonalitic)	light	71°21.2'	13°25.6'	700
2118	Zimmermannberg	anorthosite	light	71°21.7'	13°17.5'	1580
2119	Zimmermannberg	mylonitic shear zone (norite)	dark	71°21.7'	13°17.5'	1580

7.1. Massif-type anorthosite samples

7.1.1. Petrography (thinsections no. 1581, 1583, 1587A, 1587B, 1588-1A, 2118)

Macroscopically, the light-grey anorthosite rocks are fine to coarse-grained equigranular or bimodal inequigranular with nondirectional fabric and plagioclase megacrysts up to 2.0 cm in size (Fig. 7.1).


Fig. 7.1: Photograph of light-grey anorthosite as observed in the field.

The major constituent of all samples is plagioclase (c. 90 vol%). Minor components in varying amounts are clinopyroxene and alkali-feldspar (often microcline). Quartz, biotite, green hornblende, orthopyroxene, chlorite, black and brown to dark red opaque phases, muscovite/paragonite, zoisite, calcite, apatite, and zircon were identified as accessory phases (Table 7.2).

Table 7.2: *Modal compositions (in vol%) of samples taken from the O.-v.-Gruber anorthosite body $x \leq 2$ vol%. (1587A: pegmatite vein in anorthosite, 1587B: anorthosite, 1588-1A: anorthosite around shear plane).*

sample no.	1581	1583	1587A	1587B	1588-1A	2118
rock type	anorthosite	anorthosite	tonalitic pegmatite	anorthosite	anorthosite	anorthosite
plagioclase	90	90	60	90	90	90
alkali-feldspar	5	3	x	4	3	4
quartz	3	x	37	x	x	x
biotite	x	x	x	x	x	x
muscovite/paragonite	x	x		x	x	x
garnet						
green hornblende		x		x	x	x
orthopyroxene		x		x	x	
clinopyroxene		x		x	3	x
opaque phase	x	x			x	x
apatite		x				x
zircon	x	x		x		x
chlorite	x	x		x	x	x
zoisite		x		x		
calcite	x	x	x	x	x	x
titanite		x				
rutile						

Microscopically, some large (0.8 - 1.5 mm) subhedral to anhedral grains of *plagioclase* are slightly flattened and show lattice-preferred orientation, but the general microfabric is nondirectional. Plagioclase crystals may reveal antiperthitic unmixing, vermicular intergrowth with quartz and/or moderate alteration to sericite, chlorite, and calcite. Twinning after albite- and pericline twin law is common (see Fig. 8.3). Undulous extinction, bent deformation lamellae and subgrain formation give evidence of intracrystalline deformation and recovery. Occasionally, bulging of grain boundaries in addition to subgrain rotation led to the formation of aggregates of small (c. 0.2 - 0.5 mm), dynamically recrystallised plagioclase grains alongside the grain boundaries of larger feldspar crystals (Fig. 7.2e and 8.3b), thus forming "core-and-mantle" structures (as described by Passchier & Trouw, 1996).
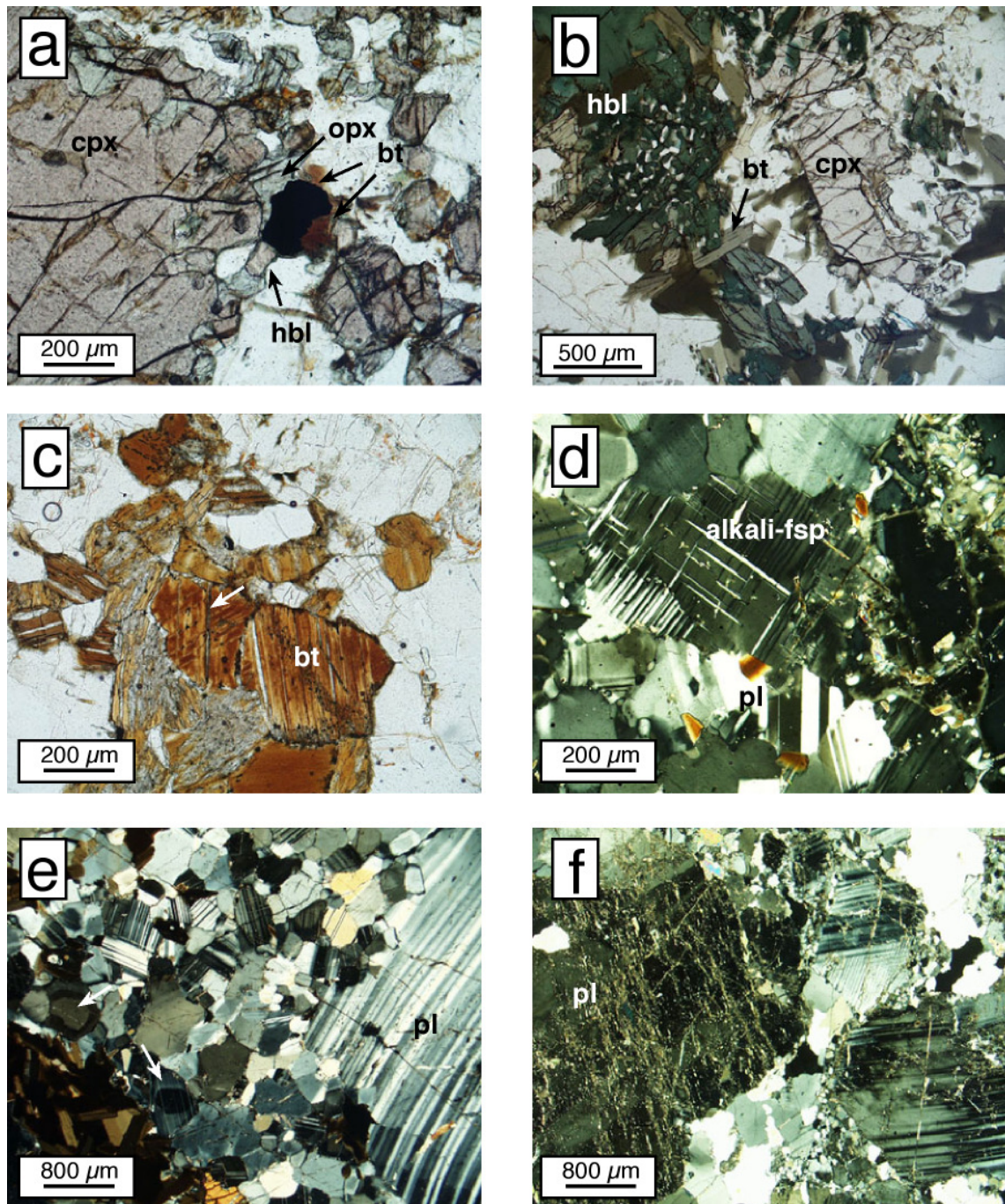
Fig. 7.2: *(a) Clinopyroxene of thinsection no. 1588-1 A, showing only weak alteration to biotite and green hornblende; (b) Vermicular relation of secondary green hornblende and quartz adjacent to clinopyroxene and biotite, sample no. 1587; (c) Pseudomorphosis of biotite (with slight opacitication) after hornblende. Amphibole mineral cleavage planes are still preserved (white arrow, thinsection no. 1583); (d) Crosshatched and discontinuous microcline-type twinning of alkali-feldspar thinsection no. 1587; (e) polygonal fabric of twinned and zoned (arrows) recrystallised plagioclases around large old grains with bent deformation lamellae thinsection no. 1587; (f) Microfabric of pegmatite vein of sample 1587 with strong sericitisation of large plagioclase crystals.*

64

Within the fine to medium grained areas, a polygonal fabric with straight or smoothly curved grain boundaries has developed, and plagioclases exhibit zonation (Fig. 7.2e). Rare intercrystalline microfractures are either open or filled with white micas and/or calcite. *Alkali-feldspar* crystals show similar deformation and alteration features and can be distinguished from plagioclase by the characteristic diffuse and discontinuous crosshatched twinning after albite- and pericline twin law (Fig. 7.2d), or rare perthitic unmixing.

Anhedral *clinopyroxene* grains, 0.1 - 4.0 mm in size, display pleochroitic colours of light green and light red. Small pyroxene crystals occur as inclusions in plagioclase. In different samples, the clinopyroxenes reveal varying states of alteration. Almost unmodified grains show weak alteration to biotite and green hornblende along mineral cleavage planes, intracrystalline microfractures or grain boundaries (Fig. 7.2a). The progression of this alteration results in the formation of subhedral to anhedral biotite (0.2 - 2.0 mm) with pleochroitic colours of dark and light green, and large (0.2 to 3.0 mm) euhedral to anhedral hornblende crystals that show vermicular intergrowth with quartz (Fig. 7.2b). The complete decomposition of amphibole leads to the formation of biotite, hematite and Fe-bearing hydrous phases, calcite, and white mica. Pseudomorphic replacement of amphibole by biotite with weak pleochroism is also observed (Fig. 7.2c). In some samples, the presence of such Fe-bearing red to orange coloured phases together with biotite and calcitic aggregates is the only indicator of a former presence of pyroxene. *Orthopyroxene* is less abundant and smaller in size (c. 0.1 to 0.5 mm. It shows pleochroitic colours of pale green and yellowish and is distinguished from clinopyroxene by its low birefringence and straight extinction.

The white and coarse grained pegmatite vein crosscutting sample 1587 is mostly comprised out of anhedral plagioclase (0.1 - 10.0 mm) and quartz (0.04 - 4.0 mm), with accessory alkali-feldspar (microcline), biotite, muscovite/paragonite, and calcite. White mica and calcite have formed as secondary alteration products within plagioclase and crystallised along intergranular microfractures. Sericitisation of plagioclase crystals of the pegmatite vein is slightly stronger than of those belonging to the adjacent anorthosite (Fig. 7.2f). Large quartz grains show undulous extinction and subgrain formation. Subgrain rotation leads to the development of small recrystallised strain-free grains with straight or smoothly curved grain boundaries. The bimodal grain size distribution forms the picture of "core-and-mantle" structures. Biotites with pleochroitic colours of dark and light brown are almost exclusively aligned along the contact zone between anorthosite and pegmatite vein.
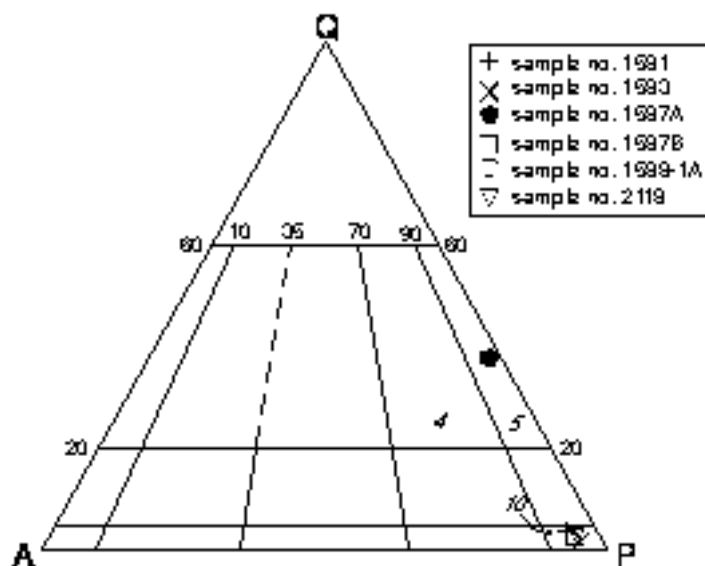
Fig. 7.3: *Classification of the samples taken from the O.-v.-Gruber anorthosite complex, according to Le Maitre (1989). Modal compositions of quartz, plagioclase and alkali-feldspar are given in Table 5.2. The pegmatite vein has tonalitc composition. All other rocks are anorthosites. If the estimated mode % of quartz was ≤ 2 vol%, the maximum value of 2 vol% was used for the recalculation to total 100%. Numbers in italics indicate the QAPF field number after Le Maitre (1989).*

7.1.2. Fluid inclusion studies (thicksections no. 1583, 1587A, 1587B, 1588-1A, 1588-1B, 2118)

Only one type of fluid inclusions was identified within all anorthosite samples. They are hosted by plagioclase and range in size between c. 5.0 and 12.0 μm (longest dimension) (Fig. 7.4a, c). Sizes down to 2.5 μm and up to 65.0 μm were also observed. Inclusion shapes vary from roundish or oval to negative-crystal shape (Fig. 7.4a and 8.4a) Fluid inclusions lie on intracrystalline planar arrays (Fig. 7.4a) and trails (Fig. 8.4d), thus giving evidence of pseudosecondary origin, as they do not crosscut grain boundaries. In some crystals, alignment of fluid inclusions along single twin lamellae was observed (Fig. 8.4c). Rarely, the accumulated appearance of fluid inclusions at the centre of large feldspar crystals, best visible in sections perpendicular to the c-axes, give evidence of relictic magmatic growth zonation in plagioclase. Inclusions, are darkish and either contain a single liquid-like phase or a liquid and a vapour phase at room temperature. A common feature observed in these inclusions is the occurrence of varying amounts and ratios of different birefringent microcrystals as enclosed solids (Fig. 8.4a and 8.4b).

During microtherometry measurements, initially homogeneous inclusions nucleate a gas bubble at c. 0.0 °C, before supercooling leads to the formation of a solid phase around –90.0 °C in all inclusions. During the heating cycle, melting of the solid phase

occurs within a narrow temperature range of –58.0 to –56.6 °C (Fig. 7.5b). Thus, the inclusions are interpreted as containing a nearly pure carbonic fluid, together with small amounts of different gaseous species.

The majority of fluid inclusions homogenise between 14.0 to 24.0 °C (Fig. 7.5a), but taken together, homogenisation occurs over a wide temperature range between –1.8 to 30.6 °C (Fig. 7.5a). In general, homogenisation is into the liquid phase. Only plagioclase hosted inclusions of the anorthosite sample that contains a pegmatite vein (1587B), homogenise into the vapour phase. A systematic relationship between Th and Tm is not present (Fig. 7.6).
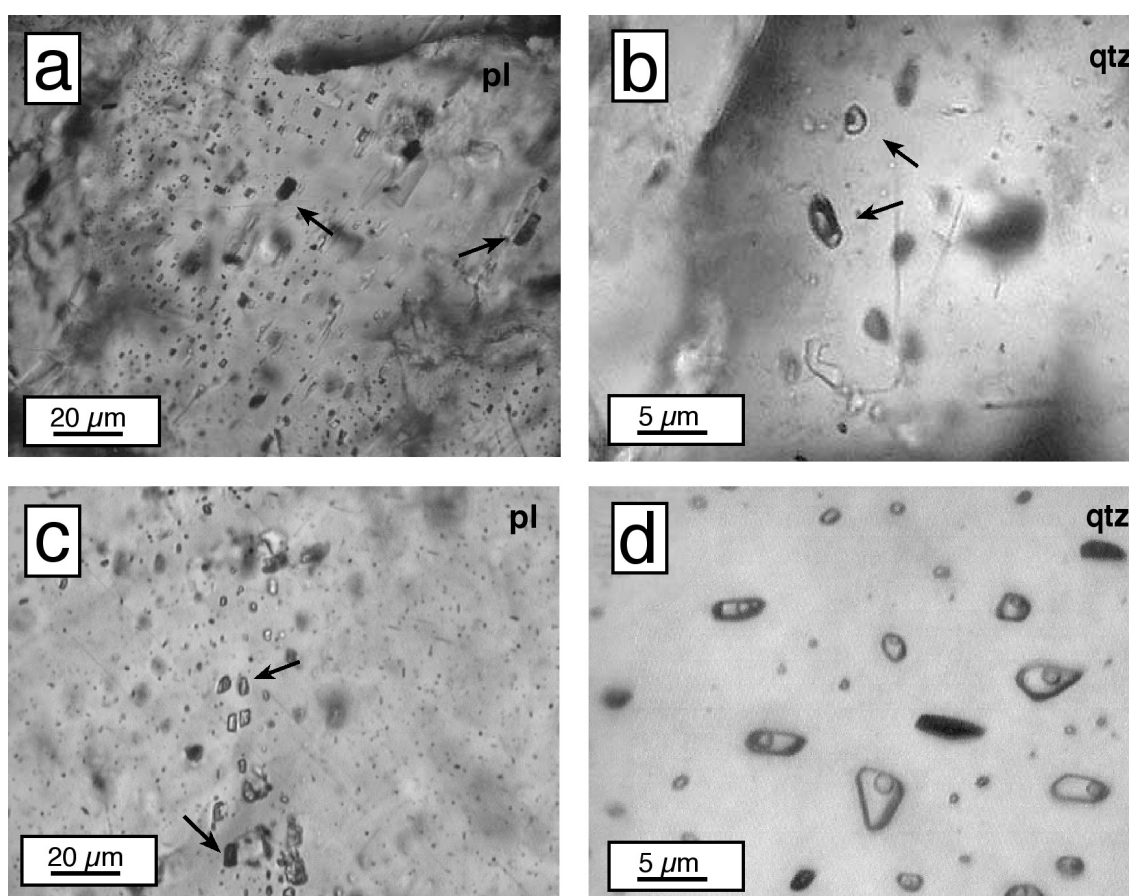
Fig. 7.4: *Intracrystalline plane (a) and trail (c) of darkish $CO_2\pm N_2$ inclusions with rectangular to negative crystal shapes hosted by plagioclase of sample no. 1588-1. Large inclusions are marked with arrows. (b) Cluster of roundish CO_2-$H_2O\pm N_2$ fluid inclusions with varying degree of fill rarely hosted by intersticial quartz of sample no. 1588. (d) Cluster of roundish quartz-hosted inclusions of pegmatitic vein (thicksection no. 1587A) with consistent degree of fill.*
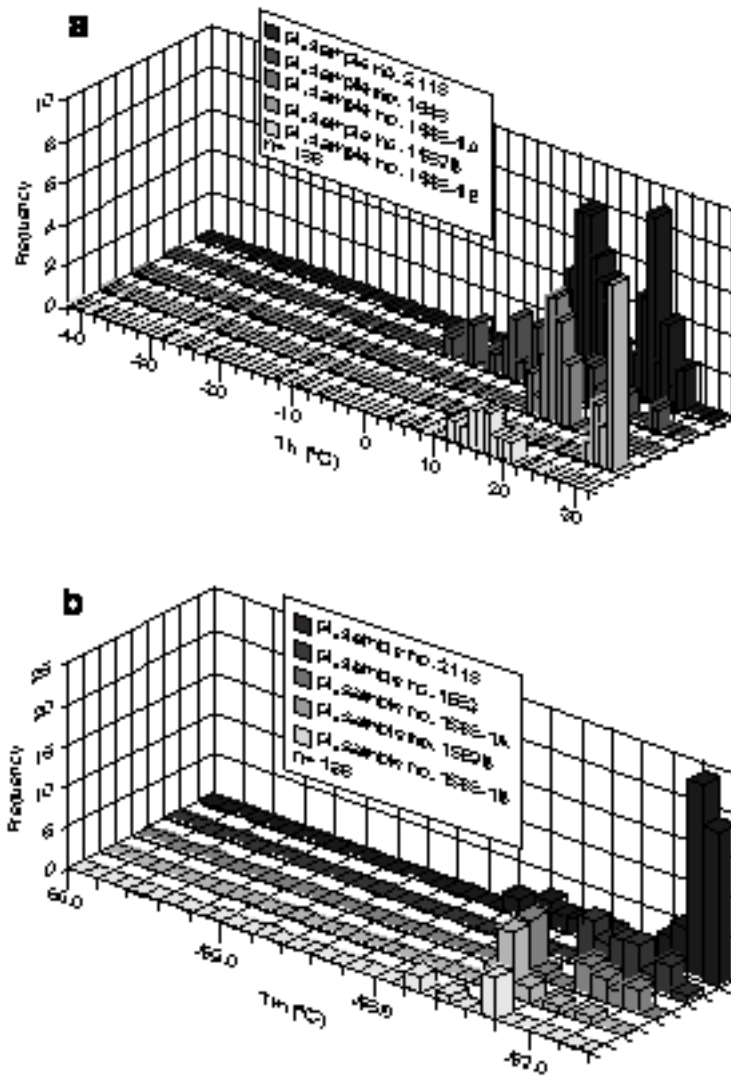
Fig. 7.5: *Histograms of homogenisation (a) and melting (b) temperatures from samples of the massif-type O.-v.-Gruber anorthosite complex. Included into this diagram are of fluid inclusions detected within the anorthositic part of thicksection no. 1588-1 B. Inclusions from thicksection 1587B (anorthosite adjacent to pegmatite) homogenise into the vapour phase.*
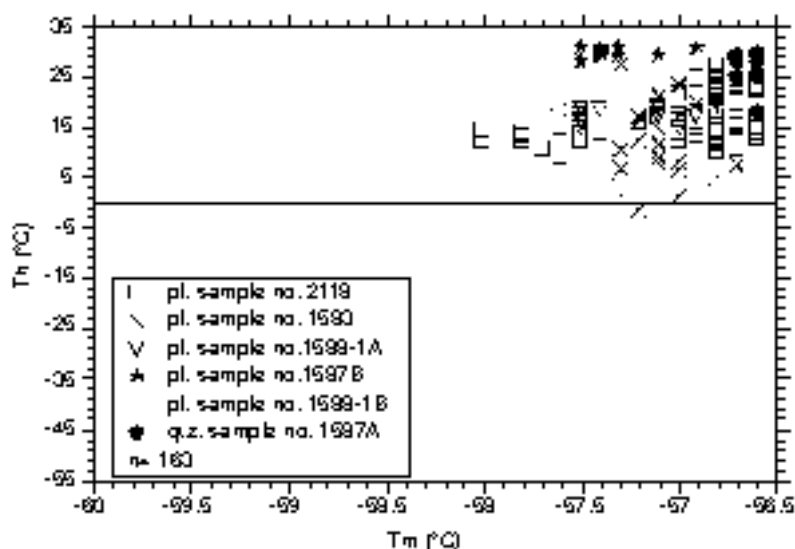
Fig. 7.6: Relationship between homogenisation and melting temperatures of fluid inclusions hosted by plagioclases of the anorthosite samples. Additionally, microthermometrical data of quartz-hosted fluid inclusions of the pegmatite (thicksection 1587A) are shown for comparison.

Raman microspectrometry confirmed CO_2 as being the major gaseous component within this type of fluid inclusions, and yield a maximum of 4.0 mol% N_2 as additional gas component (Fig. 7.6a). Graphical estimations result in much higher nitrogen amounts of 17 mol%. CH_4 and H_2O were never detected. Densities calculated according to the procedure described in chapter 4.6 range between 0.61 and 0.94 gcm^{-3} for inclusions that homogenise into the liquid phase, and 0.28 and 0.37 gcm^{-3} for those that homogenise to the vapour phase.

Due to their high refractive index compared to the surrounding plagioclase, carbonate microcrystals entrapped in fluid inclusions can facilely be identified by optical microscopy (Fig. 8.4b). With Raman spectrometry, a slight variation in carbonate compositions was detected between Mg-rich calcite (284, 714 and 1087 cm^{-1}) and pure calcite (283, 711 and 1085 cm^{-1}), even within single fluid inclusions (Fig. 7.6b).

Raman spectrometry also gave proof of the presence of sheet silicates that are often located at the inclusion walls or at carbonate crystal faces and therefore may easily be overlooked by optical microscopy in small or dark fluid inclusions. Muscovite/paragonite and pyrophyllite were identified within fluid inclusions where they appear as individual crystals or intergrown aggregates. An exact differentiation between muscovite and paragonite is not possible with this method, though. It is supposed that paragonite makes up most of the enclosed mica, as potassium is only a minor component of the plagioclase host (see Fig. 8.2).
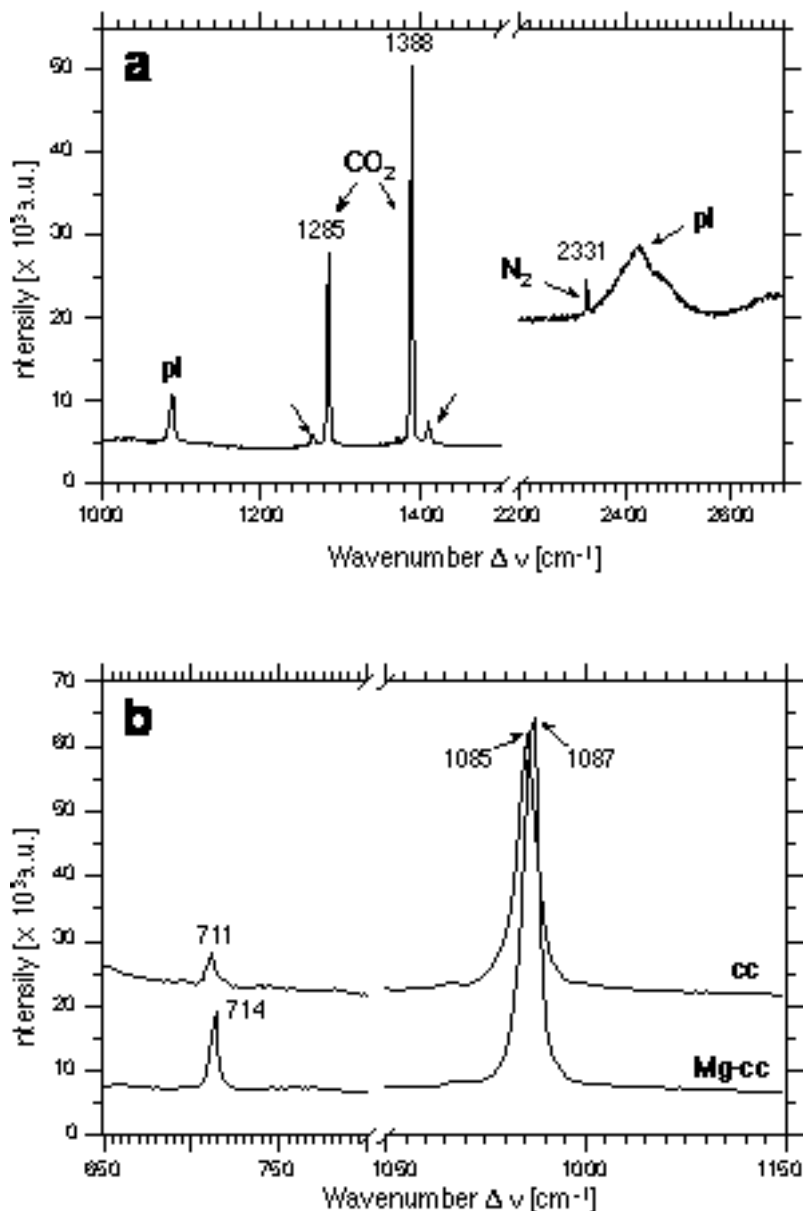
Fig. 7.7: *(a) Significant Raman peaks used for the differentiation of calcite and Mg-calcite found as enclosed solids in fluid inclusions hosted by plagioclase of sample 1588; (b) Typical Raman spectra of CO_2 and N_2, the fluid species most commonly detected in plagioclase hosted inclusions. The small arrows to the left and to the right of the main CO_2 peaks indicate the two characteristic "hot bands" of CO_2 at c. 1265 cm^{-1} and 1410 cm^{-1}.*

Some of the anorthosite samples also reveal rare single inclusions hosted by accessory xenomorphic quartz. These inclusions are approximately 3–10 μm in size, and show rounded to nearly perfect negative crystal shapes. In general they comprise an aqueous liquid and a carbonic vapour phase, the latter occupying from 30 vol% up to an apparent total fill (Fig. 7.4b; 8.4e). Decrepitation clusters are evident around some inclusions that only contain a carbonic vapour phase (Fig. 8.4f).

The only quartz-hosted fluid inclusions that yielded a complete microthermometrical dataset reveals a CO_2-melting point of –57.7 °C and clathrate

melting was observed around 7.9 °C in the presence of two CO_2-rich phases. Homogenisation of CO_2 occurred at 18.7 °C into the liquid phase. Salinity obtained from the clathrate melting temperature is equivalent to 4.2 wt% NaCl, and the bulk fluid density was calculated to 0.88 gcm^{-3}. Analysis with Raman spectrometry gave proof of the presence of CO_2 and small (≤ 2 mol%) amounts of N_2. The presence of H_2O was even confirmed in those inclusions that did not reveal a visible aqueous rim. Entrapped minerals were not detected within these inclusions.

Due to the strong alteration, no fluid inclusions are preserved in plagioclase crystals of the pegmatite vein of sample 1587 (thinsection 1587A). Quartz crystals contain fluid inclusions that vary between 3.5 and 14.5 μm in size and show irregular to roundish or negative crystal shapes (Fig. 7.4d). They are arranged in intracrystalline clusters, and usually only a single carbonic phase is visible at room temperature. Melting of a solid phase after supercooling down to -120 °C uniformly occurs at -56.6 or -56.7 °C, which hints at the presence of a pure carbonic phase (Fig. 7.6). Raman spectrometrical data verified this interpretation, as no additional gaseous species could be detected by this method. Homogenisation into the liquid phase consistently occurs between 17.7 and 29.1 °C with emphasis on 25.0 to 29.1 °C (Fig. 7.6). Calculated densities range between 0.63 and 0.80 gcm^{-3}.

7.2. Shear zones within the O.-v.-Gruber anorthosite complex

7.2.1. Petrography (thinsections no. 1588, 1588-1B, 2119)

In the field and in hand specimen, shear zones are characterised by brownish colouring, a distinct foliation, secondary garnet growth, and lattice-preferred orientation of the main mineral constituents (Fig. 7.9a, b).

Plagioclase is the dominant mineral phase (c. 60 vol%), but in contrast to the surrounding anorthosite, these samples contain garnet, orthopyroxene and clinopyroxene, alkali-feldspar (often microcline), and quartz as minor components. Green hornblende, biotite, chlorite, black (magnetite) and brown to dark red opaque phases, muscovite/paragonite, calcite, chlorite, apatite, zircon, titanite and tourmaline were identified as accessory phases. The shear plane of sample 1588-1 (thinsection 1588-1B) is only one centimetre in width, and modal fractions of the mafic minerals are increased compared to the shear zones, with the effect that plagioclase is only a subordinate phase next to garnet, but biotite occurs as a minor phase (Table 7.3).

Fig. 7.8: *Garnet bearing shear zone that has formed within the massif-type O.-v.-Gruber anorthosite complex showing typical brownish surface colour.*

Grain size distribution of the subhedral to anhedral *plagioclase* crystals is bimodal inequigranular (0.1 - 10 mm) to equigranular (0.05 - 0.4 mm). Typical intracrystalline deformation features include deformation twinning after albite- and pericline twin law, bent deformation lamellae, and undulous extinction. Subgrain formation and subgrain rotation, grain size coarsening and bulging of grain boundaries give evidence of dynamic recrystallisation and recovery. Areas with recrystallised plagioclase grains show a polygonal fabric with straight grain boundaries. Antiperthitic unmixing is often observed in larger (3.0 - 6.0 mm) plagioclase grains, as is myrmekite growth along the boundaries of K-feldspar porphyroclasts (Fig. 7.9d). Alteration to sericite does occur. *Alkali-feldspar* crystals display perthitic unmixing, fine deformation lamellae, undulous extinction, and diffuse and discontinuous crosshatched twinning after albite- and pericline law.

Quartz is inequigranular (0.04 - 3.5 mm) and preferably occurs close to domains dominated by garnet, pyroxene and opaque phases. Opaque minerals and tourmaline crystals are sometimes found as inclusions in quartz. Anhedral quartz grains may be disc-shaped and disc-quartz shows undulous extinction and subgrain formation (Fig. 7.9c). Subgrain rotation recrystallization has led to the development of high angle grain boundaries, and the formation of new grains. In sample 1588, grain sizes of anhedral to subhedral quartz varies between 0.05 to 0.4 mm.
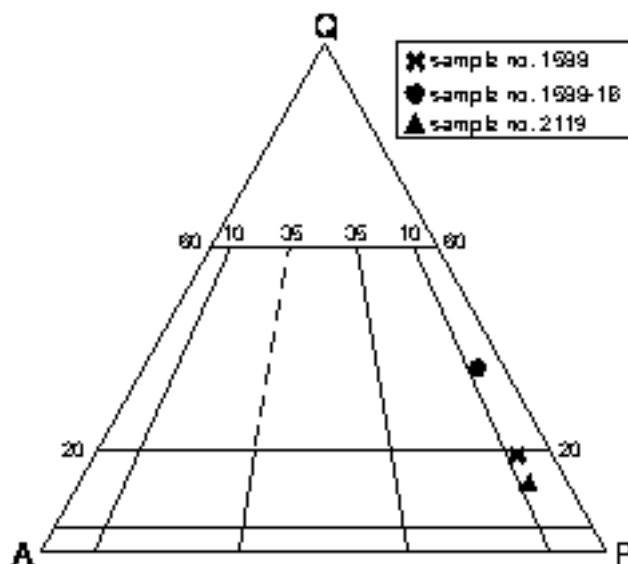
The size of subhedral *garnet* porphyroblasts ranges from 0.1 to 4.0 mm with the majority being 0.1 to 0.4 mm. Garnets are associated with a black opaque phase, biotite and green hornblende and show vermicular intergrowth with small anhedral quartz grains. The modal amount of garnet that has formed along a shear zone or shear plane is inversely proportional to the amount of pyroxene as can be seen by a direct comparison of the thinsections and estimated modal compositions (Table 7.3).
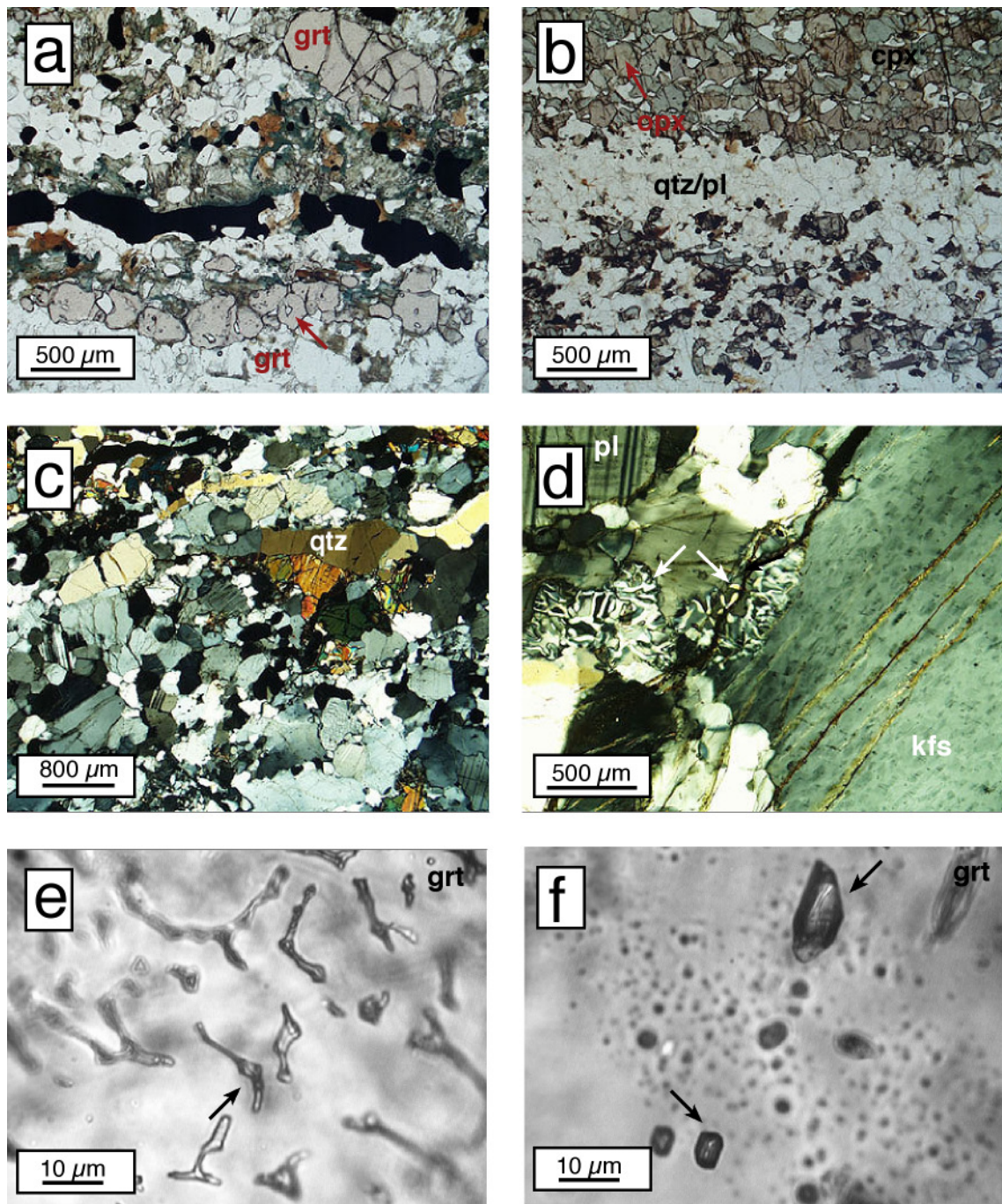
Fig. 7.9: *Microphotographs of thin and thicksections of shear zone samples. (a) Garnet blasts, sometimes with quartz inclusions (arrows), and elongated black opaque phase aligned along foliation plane of sample 1588-1B; (b) Ortho- and clinopyroxene blasts of thinsection 1588 interlayered with recrystallised plagioclase and quartz aggregates; (c) disc-shaped quartz with undulous extinction and subgrains; (d) large alkali-feldspar crystal displaying perthitic unmixing and intracrystalline fractures filled with sericitic aggregate. Myrmekitic intergrowth of quartz and plagioclase adjacent to alkali-feldspar and plagioclase with polysynthetic twinning (arrows); (e & f) rod-like and roundish CO_2-N_2 fluid inclusions hosted by garnet of sample 1588-1B.*

Table 7.3: Modal compositions (in vol%) of samples from shear zones within the O.-v.-Gruber anorthosite complex. **x** ≤ *2 vol% (1588-1B: shear plane in anorthosite). In thinsection 1588-1B modal estimations only refer to the shear plane, not to the whole thinsection as it is a c. 1.0 cm wide sharply defined layer in light-grey anorthosite.*

sample no.	1588	1588-1B	2119
rock type	mylonitic shear zone (norite)	shear plane (tonalitic)	mylonitic shear zone (norite)
plagioclase	60	25	60
alkali-feldspar	5	x	5
quartz	15	15	10
biotite	x	8	x
muscovite/paragonite	x	x	x
garnet	3	25	10
green hornblende	x	8	x
orthopyroxene	7		4
clinopyroxene	7		6
opaque phase	x	15	x
apatite	x	x	x
zircon			x
chlorite	x	x	x
calcite	x		x
tourmaline	x	x	x
titanite	x		x

Fig. 7.10: Graphic account and classification of the samples taken from shear zones and a shear plane within the O.-v.-Gruber anorthosite complex (according to Le Maitre, 1989). Modal compositions of quartz, plagioclase and alkali-feldspar are given in Table 7.3. If the estimated mode % of alkali-feldspar was ≤ 2 vol%, the maximum value of 2 vol% was used for the recalculation to total 100%. Samples 1588 and 2119 are classified as norites, whereas the composition of the shear plane in sample 1588-1 is tonalitic.

Orthopyroxene is colourless to light green with weak pleochroism, and varies in size between 0.1 to 2.0 mm. Clinopyroxene has the same variation in grain size but displays stronger pleochroism from light green to pale red and higher birefringence (Fig. 7.9b).

Nearly all major and minor mineral constituents show microfractures (Fig. 7.9d). Those observed in feldspars and garnet are often refilled with white micas and calcite or a brownish secondary phase that can also be found as alteration product along pyroxene mineral cleavage and grain boundaries.

7.2.2. Fluid inclusion studies (thicksections no. 1588, 1588-1B, 2119)

Fluid inclusions observed in these samples are either hosted by plagioclase (sample no. 2119), by plagioclase and garnet (sample no. 1588) or apatite and garnet (sample no. 1588-1B). The size of the *plagioclase-hosted* inclusions varies between 3.0 and 33.0 μm in sample 2119 and between 2.0 and 8.5 μm in sample 1588. In the latter they are darker and much less abundant. Inclusions predominantly have roundish to negative crystal shapes, but irregular forms can be observed as well. Throughout the crystals the majority of inclusions is arranged in intracrystalline clusters or trails and single inclusions are rare. *Garnet hosted* fluid inclusions range in size between 3.5 and 26 μm. Except for a few single inclusions, they are distributed in intracrystalline clusters and show irregular tube-like or roundish to negative-crystal shapes.

At room temperature, most plagioclase and garnet hosted inclusions contain a single liquid-like carbonic phase, and some comprise a varying number of solid phases that were identified as being calcite, Mg-calcite or pyrophyllite. Minor amounts of nitrogen (max. 4 mol%) have been detected by Raman spectrometry and rarely, amounts as high as 8 mol% were estimated using the diagrams provided by Thiery *et al.* (1994). Homogenisation of all fluid inclusions occurs into the liquid phase. Inclusions hosted by garnets and plagioclases of sample 1588 show a wide range of homogenisation temperatures between -10.4 and +27.2°C and -38.6 and +22.9°C, respectively. Fluid inclusions detected in sample 2119 show a similar spread of Th (-12.8 to +23.8 °C) (Fig. 7.11a). Melting temperatures are consistent, as well, and range from -59.1 to -56.6 °C (Fig. 7.11b). A systematic relationship between Th and Tm is not present (Fig. 7.12). Calculated densities lie between 0.64 and 0.98 gcm^{-3} in sample no. 2119, and between 0.56 and 0.96 gcm^{-3} (garnet) and 0.52 and 1.07 gcm^{-3} (plagioclase) in sample 1588 .
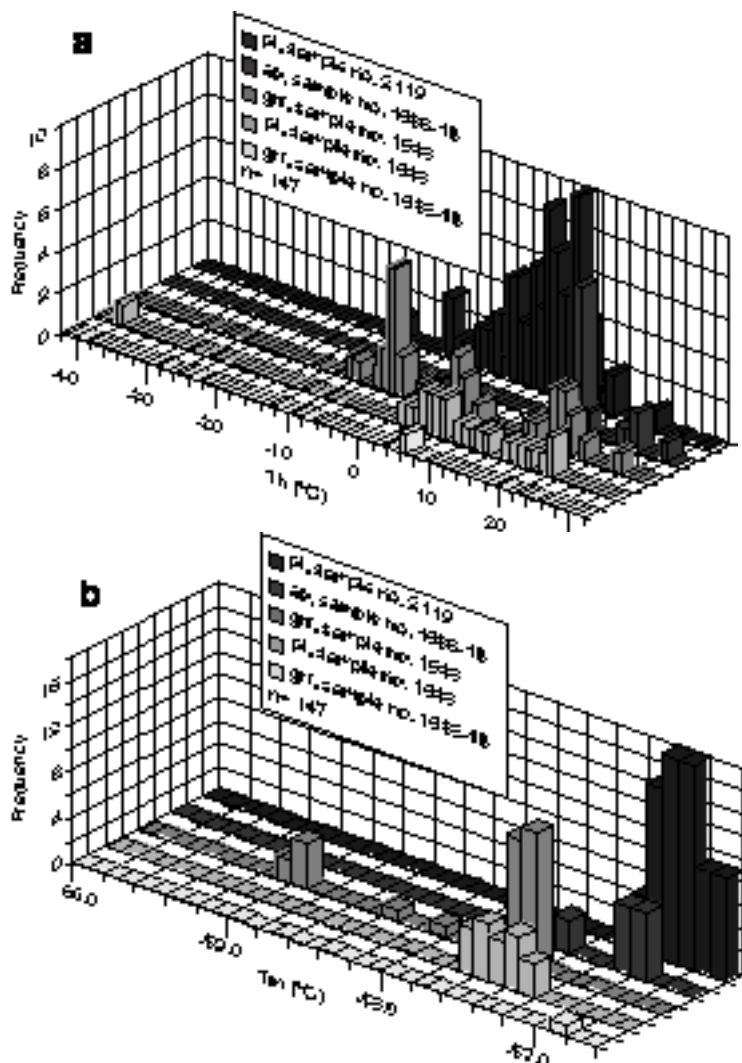
Fig. 7.11: *(a) Homogenisation temperatures of plagioclase, garnet and apatite hosted fluid inclusions from shear zone samples and a narrow shear plane. Homogenisation always occurs into the liquid phase. (b) Melting temperatures of CO_2-dominated fluid inclusions. Melting point depression of max. 2.5°C is caused by the presence of minor amounts of N_2.*

Garnet and *apatite* crystals of the narrow shear plane (thinsection 1588-1B) contain intracrystalline clusters and trails of small (2.0 to 9.5 μm) inclusions with roundish to negative crystal shapes that show melting of a solid phase at a narrow temperature interval from -57.5 to - 56.8 °C. Homogenisation into the liquid phase of inclusions hosted by apatite occurs at 15.5 to 29.7 °C. In garnet-hosted inclusions homogenisation to the liquid phase was observed only once at 6.3 °C. All other inclusions revealed fading of the miniscus of the vapour bubble at c. 30.1 °C, which indicates critical homogenisation. Nevertheless, due to the small inclusion size, the darkish appearance of the inclusions and the colouring of the garnet, observations are ambiguous and equivocal. Density of the garnet hosted inclusion is 0.87 gcm^{-3}, whereas densities of apatite hosted inclusions vary between 0.74 and 0.77 gcm^{-3}
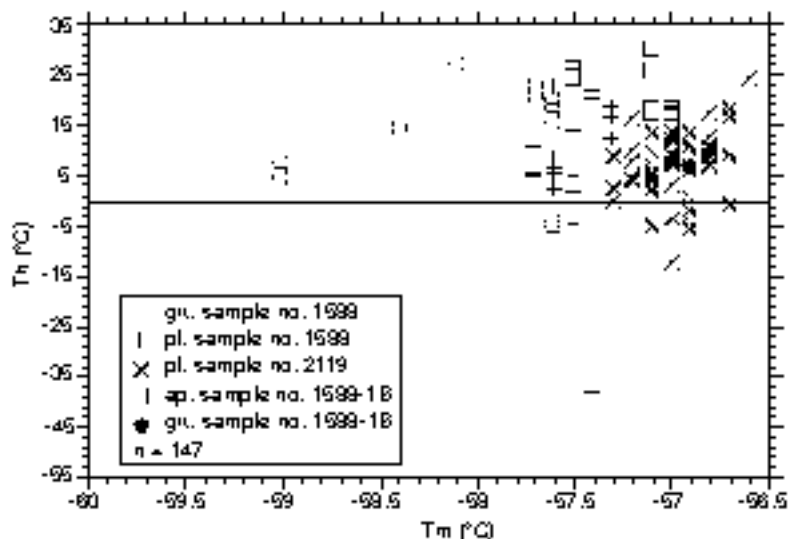
76

Fig. 7.12: *Relationship between Th and Tm of plagioclase hosted inclusions from shearzone samples*

7.2.3. Mineral chemistry of feldspars, pyroxenes and garnets of samples no. 2118 and 2119

Electron microprobe analyses of varying mineral phases were carried out on samples 2118 and 2119 to enlighten possible changes in mineral chemistry during the deformational event that led to the shear zone formation. The plagioclases of the anorthosite sample no. 2118 have a uniform compositional range varying between $An_{40}Ab_{57}Or_3$ and $An_{46}Ab_{53}Or_1$ (Fig. 7.13).
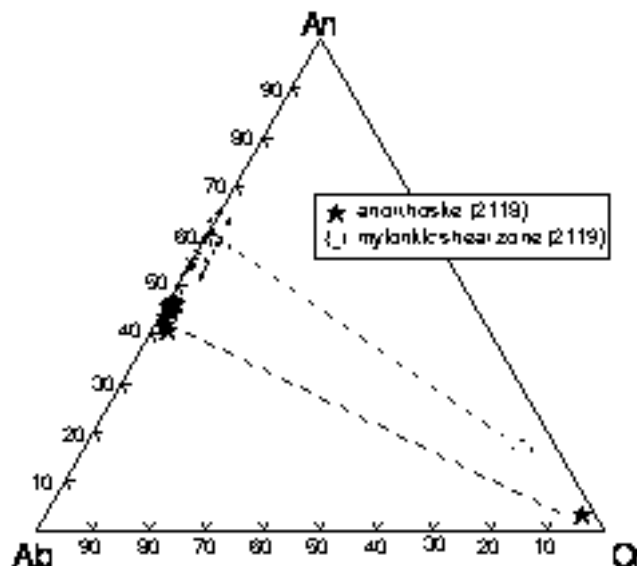

Fig. 7.13: *Compositions of plagioclase and K-feldspar (in mol%) from anorthosite and mylonitic shear zone samples no. 2118 and 2119 plotted in the albite (Ab)-anorthit (An)-orthoclase (Or) system.*

Plagioclase crystals of the mylonitic shear zone sample have slightly higher An values of $An_{51}Ab_{47}Or_2$ to $An_{63}Ab_{36}Or_1$ (Fig. 7.13). The transition is smoothly, and compositional values may overlap, as further investigations of anorthosite hosted plagioclases ($An_{46}Ab_{53}Or_1$ to $An_{53}Ab_{46}Or_1$) from samples no. 1583 and 1588-1 have revealed (*cf.* chapter 8, Fig. 8.2). Rare K-feldspar exsolution lamellae in plagioclase have a composition of $An_3Ab_3Or_{94}$ in anorthosite, and of $An_7Ab_{16}Or_{77}$ in shear zone samples. This depicts an identical trend of enrichment of the anorthite component in K-feldspars during the deformational event.

The graphic representation of pyroxene compositions shows that clinopyroxenes of sample 2118 are either Fe-rich diopsides with a slight shift towards Fe-poor hedenbergite, or Ca-rich augites with counterbalanced fractions of magnesium and iron (Fig. 7.14). In sample 2119, clinopyroxene compositions are predominantly in the range of Fe-poor hedenbergite with a weak tendency towards Ca-rich augite. Clinopyroxene compositions of samples 2118 and 2119 mainly differ in higher Fe-values of pyroxenes hosted by the shear zone sample. Orthopyroxene of sample 2119 is in the range of ferrosilite.
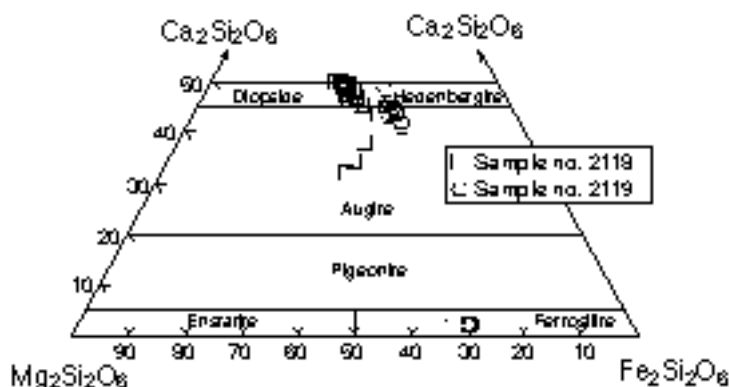

Fig. 7.14: *Chemical composition of pyroxenes (in mol%) of anorthosite and shearzone samples 2118 and 2119*

Endmember calculations of secondary garnet blasts from the shear zone sample 2119 exhibit that the garnet solid solution has a relatively narrow compositional range. It varies only slightly between $Alm_{66}Grs_{27}Prp_6Sps_1$ and $Alm_{70}Grs_{20}Prp_8Sps_2$. Andradite does not occur during endmember calculations, as total iron was completely calculated as ferrous component of almandine.
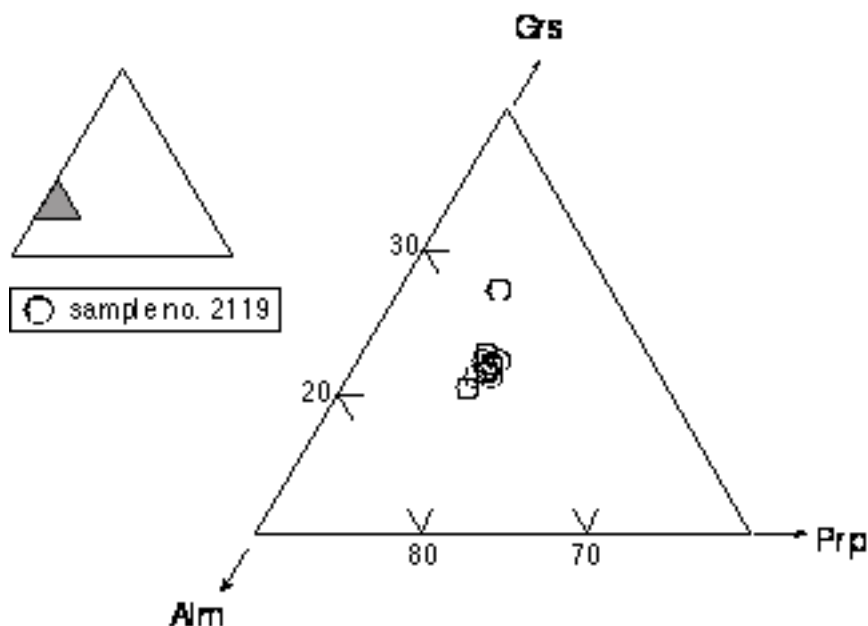
Fig. 7.15: *Compositions of secondary garnet (in mol%) of sample 2119 projected onto the spessartine free base of the garnet endmember system Alm-Prp-Grs-Sps.*

7.3. Discussion

The Otto-von-Gruber-Gebirge provides a typical example of a Proterozoic massif-type anorthosite complex. In this study, several samples from the weakly deformed central part of the plutonic body, and from mylonitic shear zones that have formed within. They have been investigated with regard to their petrography, preserved microstructures, fluid inclusion content, and mineral chemistry.

Modal analyses have reconfirmed the field observation that the voluminous intrusion predominantly comprises rocks of anorthositic composition (Fig. 7.3). It is composed of up to 90 vol% plagioclase in the range of $An_{40-46}Ab_{53-57}Or_{1-3}$. During shear zone formation, the modal composition changed towards higher quartz contents (plus garnet and orthopyroxene formation), and the samples have been classified as norites (thus belonging to the charnockitic rocks as they contain orthopyroxene) and tonalite (Fig. 7.10). The anorthosites display a uniform mineral assemblage of plagioclase-clinopyroxene-K-feldspar, whereas the samples collected from the shear zones are characterised by the metamorphic mineral assemblage of garnet-orthopyroxene-clinopyroxene-plagioclase-quartz. The comparison of pyroxene analyses from anorthosites and shear zones reveals that clinopyroxene becomes enriched in iron. Newly grown orthopyroxene is characterised by an iron-dominated ferrosilitic composition, as is secondary garnet, which exhibits a homogeneous, almandine-rich, composition (Figs. 7.14, 7.15). Plagioclase of both rock types ranges between

$An_{40-63}Ab_{36-57}Or_{1-3}$, with the highest An values measured in the shear zone samples (Fig. 7.13). A very primitive composition of $An_{74}Ab_{26}Or_0$ has been reported from the core of a plagioclase porphyroclast from the central O.-v.-Gruber anorthosite body by Markl *et al.* (in press). It is suggested that this composition reflects the beginning of plagioclase crystallisation from a primitive basaltic magma. Ashwal (1993), who has reported even more primitive plagioclase compositions from undeformed anorthosite complex, argues that compositional changes towards lower An contents are indicative for recrystallisation of plagioclase during metamorphic overprint. Based on these considerations, lower An values of 40 to 46 mol% are interpreted to reflect the effect of metamorphic recrystallisation. Subsequent shearzone formation again resulted in an increase of anorthite component in plagioclase and K-feldspar. This interpretation is also in conformity with the general observation that an enrichment in anorthite component in plagioclase indicates a progression in pressure and/or temperature, as already considered by Becke (1903). A comparison of pre- and postmetamorphic mineral assemblages reveals, that the mineral reactions would not have taken place in an isochemical system. Thus, the change in chemical composition during the time span of shear zone formation - increase of femic components and decrease of sodium- must have been allochemical, possibly under influence of an ion-rich fluid phase. The pseudomorphosis of biotite after amphibole (Fig. 7.2c) hints at a high K-mobility during retrogression. Additionally, the alteration of pyroxene to hornblende and biotite, as well as sericitisation of plagioclase observed in all samples is typical for retrogression under presence of an aqueous fluid phase.

Conspicuous microstructures observed in feldspar of anorthosites and shear zones include undulous extinction, deformational twinning, bent deformation lamellas, "core-and-mantle" stuctures, myrmekite growth and the formation of real subgrain structures. Bent deformation lamellae, undulous extinction and "core-and-mantle" stuctures are indicative for deformation at temperatures around 450 to 550 °C (Passchier & Trouw, 1996). Quartz from the shear zones reveals a disc-shaped habit which is characteristic of deformation under granulite facies conditions (Shelley, 1993). The pegmatitic mobilisate of tonalitc composition reveals microstructures very similar to those of the surrounding anorthosite, and is therefore considered to be concomitant to the deformation of the anorthosite body. Mineral deformation is not restricted to high grade conditions but continues towards lower temperatures and pressures. Processes responsible for recrystallisation or brittle fracturing are important during retrogression, and may strongly effect fluid inclusions that formed during prograde or peak-metamorphic conditions.

Thorough fluid inclusion studies have revealed, that the current fluid content of the samples collected from the O.-v.-Gruber anorthosite complex is $CO_2 \pm N_2$ dominated

with the melting temperatures of solid CO_2 varying between -59.1 and -56.6 °C. The amount of nitrogen detected is mostly in the range of 2-4 mol%. Nearly all fluid inclusions homogenise into the liquid phase. The uniformity in fluid composition ($CO_2 \pm N_2$) is accompanied by largely homogeneous inclusion shapes (roundish to negative crystal shape), and the frequent occurrence of enclosed solids. The latter were identified as carbonates and/or varying sheet silicates. The microcrystals predominantly occur in in plagioclase hosted inclusions, but some inclusions hosted by garnet contain solids as well. Fluid inclusions are exclusively arranged along intracrystalline clusters and trails, and no evidence of secondary origin or influx of different (late or secondary) fluid generations was found. The only evidence for the presence of any free H_2O derived from microthermometry and Raman spectrometrical investigations is given by extremely rare H_2O-CO_2-bearing fluid inclusions hosted by intersticial quartz of the anorthosite samples.

A comparison of all plagioclase hosted inclusions from anorthosite and shear zone samples exhibits, that the majority of fluid inclusions from the anorthosites homogenises at higher temperatures than those hosted by plagioclase of the shear zones (Fig. 7.16).
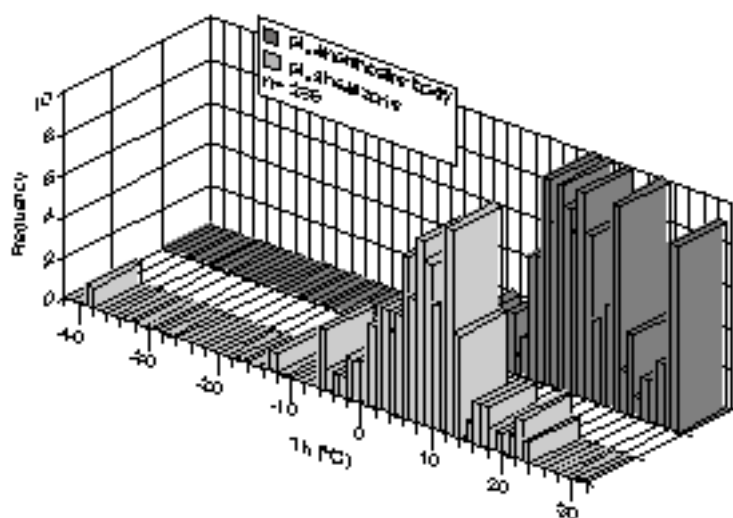

Fig. 7.16: Compilation of all homogenisation temperatures measured from plagioclase-hosted fluid inclusions from the O.-v.-Gruber anorthosite complex

This tendency is also reflected by the results of density calculations (high Th generally corresponding to low densities). The whole range of densities in the shear zones spreads from 0.73 to 1.07 gcm^{-3}, with densities > 1.0 gcm^{-3} just reached once. Considering only those inclusions that homogenise into the liquid phase, the whole range of densities of anorthosite hosted inclusions lies between 0.61 and 0.94 gcm^{-3}. Very low densities (0.28 to 0.38 gcm^{-3}) were exclusively calculated from irregular to roundish inclusions that homogenise into the vapour phase. They are located in

immediate vicinity of the pegmatite vein. Quartz hosted inclusions from the pegmatite itself yield densities of 0.63 to 0.80 gcm^{-3}. Densities from garnet and apatite hosted inclusions from the shear zones fall in the range of 0.56 to 0.96 gcm^{-3} (limits determined from garnet hosted inclusions). Consequently, all densities calculated from homogenisation temperatures (Th (l)) measured in other minerals than plagioclase fall well into the range already encompassed by the most abundant host mineral.

The relatively wide spread of densities and slight variation in fluid composition within the homologous inclusion assemblages can be best explained by the different reaction of single inclusions on the influence of post-entrapment change. Evidence for brittle failure during decompressional uplift is given by a positive correlation of inclusion size and homogenisation temperatures (Fig. 7.17). Large inclusions tend to decrepitate easier than small inclusions which results in a fluid loss and generation of larger inclusion volumes (*e.g.* Swanenberg, 1980; Bodnar *et al.*, 1989). A further indicator is the occurrence of decrepitation clusters around rare quartz hosted inclusions (Fig. 8.4f). Evidence for post-entrapment change through reequilibration processes is given by the predominantly roundish to negative crystal shapes, and by microstructural features evident in the host minerals. The modification of inclusions is often accompanied by selective loss of N_2 or H_2O. The very low density of inclusions found adjacent to the pegmatite vein most probably result from destruction and fluid loss during locally restricted melt injection.
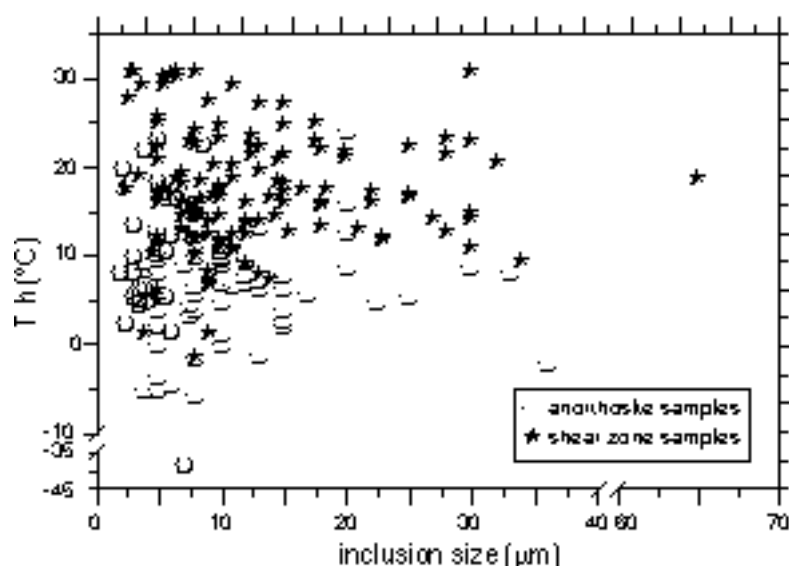

Fig. 7.17: *Correlation between homogenisation temperatures and inclusion sizes of anorthosites and shear zone samples. Smaller inclusions display a wide range of Th, whereas large inclusions generally do not reveal low homogenisation temperatures (with one exception).*

The results from microthermometrical studies (Th, Tm) reveal that the composition of the actual fluid content from the O.-v.-Gruber anorthosite complex is relatively

homogeneous. In a first approach, isochores were calculated for selected inclusions containing a maximum amount of 4 mol% N_2 and compared with published P-T data deduced from independent thermobarometrical studies.

Representative isochores depicted in Fig. 7.18 indicate the maximum and minimum P-T conditions from garnet and plagioclase hosted inclusions of the shear zones, and plagioclase hosted inclusions of the anorthosite samples, respectively. The absolute maximum P values result from high density, garnet and plagioclase hosted inclusions that were rarely detected in the shear zone samples (0.96 and 1.07 gcm^{-3}). The intrusion of the anorthosite body into the metamorphic basement lithologies of cDML occurred at c. 600 Ma, subsequently followed by a first stage of Pan African I metamorphism at 580-550 Ma (Jacobs *et al.*, 1998). The isochores intersect with metamorphic conditions of the Pan African I event (M2) as given by Markl & Piazolo, 1998 (Fig. 7.18). Thus it is concluded that despite the frequent evidence for post-entrapment change, these rare inclusions still reflect peak metamorphic conditions.
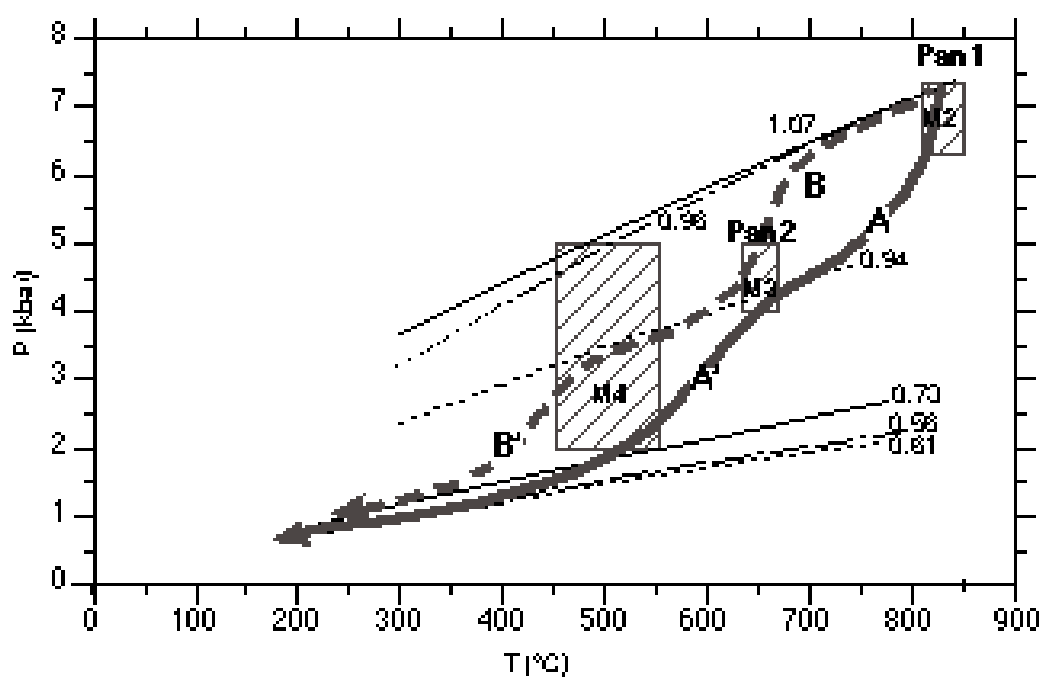
Fig. 7.18: *P-T diagram with isochores derived from fluid inclusion data of plagioclase hosted inclusions of anorthosites and shear zone samples. Given isochores represent maximum and minimum density values of $CO_2 \pm N_2$ inclusions detected in plagioclase of anorthosite (dashed lines), and plagioclase (solid lines) and garnet (dash-dot-lines) of shear zone samples. The majority of isochores calculated from plagioclase, garnet, apatite or quartz hosted inclusions fall in the field encompassed by maximum and minimum isochores from the anorthosite samples (dashed lines). Numbers refer to the densities in gcm^{-3}. Boxes indicate metamorphic conditions of Pan African I (**Pan1**), Pan African II (**Pan2**) and retrogression (M4) cf. chapter 5. The possible P-T paths resulting from the intersection of isochores with independent P-T constraints are indicated by the grey arrosw, description is given in the text.*

The isochore calculated from maximum density values of the anorthosite inclusion (0.94 gcm^{-3}) is interpreted to represent maximum pressure conditions prevailing during a further metamorphic event, as the vast majority of inclusions reveal similar or lower densities (0.71 to 0.84 gcm^{-3} in anorthosites and 0.81 and 0.92 gcm^{-3} in shear zone samples). The resulting pressure estimation is in accordance with independent P-T conditions, given for the second stage of Pan-African metamorphism (Pan2, M3 from Markl & Piazolo, 1998).

A multitude of calculated isochores (not depicted in Fig. 7. 18) falls into the range encompassed by the isochore reflecting M3 conditions (0.94 gcm^{-3}) and minimum value isochores derived from plagioclase and garnet hosted inclusions of anorthosites and shear zones (0.73, 0.56 and 0.61 gcm^{-3}). Density values (and indicated pressures) decrease gradually and terminate at the minimum value isochores.

Near isobaric cooling (P-T path **B** in Fig. 7.18) from high-grade granulite facies conditions would result in volume decrease without major loss of fluid content, and abundance of high density inclusions (≥ 1.0 gcm^{-3}), even when followed by a stage of rapid isothermal decompression (Lamb & Morrison, 1997; Touret, 2001). The absence of any significant amounts of high density inclusions in the O.-v.-Gruber anorthosite complex, in addition to evidence of decrepitation (Fig. 7.17) though is in favour of a periode of isothermal decompression for the retrograde stage between the Pan African I and Pan African II metamorphic stage (path **A** in Fig. 7.18). Fluid inclusion densities were "reset" at M3 conditions and a second period of retrogression followed.

Density values reflecting the post-M3 phase (ranging between 0.94 and 0.56 gcm^{-3}) decrease gradually and occur rather evenly distributed throughout all samples. This indicates an even influence of reequilibration processes acting over a long period of time. Thus, a gradual (nearly linear) decrease in P-T conditions is proposed (path **A'**) for the post M3 retrograde stage, which has only very roughly been confined by other thermobarometric studies (M4 taken from Markl & Piazolo, 1998; Colombo & Talarico, in press). The presence of slightly higher average density values in shear zone samples is probably an effect of shear zone reactivation or a less pronounced influence of retrograde fluid inclusion modification. Again, the absence of a significant number of high density inclusions (≥ 0.92 gcm^{-3}) speaks against a mode of isobaric cooling (path **B'**).

It is evident from the fluid inclusion studies, that the majority of inclusions under investigation have changed their initial volumetric and compositional properties towards lower densities. A partial loss of the fluid phase during change after inclusion formation often has the character of selective loss of one fluid component (*e.g.* H_2O or N_2). Fluid pressure indicated by isochores calculated from inclusions hosted by well identified metamorphic minerals (e.g. garnet) is almost systematically lowered about 1-

2 kbar, compared to metamorphic pressures derived from solid-equilibria estimations (Touret & Huizenga, 1999). This feature has often been reported from granulite lithologies and may be explained by systematic H_2O -loss through water leakage (*e.g.* Touret, 2001). Heinrich & Gottschalk (1995) have suggested that peak metamorphic fluids that were captured in prograde metamorphic minerals react with the surrounding host somewhere along the retrograde path, leading to a severe change in volume and loss of some fluid components. That a free aqueous phase must have been present at some stage of the geologic evolution of the O.-v.-Gruber anorthosite complex is unequivocally documented by extremely rare quartz-hosted inclusions that contain a CO_2-H_2O fluid. Further indicators are sericitisation and calcitisation of plagioclase (most dominantly developed in the pegmatite vein), and slight alteration of pyroxene to biotite and amphibole. That up to 15 vol% H_2O, forming a small rim around the vapour bubble, might be overlooked during microthermometry studies has already been reported by early workers (*cf.* Roedder, 1984). Furthermore, besides the models that largely connect granulite petrogenesis to "dry" conditions with low water activities (*e.g.* Newton *et al.*, 1980; Santosh *et al.*, 1990), more recent studies do not preclude the presence or even participation of an aqueous phase during granulite facies metamorphism (*e.g.* van den Kerkhof, & Grantham, 1999; Newton *et al.*, 1998). The initial anorthositic magma system must have contained certain amounts of dissolved H_2O and CO_2, and as no evidence for the influx of significant amounts of a later fluid phase was detected it is presumed that the initial fluid was comprised out of $CO_2\pm H_2O\pm N_2$.

Thorough Raman spectrometry analyses have ruled out the possible presence of any "hidden" water in the plagioclase and garnet hosted $CO_2\pm N_2$ inclusions under investigation. Based on the frequent findings of hydrous microsolids (sheet silicates) and carbonates in plagioclase and garnet hosted inclusions, it is suggested that the H_2O component of the initial fluid reacted with the surrounding mineral host under formation of so-called "step-daughter" phases. The mechanism of post-entrapment change through the reaction of an entrapped fluid with its mineral host, has only been reported by a few workers, so far (e.g. Heinrich & Gottschalk, 1995; Svensen *et al.*, 2001). The effect of volumetric and compositional change on plagioclase hosted inclusions has not been described before. Thus the example studied was used to model and evaluate the modifications a CO_2-N_2 bearing fluid hosted by plagioclase would undergo during retrograde metamorphism, and the effect on isochore calculations if it could be proved that the initial inclusion contained significant amounts of H_2O.

The following chapter consists of an individual paper on modelling of fluid host interactions of plagioclase with an enclosed H_2O-CO_2-bearing fluid, leading to the formation of "step-daughter" microcrystals within fluid inclusions under complete consumption of the aqueous phase. It contains own chapters on introduction, geological setting, discussion, and conclusions, and separate references. All data used are presented either in the text or the appendices A and B. With the detailed study of fluid inclusions of anorthosite samples 1583 and 1588-1, the results of the publication have a close relationship to the data discussed in chapter 7 of this thesis.

Chapter 8

Fluid inclusions as micro-chemical systems: evidence and modelling of fluid-host interactions in plagioclase

Bärbel Kleinefeld* & Ronald. J. Bakker°

*Faculty of Geosciences, University of Bremen, Postfach 330440,
D-28334 Bremen (Germany), bkleinefeld@uni-bremen.de*

*°Institute of Geosciences, Mineralogy & Petrology,
University of Leoben, Peter-Tunner-Str. 5, A-8700 Leoben (Austria)*

Abstract

Dense, CO_2-rich fluid inclusions hosted by plagioclases, An_{45} to An_{54}, of the O.-v.-Gruber anorthosite body, central Dronning Maud Land, East Antarctica, have shown to contain varying amounts of small calcite, paragonite and pyrophyllite crystals, as detected by Raman microspectrometry. These crystals are reaction products that have formed during cooling of the host and the original CO_2-rich H_2O-bearing enclosed fluid. Variable amounts of these reaction products illustrate, that the reaction did not take place uniformly in all fluid inclusions, possibly due to differences in kinetics as caused by differences in shape and size, or due to compositional variation in the originally trapped fluid. The reaction *Albite + 2Anorthite + 2H₂O + 2CO₂ = Pyrophyllite + Paragonite + 2Calcite* was thermodynamically modelled with consideration of different original fluid compositions. Although free H_2O is not detectable in plagioclase-hosted inclusions, the occurrence of OH-bearing sheet silicates indicates that the original fluid was not pure CO_2, but contained significant amounts of H_2O. Compared to an actual fluid inclusion it is obvious, that volume estimations of solid phases can be used as a starting point to reverse the retrograde reaction and recalculate the compositional and volumetrical properties of the original fluid. Isochores for an unmodified inclusion can thus be reconstructed, leading to a more realistic estimation of P-T conditions during earlier metamorphic stages or fluid capturing.

Introduction

The interpretation of many fluid inclusion studies is based on the assumption that the entrapped fluid has not changed its composition and density during the long exhumation history. Fluid inclusions, both primary and secondary, form during precipitation processes of a mineral host. At this stage, the enclosed fluid and its host crystal are not chemically reactive. However, at temperatures and pressures different from the formation conditions, the micro-system may become unstable and therefore react. Quartz, the most studied host mineral, is not chemically reactive with most of the enclosed fluids over a wide range of P-T conditions. The occurrence of chemical reactions between the entrapped fluid and a reactive mineral host (e.g. feldspar and pyroxene) has been reported so far by only a few workers.

Andersen *et al.* (1984) described inclusions in pyroxene from mantle xenoliths with a residual composition of nearly pure CO_2 and two secondary solids of carbonate and amphibole. It was suggested that both phases resulted from reaction between the pyroxene host and an original H_2O-CO_2-rich entrapped fluid. They used SEM and microprobe techniques to identify the varying entrapped minerals in fluid inclusions, and Raman microspectrometry for the analysis of fluid components. The density change of the remaining fluid was modelled against the volume change of the solid phase involved in the reaction. The reaction of melt inclusions with a garnet host was described by Schulze (1985). Included olivine is supposed to react with garnet to form spinel and pyroxene, which are later transformed into serpentine. Davis *et al.* (1990) reported the reaction of a salt-saturated aqueous solution in fluid inclusions with a halite host during a freezing-heating experiment. A rim presumably composed of hydrohalite formed just after the melting of ice. Heinrich & Gottschalk (1995) introduced the term "back-reactions" for decarbonation reaction during retrogression in wollastonite-hosted fluid inclusions leading to the formation of quartz and calcite. On heating in the microstage, the progress of the prograde reaction is estimated visually and then thermodynamically modelled, using compositions and densities of similar but unmodified fluids entrapped in neighbouring quartz. Svensen *et al.* (1999, 2001) considered that some of the many entrapped crystals (e.g. calcite, quartz and K-feldspar) within fluid inclusions in omphacite and garnet may be reaction products of fluid and host ("step-daughter-crystals"), whereas the others were accidentally trapped during multiple re-opening, or precipitated out of a supersaturated fluid.

Thermodynamic modelling of fluid-host reactions as applied to wollastonite by Heinrich & Gottschalk (1995) allows a more precise and realistic interpretation of fluid inclusions analysed in metamorphic rocks. In this study we have combined the varying approaches of the previously described studies, including the exact analysis of reaction

products as well as the thermodynamic evaluation of the stability field of phases involved and their proper mass balance. Plagioclase from the O.-v.-Gruber anorthosite complex, central Dronning Maud Land, East Antarctica, contains CO_2-rich fluid inclusions with several solid phases, which were identified as carbonates and sheet-silicates by Raman microspectrometry. The aim of this study is to prove, that the enclosed solids formed by chemical reaction between the fluid and the host mineral.

Geological Setting

Central Dronning Maud Land (cDML) is situated within the East Antarctic/African Orogen, the Late Neoproterozoic-Lower Palaeozoic collision zone between East and West-Gondwana (Jacobs *et al.*, 1998). One striking feature of this region is the occurrence of a massif-type anorthosite body that crops out over approximately 250 km^2 within the Otto-von-Gruber-Gebirge, East Antarctica (Fig. 1).
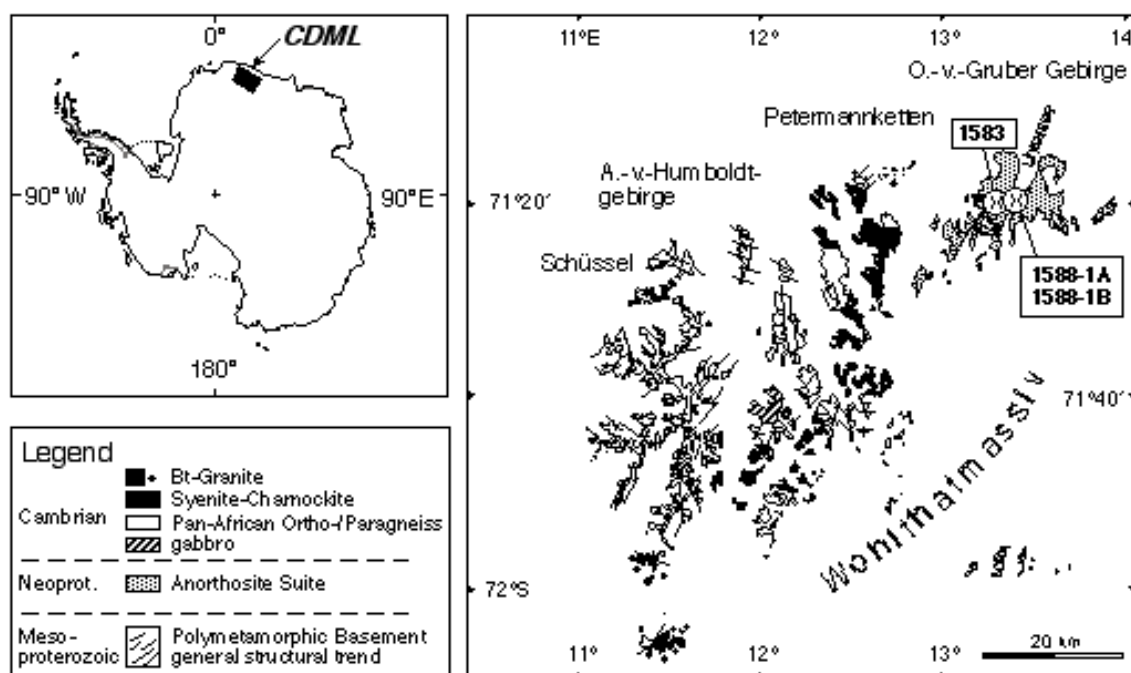
Fig. 1: Geological overview map of the Wohlthatmassiv, central Dronning Maud Land (cDML) and sample localities (modified after Jacobs et al., 1998).

The volcanic and sedimentary basement rocks of cDML experienced an early Grenville-age metamorphic overprint at high- to medium-pressure granulite facies conditions (D1 and M1 according to Bauer *et al.*, in press), that was associated with the syntectonic intrusion of granite sheets and plutons at c. 1085 to 1075 Ma (Jacobs *et al.*, 1998). Voluminous anorthositic magmas were emplaced at c. 600 Ma and the margins of the anorthosite body were strongly deformed at c. 580-550 Ma (Jacobs *et al.*, 1998). Deformation took place at medium-pressure granulite facies conditions of about 6.8 ± 0.5 kbar and 830 ± 20 °C and is interpreted as representing the collisional stage between

East and West-Gondwana, i.e. Pan- African I (Markl & Piazolo, 1998; D2 and M2 in Bauer *et al.*, in press). During deformation the anorthosite body behaved like a large delta-clast that still exhibits undeformed magmatic textures in its central parts (Bauer *et al.*, in press).

A subsequent tectono-metamorphic event (Pan-African II) started with the syntectonic intrusion of granitoids and gabbros at approximately 530 Ma and finally culminated in voluminous anorogenic charnockite and syenite magmatism at 510 Ma (Mikhalsky *et al.*, 1997; Jacobs *et al.*, 1998). Metamorphic conditions were at low–pressure granulite facies of 4 - 5 kbar and temperatures of about 640 ± 10 °C (Markl & Piazolo, 1998; D3/M3 in Bauer *et al.*, in press). A poorly developed and yet undated retrogression at pressures of approximately 2 - 5 kbar and 480 - 580 °C post-dates the voluminous intrusion of granitoids at 510 Ma (Markl & Piazolo, 1998; D4 in Bauer *et al.* in press).

Thermobarometric studies indicate a clockwise P-T-path characterised by an isothermal decompression evolution for the early Pan-African I event, whereas the structures of the Pan-African II event are ascribed to a late-orogenic extensional collapse of the East Antarctic-African Orogen (Jacobs *et al.*, in press).

Analytical Methods

Thin- and thick-sections were made from selected samples, and investigated by optical petrography, electron microprobe analysis, microthermometry and Raman microspectrometry. Microthermometric measurements were carried out with a Linkam MDS 600 stage operating over a temperature range from -190 to 35 °C. Within these limits it was calibrated using synthetic fluid inclusions provided by Fluid Inc. at -56.6 and 0.0 °C, i.e. melting of pure CO_2 and pure H_2O, respectively. The analytical accuracy is ± 0.1 °C. The stage is mounted on an Olympus BX 60 microscope, modified and supplied by Fluid Inc. A Dilor LABRAM confocal-Raman spectrometer equipped with a frequency-doubled Nd-YAG laser (100 mW, 532.2 nm) with a LMPlanFI 100x/0.80 objective lens (Olympus) was used to identify fluid and solid phases in inclusions. Wavenumber measurements have an accuracy of 1.62 cm^{-1} at low $\Delta \nu$ (Raman shift around 0 cm^{-1}) and 1.1 cm^{-1} at high $\Delta \nu$ (around 3000 cm^{-1}). To analyse a homogeneous carbonic gas mixture by microspectrometry, samples were held at controlled temperatures of c. +33 °C with a Linkam THMSG 600 heating-freezing stage. As the Raman signal for ice is more pronounced than for water, inclusions are analysed at -120°C to verify the presence or absence of invisible small amounts of H_2O.

As the amount of N_2 detected by Raman microspectrometry does not exceed 2 mol%, fluid properties were calculated as being equivalent to pure CO_2. The error in molar volume estimation resulting from this assumption is by far smaller than liquid-

vapour equilibrium calculations with published equations of state. Thus, molar volumes of these fluid inclusions are obtained from the homogenisation temperatures using the equation of Duschek *et al.* (1990) for pure CO_2 and isochore calculations are based on the equation of state of Span & Wagner (1996). Isochores for H_2O-CO_2 mixtures are calculated with the equation of state of Holloway (1977, 1981). The fluid properties of homogeneous H_2O-CO_2-NaCl mixtures are calculated with the equation of state of Anderko & Pitzer (1993) and Duan *et al.* (1995). The salinity of rare H_2O-CO_2-NaCl fluid inclusions hosted by quartz is calculated using the program *Q2* from the software package *CLATHRATES* (Bakker, 1997). All other fluid properties were computed with the software package *FLUIDS* (Bakker, in press).

An ARL-SEMQ 30 microprobe equipped with four wavelength-dispersive spectrometers (WDS) with TAP, LiF and PET diffraction crystals, and a LINK AN 10/25S energy-dispersive spectrometer (EDS) was used to measure plagioclase compositions. Beam conditions were 20 kV and 15 nA. A plagioclase standard from the Leoben University was used for calibration. The Bastin correction was applied to the obtained data.

Petrography and Electron Microprobe Analysis

The light-grey anorthosite rocks are fine to coarse-grained equigranular and bimodal inequigranular with plagioclase megacrysts up to 1.5 cm in size. The major constituent is plagioclase (c. 90 vol%) of An_{45} to An_{54} (Fig. 2). Minor components in varying occurrence are K-feldspar (microcline) and clinopyroxene. Quartz, biotite, hornblende, orthopyroxene, chlorite, opaque (oxides and sulfides), sheet-silicates, and carbonates form accessories, some of which are related to the metamorphic overprint.
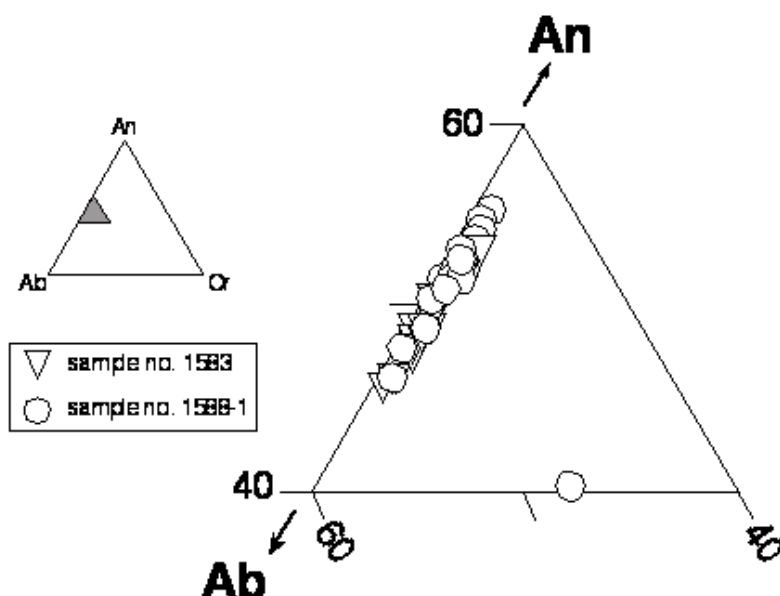

Fig. 2: Feldspar compositions obtained from electron microprobe analysis plotted in the ternary Or-Ab-An diagram.

Large subhedral to euhedral grains of plagioclase are slightly flattened and may show lattice-preferred orientation. Antiperthitic unmixing is often observed in larger grains. Twinning on albite- and pericline law planes is common (Fig. 3a). Bent deformation lamellae and undulose extinction in addition to subgrain formation and subgrain rotation and bulging of grain boundaries give evidence of intracrystalline deformation and recovery, probably related to the Pan-African I metamorphic event. Aggregates of small, dynamically recrystallised grains surround the larger feldspar clasts (Fig. 3b) and thus form "core-and-mantle" structures (as described by Passchier & Trouw, 1996). Within these fine-grained areas a polygonal fabric with relatively straight grain boundaries has developed. Rare intercrystalline microfractures are either open or filled with sheet silicates and/or calcite. Some plagioclase crystals show strong alteration to sericite and calcite, whereas ortho- and clinopyroxene may be altered to hornblende and biotite along small intracrystalline fractures and grain boundaries.
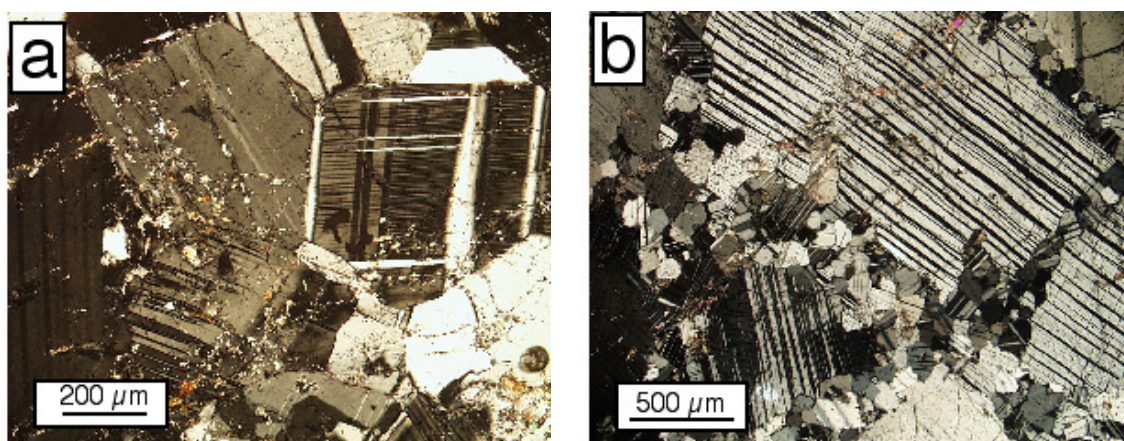

Fig. 3: *Microphotographs of albite and pericline-twins in plagioclase of sample 1583 (a) and "core-and-mantle" structures of sample 1588-1 (b).*

Results of fluid inclusion studies

Fluid inclusion petrography

One single type of fluid inclusions hosted by plagioclase was identified within all anorthosite samples. Inclusions have an average length of 7 - 15 μm (longest dimension), but sizes down to 2.5 μm and up to 65 μm were also observed (Table 1). Inclusion shapes vary from roundish or oval to negative-crystal shapes (Fig. 4a). At room temperature, they contain a single liquid-like carbonic phase and occasionally several birefringent solid phases (Fig. 4b). The solid/fluid ratio varies significantly among adjacent inclusions. Fluid inclusions are arranged as intracrystalline clusters (Fig. 4c) and trails (Fig. 4d), thus giving evidence of pseudosecondary origin, as they do not crosscut grain boundaries.

Table 1: *Microthermometrical data, length (in μm) and molar volume (in cm³mole⁻¹) of carbonic (car) fluid inclusions. Melting (T_m) and homogenisation temperatures (T_h) are given in °C. Homogenisation is always into the liquid phase. The solid phases calcite (cal), Mg-calcite (mg-cal), dioctaedral mica (dm) and pyrophyllite (prl) were identified with Raman spectrometry. Numbers in brackets indicate the volume percentage of the specific solid phase. The occurrence of at least one solid phase that was not further identified is indicated by "+".*

Inclusion no.	Length (μm)	Solid Phases	T_m (car) °C	T_h (car) °C	V_M (cm³mole⁻¹)
1583-1-01	14.3	+	-57.1	14.3	53.20
1583-1-02	7.5	+	-57.2	12.2	52.13
1583-1-03	9.0	+	-57.3	6.6	49.71
1583-1-04	4.5	+	-57.3	10.2	51.20
1583-1-05	5.0	+	-57.3	5.8	49.41
1583-1-06	13.0	mg-cal	-57.1	7.5	50.06
1583-1-07	9.0	+	-57.3	27.3	65.64
1583-1-08	11.0	mg-cal	-57.3	10.6	51.38
1583-1-09	30.0	mg-cal	-57.0	22.8	59.39
1583-1-10	9.0		-57.0	7.9	50.22
1583-1-11	9.0		-57.0	6.3	49.60
1583-1-12	9.0	mg-cal	-57.0	1.1	47.80
1583-1-13	7.5	+	-57.2	15.6	53.93
1583-1-14	14.0	cal (25), dm (12)	-56.7	7.1	49.91
1583-1-15	11.0	+	-56.8	10.8	51.47
1583-1-16	5.0	+	-56.8	4.6	48.97
1583-1-17	10.0		-56.8	17.5	55.11
1583-1-18	14.0	cal	-57.2	16.5	54.47
1583-1-19	11.0	+	-56.9	18.5	55.79
1583-1-20	7.0	mg-cal	-56.9	19.2	56.29
1583-1-21	65.0	mg-cal (11), dm (3)	-56.8	18.5	55.79
1583-3-03	15.0	mg-cal (5), dm-prl (6)	-57.1	8.7	50.55
1583-3-04	27.0	mg-cal (34), dm-prl (9)	-57.1	20.9	57.64
1583-3-05	7.0	mg-cal (6), dm-prl (6)	-57.1	11.4	51.74
1583-3-06	30.0	mg-cal (34), dm-prl (4)	-57.0	17.0	54.79
1583-3-07	17.0	Mg-cal (34)	-57.2	-1.8	46.92
1583-3-08	8.0	mg-cal (5), dm-prl (7)	-57.3	1.0	47.77
1588-1A-1-01	13.0		-56.8	19.4	56.44
1588-1A-1-02	9.5	+	-56.9	16.8	54.66
1588-1A-1-03	9.5		-56.8	19.9	56.82
1588-1A-1-04	11.0		-56.8	19.9	56.82
1588-1A-1-05	8.0		-57.0	14.5	53.31
1588-1A-1-06	5.5		-57.0	17.3	54.98
1588-1A-1-07	5.5	+	-56.9	17.1	54.85
1588-1A-1-08	2.5		-57.1	17.4	55.04
1588-1A-1-09	7.0		-57.1	18.0	55.44
1588-1A-1-10	2.5	+	-57.0	17.2	54.91
1588-1A-1-11	3.5		-57.1	18.9	56.07
1588-1A-1-12	6.0		-57.1	16.6	54.54
1588-1A-2-13	22.0	cal, mg-cal (2)	-57.5	15.7	53.99
1588-1A-2-14	8.5	+	-57.5	14.4	53.26
1588-1A-2-15	15.0	mg-cal	-57.5	18.0	55.44
1588-1A-2-16	18.5	cal, prl	-57.5	17.4	55.04
1588-1A-2-17	6.5	mg-cal	-57.5	18.4	55.72
1588-1A-2-18	10.0	mg-cal	-57.5	17.4	55.04
1588-1A-2-19	8.5	mg-cal	-57.4	18.2	55.58
1588-1A-2-20	8.5	cal	-57.5	16.2	54.29
1588-1B-3-22	30.0	mg-cal (8), prl (4)	-57.3	14.1	53.1
1588-1B-3-23	7.0		-57.3	15.9	54.11
1588-1B-3-24	10.0		-57.3	17.2	54.91
1588-1B-3-25	15.5		-57.3	12.5	52.27
1588-1B-3-26	14.5	mg-cal	-57.3	20.6	57.38
1588-1B-3-27	14.5		-57.6	18.1	55.51
1588-1B-3-28	16.5		-57.8	17.2	54.91
1588-1B-3-29	15.0		-57.6	15.7	53.99

Rarely, the accumulated appearance of fluid inclusions at the centre of large feldspar crystals, best visible in sections perpendicular to the c-axis, give evidence of relictic magmatic growth zonation in plagioclase. In some crystals, alignment of fluid inclusions along single twin lamellae was observed.

Aside from this dominant type of fluid inclusions hosted by plagioclase, accessory xenomorphic quartz also contains some inclusions. These are approximately 3–10 μm in size, rounded to negative crystal shape. In general they comprise an aqueous liquid and a carbonic vapour phase, the latter occupying from 30 vol% up to an apparent total fill (Fig. 8.4e). Decrepitation clusters occur around some inclusions that contain only a carbonic vapour phase (Fig. 4f).

Composition of plagioclase adjacent to fluid inclusions

Electron microprobe analysis reveals that there is no evidence for significant chemical gradients in feldspar around single fluid inclusions (Fig. 5). Potassium variation is close to nil whereas for Al, Ca and Na show ranges of c. 2 wt% (Fig. 5). No systematic relationship between composition and distance from inclusion could be detected. The average composition of plagioclase around this particular inclusion is $An_{46}Ab_{53}Or_1$ to $An_{53}Ab_{46}Or_1$ (see Appendix A, Table A1).

Microthermometry and Raman microspectrometry of the enclosed fluid

Upon cooling from room temperature, the inclusions first nucleate a gas bubble around 0 °C before supercooling leads to the formation of a solid phase around –90 °C. Upon heating, melting of the solid phase occurs within a narrow temperature range of –57.8 to –56.8 °C (Fig. 6 and Table 1). CO_2 was confirmed by Raman microspectrometry as being the major gaseous component within all fluid inclusions hosted by plagioclase. The lowering of the final melting temperature of pure CO_2 is caused by the addition of small amounts of N_2 (maximally 2 mol%) whereas CH_4 and H_2O were never detected. All fluid inclusions homogenise into the liquid phase over a broad temperature interval of –1.8 to 27.3, with the majority homogenising between 14 to 20 °C (Fig. 6 and Table 1). There is no systematic relationship between Th and Tm.

Quartz-hosted fluid inclusions reveal a similar CO_2-melting point of –57.7 °C and additional clathrate melting was observed around 7.9 °C. Homogenisation of CO_2 occurred at 18.7 °C into the liquid phase. The calculated salinity obtained from the clathrate melting temperature is equivalent to 4.2 wt% NaCl. In addition to CO_2, small amounts of N_2 were identified with Raman microspectrometry. The presence of H_2O was even confirmed in those inclusions that did not show a visible aqueous rim (e.g. Fig. 4f). Entrapped minerals were not detected within these inclusions.
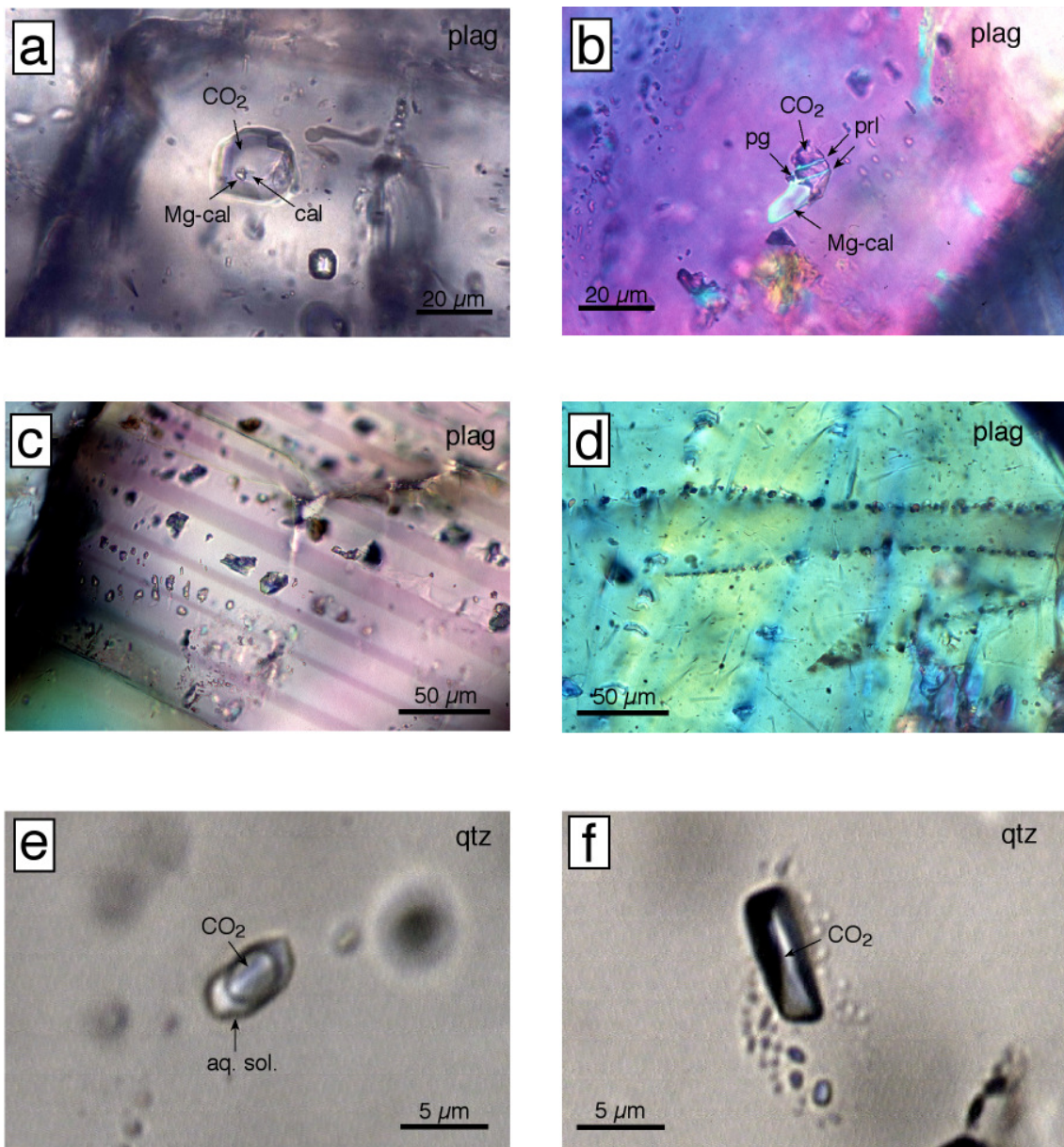
Fig. 4: *Microphotographs of CO_2-rich fluid inclusions hosted by plagioclase: (a) negative-crystal shaped inclusions containing carbonate crystals; (b) containing various birefringent crystals; (c) cluster between albite twins; (d) pseudosecondary trails; (e) two phase inclusion in quartz, containing a CO_2-rich bubble and a H_2O-rich rim; (f) decrepitation cluster around an apparently carbonic-rich fluid inclusion in quartz.*
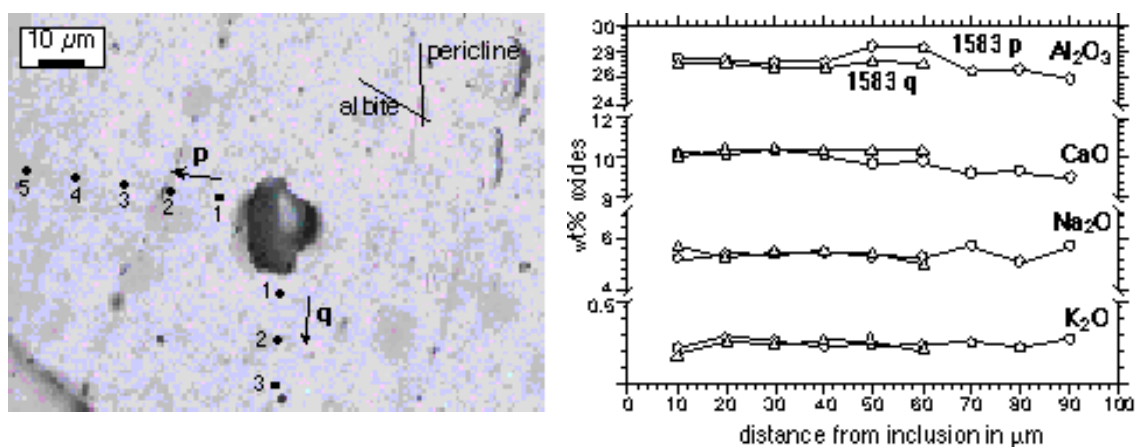
Fig. 5: *Al$_2$O$_3$, CaO, Na$_2$O and K$_2$O concentrations (in wt%) along two profiles around a fluid inclusion. "0 µm" marks the inclusion wall. Profiles "p" and "q" are perpendicular to each other. The orientation of albite and pericline twins is schematically indicated by thin lines.*
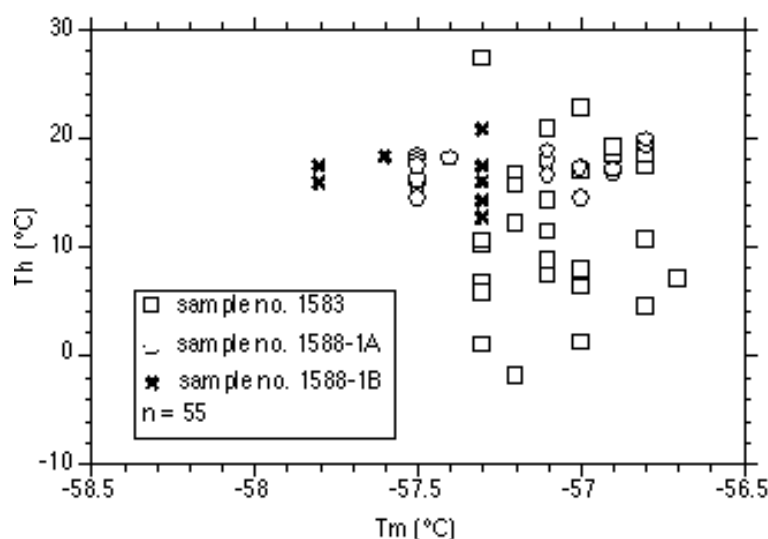

Fig. 6: *Th-Tm plot of CO$_2$-dominated fluid inclusions hosted by plagioclase. Freezing-point depression is caused by N$_2$-contents of up to 2 mol%; all inclusions homogenise into the liquid phase.*

Raman microspectrometry of enclosed solids

Because of their high refractive index compared to the surrounding plagioclase, carbonate crystals entrapped in fluid inclusions can easily be identified by optical microscopy (Fig. 8.4b). Raman spectrometry is able to detect even slight variations in carbonate composition (Bischoff, 1985), and a shift of Raman peaks from 284, 714 and 1087 cm^{-1} to 283, 711 and 1085 cm^{-1} shows, that the enclosed minerals are Mg-enriched (< 10 mol% MgCO$_3$) or pure calcite (Table 1), respectively.

Sheet silicates are often located at the inclusion walls or at carbonate crystal faces and may easily be overlooked in small or dark fluid inclusions. The Raman peaks of muscovite and paragonite are similar, not further differentiated in this study and therefore more generally referred to as di-octahedral mica. Nevertheless, paragonite is

thought to makeup most of the enclosed mica, as potassium is only a minor component of the feldspar host. The Raman spectra for di-octahedral mica and pyrophyllite are similar up to a Raman shift of about 1200 cm^{-1} (Fig. 7). Both have an intense peak at 264 cm^{-1}, whereas the second peak is slightly higher for pyrophyllite (708 cm^{-1}) than for di-octahedral mica (702 cm^{-1}). Most diagnostic peaks appear at higher wavenumbers, between 3600 and 3700 cm^{-1}, where different types of O-H bonds in the mineral structure are detectable. The sharp peak for pyrophyllite at 3674 cm^{-1} is clearly distinct from the broad peak for di-octahedral mica at 3626 cm^{-1} (Fig. 7b). Both minerals were identified within fluid inclusions where they appear as individual crystals or intergrown aggregates (Fig. 7, Table 1).
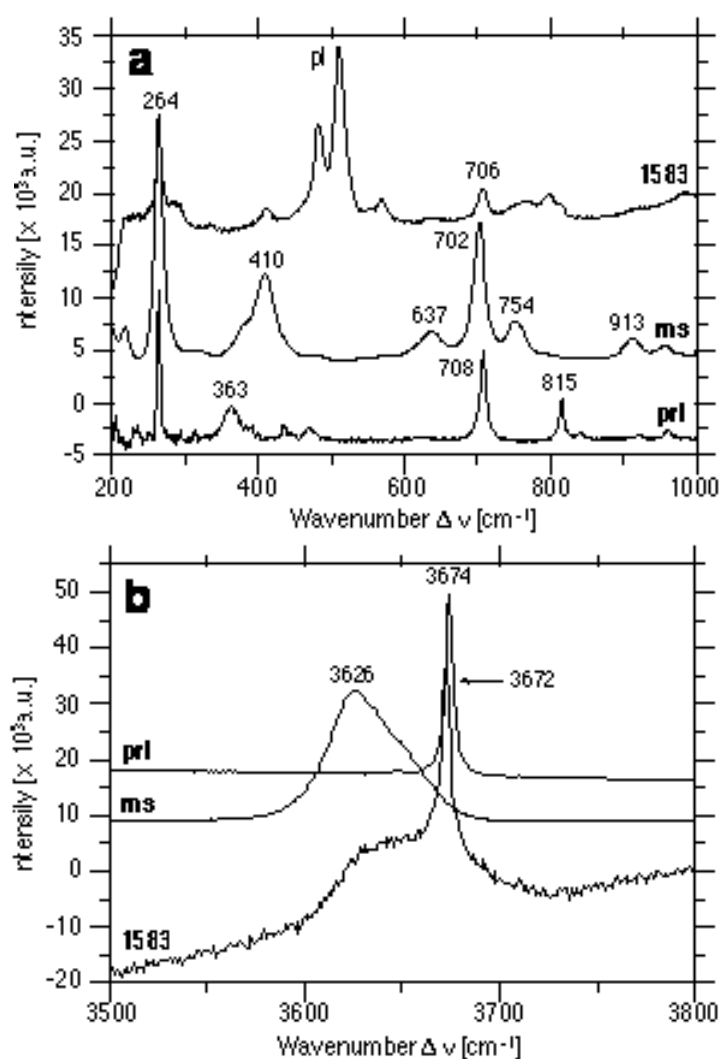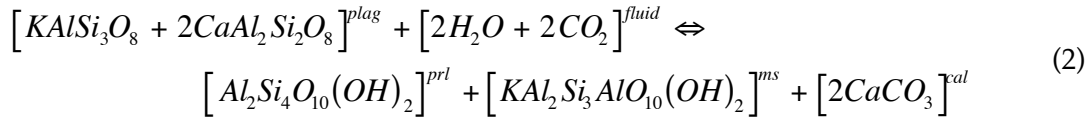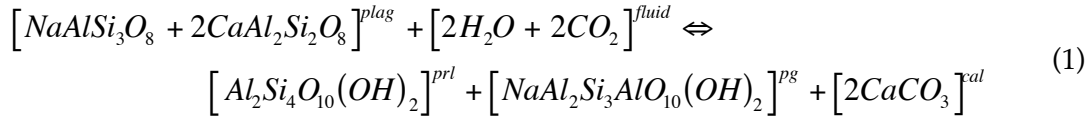

Fig. 7. *Raman spectra of sheet silicates from sample 1583 in different ranges of the Raman shift Δv: (a) 200 to 1000 cm^{-1}; (b) 3500 to 3800 cm^{-1}. Standard spectra of muscovite (ms) (substitutional for the di-octahedral micas) and pyrophyllite (prl) are indicated as a reference. pl = background peak of plagioclase host.*

Discussion

The microchemical reaction

Fluid-inclusion studies have proved that feldspar-hosted inclusions from the O.-v.-Gruber anorthosite body commonly contain a dense CO_2-rich gas mixture together with different volume fractions of solids, i.e. calcite, pyrophyllite and a di-octahedral mica. The frequent occurrence of this characteristic feature throughout the samples rules out the possibility of accidental trapping (capturing). Additionally, the lack of H_2O, and the varying amounts of solids present suggest that it is very unlikely that the solids formed as daughter crystals out of a supersaturated fluid/melt. It is therefore assumed that the solids have developed as products of reaction (1) or (2).

$$\left[NaAlSi_3O_8 + 2CaAl_2Si_2O_8 \right]^{plag} + \left[2H_2O + 2CO_2 \right]^{fluid} \Leftrightarrow$$
$$\left[Al_2Si_4O_{10}(OH)_2 \right]^{prl} + \left[NaAl_2Si_3AlO_{10}(OH)_2 \right]^{pg} + \left[2CaCO_3 \right]^{cal} \tag{1}$$

$$\left[KAlSi_3O_8 + 2CaAl_2Si_2O_8 \right]^{plag} + \left[2H_2O + 2CO_2 \right]^{fluid} \Leftrightarrow$$
$$\left[Al_2Si_4O_{10}(OH)_2 \right]^{prl} + \left[KAl_2Si_3AlO_{10}(OH)_2 \right]^{ms} + \left[2CaCO_3 \right]^{cal} \tag{2}$$

As the plagioclase is low in potassium (Fig. 2), it is more likely that reaction (1) predominated during the interaction between the host mineral and the fluid. The thermodynamic data of the individual components involved in the reaction were taken into account to determine the P-T stability field of products and reactants (Appendix B). The proposed reaction within fluid inclusions takes place if the rock P-T conditions move into the stability field of the products. The position of the reaction curves in a P-T diagram is dependent on the initial fluid composition (Fig. 8). A mixture of 50 mol% H_2O and 50 mol% CO_2 defines the maximum reaction temperature in the amphibolite facies, whereas the reaction temperatures are lower for all other mixtures. The immiscibility fields of H_2O-CO_2 mixtures, according to Tödheide & Franck (1963), do not interfere with the reaction for any fluid composition (Fig. 8 and Appendix B). The immiscibility fields of CO_2-rich fluids in the H_2O-CO_2-NaCl system also do not have interference with the reaction (Appendix B). Reaction (1) occurs at temperatures well below those given for metamorphic conditions in cDML by Markl & Piazolo (1998) and therefore it must have taken place at a late stage of crustal evolution (post M4). The presence of carbonate and sheet silicates in most fluid inclusions indicates that the reaction has indeed proceeded. The occurrence of sheet silicates requires the presence of H_2O within the inclusions before the reaction took place.
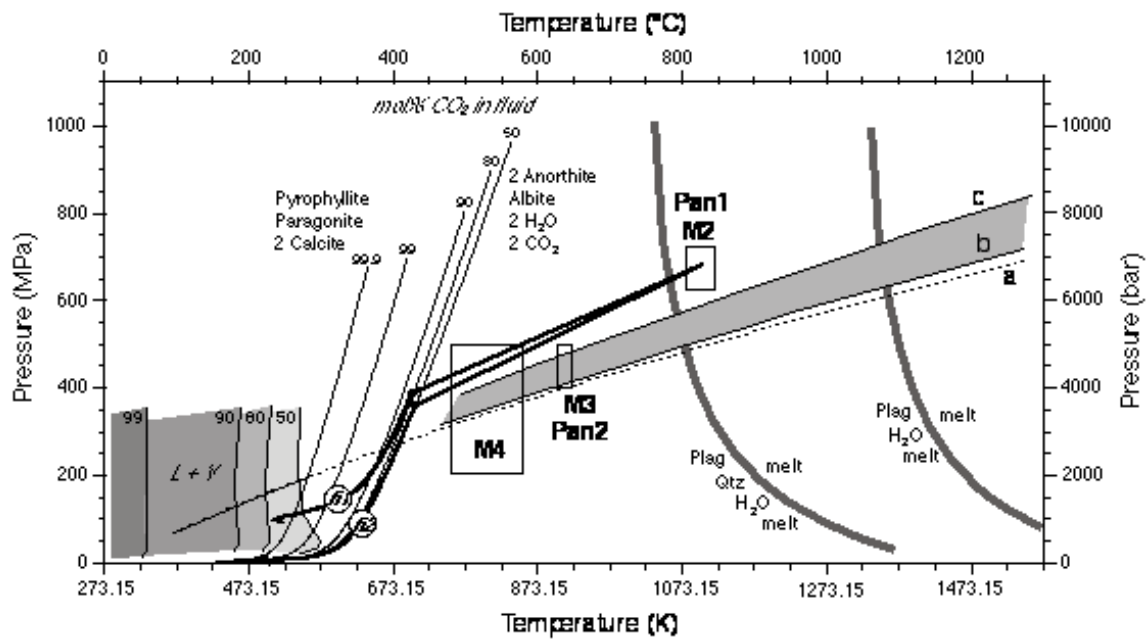
Fig. 8: Temperature-pressure diagram with reaction curves calculated for fluid compositions of 50, 80, 90, 99 and 99.9 mol% CO_2. The immiscibility field of the corresponding H_2O-CO_2-fluid mixture after Tödheide & Franck (1963) is illustrated at relatively low temperatures (L+V). M2, M3 and M4 indicate the metamorphic conditions as described in the text. Pan1 and Pan2 illustrate the P-T conditions of the Pan-African event, collisional stage I and II, respectively. Isochores for hypothetical inclusions fi1 and fi2 that formed at M2, and the path of reaction progress according to the change in fluid composition during interaction between fluid and host-mineral are shown by thick black lines. The isochore for inclusion 1583-3-08, presently containing pure CO_2 is indicated by dashed curve a. Also shown are corrected isochores according to our model (curve b for 97.2 mol% CO_2 and 45.55 cm^3mole^{-1}, and curve c for 93.6 mol% CO_2 and 42.66 cm^3mole^{-1}). The shaded area between curve b and c represents the uncertainty in the reconstruction of this specific inclusion. The approximate liquidi of the systems An-Ab-H_2O and An-Ab-Qtz-H_2O, according to Johannes (1978, 1989) are illustrated at relatively high temperatures (thick grey lines), indicating possible formation conditions of fluid inclusions in crystallising plagioclase.

The quartz hosted fluid inclusions have a comparable distribution and contain similar gaseous components. Therefore it is suggested that both, quartz- and plagioclase-hosted inclusions, have a common origin. As quartz is non-reactive and these inclusions still contain small amounts of H_2O (Fig. 4e), the original fluid composition in plagioclase is considered to have had a water component, too. We propose that a CO_2-H_2O-rich fluid was originally trapped as fluid inclusions, and that this reacted with its plagioclase host, leading to complete consumption of the subordinate aqueous fluid-component, the formation of a residual carbonic liquid and the crystallisation of carbonates and sheet silicates (Fig. 9a, c). The actual fluid preserved in quartz must not unequivocally reflect the original fluid properties as quartz-hosted inclusions might have changed by mechanical and diffusional processes since their formation. These reequilibration processes may result in decrepitation and preferential water loss as has been proved by experimental work (e.g. Sterner &

Bodnar, 1989; Bakker & Jansen, 1991). Decrepitation clusters and a variation in the enclosed amount of water have been observed in fluid inclusions in quartz (Fig. 4f).

The lack of any carbonates or sheet silicates in some of the plagioclase-hosted CO_2-rich inclusions and the variable volume fraction of the reaction products can be explained by a variation in the original fluid composition. Furthermore, the same reequilibration processes that have previously been described for quartz may have effected the plagioclase. Microstructures preserved in plagioclase crystals imply, that these processes have occurred (Fig. 3). Kinetics may be responsible for the non-completion of reactions which again results in a diversity of inclusion contents.
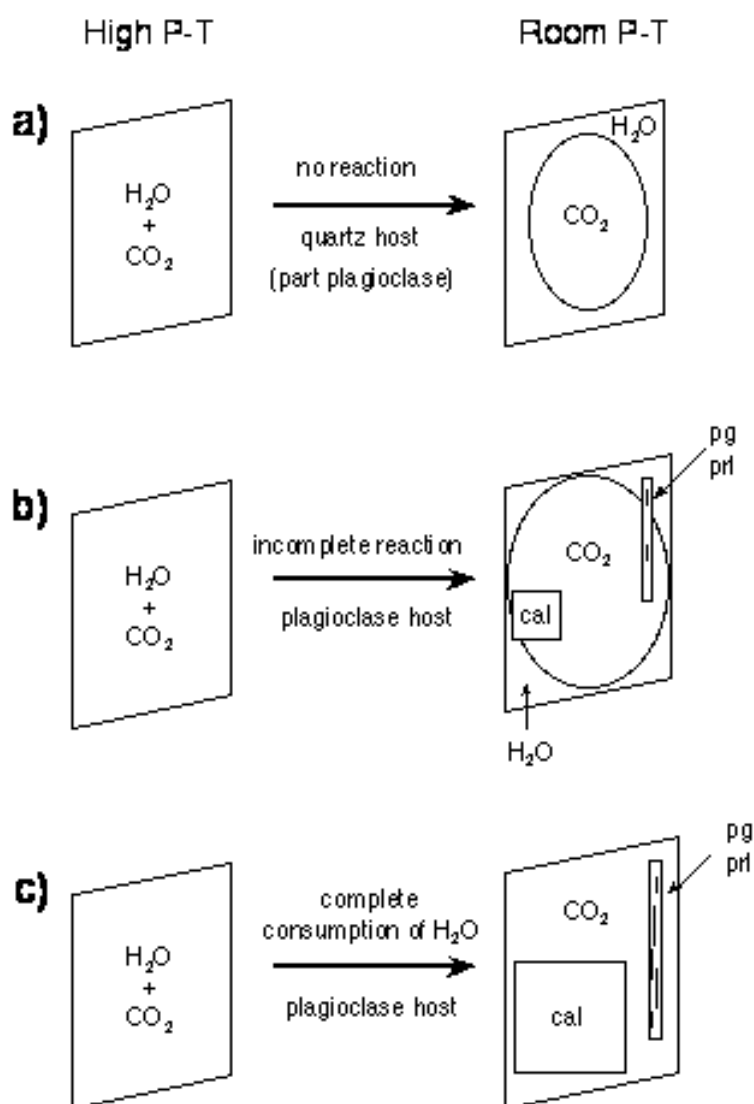
Fig. 9: Schematic reaction progress in a closed fluid-inclusion system with an originally homogeneous H_2O-CO_2 fluid not containing any solid phases at high P-T. a) No reaction for inclusions in quartz and part of the plagioclase. b) After occurrence of part of the reaction in only plagioclase. c. After complete consumption of H_2O and formation of larger calcite, paragonite and pyrophyllite volume fractions.

The model

Considering a fluid inclusion as a closed system, a quantitative model was established to describe volumetric and compositional changes caused by reaction (1). Two hypothetical fluid inclusions of the H_2O-CO_2 binary (*fi1* and *fi2* in Fig. 8) are assumed to have been trapped at M2 metamorphic conditions, with initial fluid compositions of 80 mol% CO_2 and 50 mol% CO_2, respectively (molar volumes are 38.93 cm^3mol^{-1} and 33.32 cm^3mol^{-1} respectiveley). With favourable kinetics, both inclusions start to react when the system reaches the corresponding reaction curves at about 450 °C. With progressive reaction, these inclusions develop in different ways. The molar volume of *fi1* reaches a maximum value of about 59.5 cm^3mol^{-1} at lower temperatures, which is a nearly pure CO_2 liquid-like fluid, whereas *fi2* continuously increases its molar volume up to a vapour-like fluid (Fig. 10a). The fluid composition in *fi2* does not change. The *Fi1* volume percentages will be 10.7 calcite, 18.5 pyrophyllite and 19.1 paragonite after the reaction is nearly complete at lower temperatures (Fig. 10b). The volume percentages of solid reaction products in *fi2* are higher, i.e. 16.9 calcite, 29.3 pyrophyllite and 30.3 paragonite. These amounts may not be reached if the reaction ceases when the kinetics becomes unfavourable at lower temperatures. Vice versa, the evaluation of the amount of reaction products allows the recalculation of the composition and molar volume of the initial fluid.

Using a natural example, fluid inclusion *1583-3-08* (Table 1) presently contains a dense pure CO_2 liquid, c. 5 vol% calcite and c. 7 vol% of paragonite and pyrophyllite as visually estimated, corresponding to 1.355 mmole and 0.54 mmole, respectively, in a hypothetical fluid inclusion of 1 cm^3 total volume. At 1.0 °C, its CO_2 content homogenises to the liquid phase, which corresponds to a molar volume of 47.77 cm^3mol^{-1}, or a total mount of 18.42 mmole CO_2 in 1 cm^3 total volume. In order to model the density change of the fluid phase, the equation from Andersen *et al.* (1984) has been slightly modified to take into consideration the temperature and pressure effect on molar volumes of the solid phases (from Berman, 1988). To reverse reaction (1) and recalculate the original fluid composition and density, there are two possible formulations with which to start. First, the estimated amount of bound H_2O in sheet silicates (7 vol%) is used as fixed parameter. In this case, 0.54 mmole of H_2O and CO_2 is calculated to have been consumed by the reaction with the formation of 0.54 mmole calcite and sheet silicates. Therefore the original inclusion must have contained 0.54 mmole H_2O and 18.96 mmole CO_2 (i.e. 2.8 mol% H_2O and 97.2 mol% CO_2) resulting in a molar volume of this fluid of 45.55 cm^3mol^{-1}. However, the actual inclusion contains a total amount of 1.355 mmole calcite, meaning that there is 0.815 mmole calcite in excess (i.e. 3 vol%). This suggests that part of the observed carbonate may have been accidentally trapped during initial inclusion formation, or perhaps the measurement of

7 vol% of sheet silicates is in error.

In the second approach, calculations were performed assuming that calcite will be consumed completely during the inversion of reaction (1). In this case, more sheet silicates than the amount estimated by optical observations must be taken into account for the reaction to proceed, i.e. 0.6775 mmole paragonite and 0.6775 mmole pyrophyllite. Sheet silicates often form as thin layers on inclusion walls and on carbonates, and might therefore be easily overlooked during optical microscopy. As illustrated in Fig. 10b, the calculated amount of sheet silicates produced by the progress of reaction (1) is always higher than the amount of carbonates. This situation is in agreement with the observed room-temperature volume ratios of carbonates to sheet silicates. The initial fluid derived in this way contains 6.4 mol% H_2O and 93.6 mol% CO_2, with a molar volume of 42.66 cm^{3}mol^{-1}.

After reaction (1) has completed, the maximum amount of calcite within fluid inclusions that formed at M2 conditions is about 16.9 vol% (see Fig. 10b). However, several observed inclusions are estimated to contain up to 34 vol% calcite, e.g. inclusion no. *1583-3-07* (Table 1). Taking into account difficulties in volume-fraction estimations of sheet silicates, this inclusion would have originally contained 28.6 mol% H_2O and 71.4 mol% CO_2, with an extremely high molar volume of 24.99 cm^{3}mol^{-1}. These reconstructed fluid properties are unrealistic within the known framework of geological events for the samples. It is therefore likely that part of the calcite was indeed accidentally trapped. As the plagioclase also contains small solid inclusions of pure carbonate, it is possible that the fluid inclusions are pinned to its grain-boundaries.

Although the model results diverge slightly from the estimated volume percentages of the solid phases at room temperature, they accord with respect to the characteristics of the original fluid inclusion: it must have contained some water, it was of higher density, and the formation of solid phases via reaction with the inclusion walls reduced the total free fluid volume by about 1 to 2.5 vol%. Thus, cooling of the host rock from M2 metamorphic conditions caused a simultaneous decrease in density and total volume, while at the same time various solids formed upon complete consumption of the aqueous component.
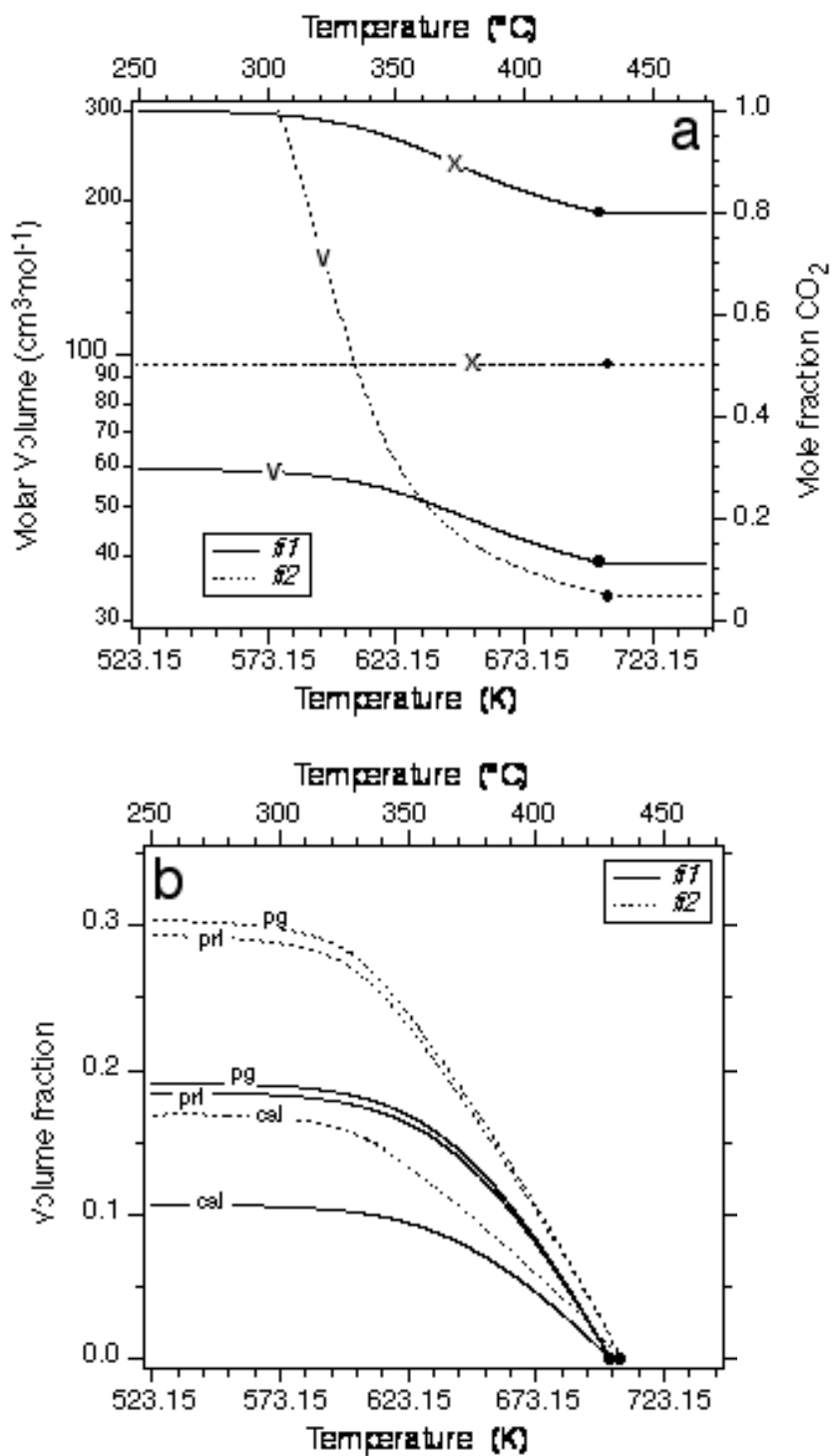
Fig. 10: *Influence of the retrograde reaction on hypothetical fluid inclusions fi1 (initially 80 mol% CO_2) and fi2 (initially 50 mol% CO_2). The solid dots indicate the starting point of the reactions. a) The change in molar volume and fluid composition caused by cooling after the reaction curves are reached at about 450 °C. b) Amount of solid reaction products forming during cooling.*

Reconstructed isochores

Recalculated isochores of the assumed original fluid compositions and densities, e.g. lines b and c in Fig. 8, are shifted towards higher pressures than those estimated for the present state of inclusions at room temperature (line a in Fig. 8.8). Considering the fluid inclusions formed at an early stage of the rock development, they may have originated immediately after crystallisation of a plagioclase-rich melt of intermediate composition. The pseudo-secondary character of most inclusion trails confirms this early formation at granulite facies conditions. As the presence of a host crystal is a necessity for the formation of fluid inclusions, the liquidus of the plagioclase system theoretically defines the maximum formation conditions. However, it is more likely that inclusions formed shortly after completion of the crystallisation of the magma, i.e. at solidus conditions. The original magma systems must have contained certain amounts of dissolved CO_2 and H_2O. The system albite-anorthite-H_2O (Johannes, 1978) has a liquidus at about 1100 °C at 500 MPa water pressure (Fig. 8.8). The addition of small amounts of quartz to this system can drastically lower the liquidus temperature to about 800 °C at 500 MPa and to about 900 °C at 200 MPa (Johannes, 1978, 1989). Data for a CO_2 bearing system are not available, but it will transpose both liquidus and solidus to higher pressures at a selected temperature.

The intersection of the corrected isochores from fluid inclusion 1583-3-08 (Fig. 8.8) with the albite-anorthite-H_2O liquidus are at about 1080 °C and 650-730 MPa. However, much higher pressures will be obtained from those inclusions that contain a higher volume percentage of reaction products. This may give important constraints on possible P-T conditions for the emplacement of the anorthositic magmas between M1 and M2 metamorphism (Jacobs *et al.*, 1998), which could not be estimated by other means.

Conclusions

The combined use of laser-Raman spectrometry and microthermometry has characterised a complete micro-chemical reaction system hosted by plagioclase. Submicroscopic phases (fluid and solid) covering inclusion walls, and optically visible solids were identified as carbonates, muscovite/paragonite and pyrophyllite, together with a nearly pure, dense CO_2 fluid phase. These solids are assumed to have developed as products of reaction between the fluid and its host. The OH-bearing sheet silicates are interpreted as proof of an aqueous component within the originally entrapped fluid. The amount of H_2O initially available in the trapped fluid is considered to control the extent of the retrograde reaction. With all involved phases identified, the reaction was thermodynamically modelled and the P-T stability conditions of products

and reactants were determined, as a function of the fluid compositions. Quantitative analysis on the basis of volume estimates of the solid reaction-products found in plagioclase-hosted fluid inclusions were used to recalculate the composition and molar volume of the original fluid. The deviation in the ratio of carbonate to sheet silicates formed within the hypothetical and the real inclusions lies within the uncertainty limits of the method. Thin layers of sheet silicates can be easily overlooked during microscopy and it is possible that part of the carbonate was accidentally trapped at the time of inclusion formation. The results have shown that detailed fluid inclusion studies combined with thermodynamic modelling can be used to trace back and evaluate the changes that a fluid inclusion has undergone since its formation. Thus, valuable petrogenetic information can be derived and used for more precise estimation of P-T conditions during earlier metamorphic stages or fluid entrapment.

Acknowledgements

Appendix A

Table A1.: Microprobe analysis of plagioclase around the fluid inclusion illustrated in Fig. 5.

Sample   O.-v.-Gruber anorthosite - sample no.1583

Mineral   Plagioclase

Analysis	p.1	p.2	p.3	p.4	p.5	p.6	p.7	p.8	p.9	q.1	q.2	q.3	q.4	q.5	q.6
SiO_2	54.57	55.05	55.15	56.03	54.73	54.50	56.34	55.66	56.36	56.19	55.52	56.01	56.31	53.97	54.97
TiO_2	0.00	0.00	0.00	0.00	0.00	0.00	0.00	0.00	0.00	0.00	0.00	0.00	0.00	0.00	0.00
Al_2O_3	27.40	27.23	27.11	27.14	28.27	28.23	26.48	26.58	25.89	27.02	27.01	26.63	26.67	27.20	27.04
Cr_2O_3	0.00	0.00	0.00	0.00	0.00	0.00	0.00	0.00	0.00	0.00	0.00	0.00	0.00	0.00	0.00
FeO	0.10	0.17	0.17	0.10	0.07	0.15	0.10	0.12	0.07	0.05	0.17	0.05	0.07	0.17	0.10
Fe_2O_3	0.00	0.00	0.00	0.00	0.00	0.00	0.00	0.00	0.00	0.00	0.00	0.00	0.00	0.00	0.00
MgO	0.05	0.05	0.05	0.00	0.00	0.00	0.10	0.00	0.05	0.00	0.05	0.05	0.00	0.05	0.10
MnO	0.00	0.00	0.00	0.00	0.00	0.00	0.00	0.00	0.00	0.00	0.00	0.00	0.00	0.00	0.00
CaO	10.13	10.01	10.24	10.05	9.63	9.69	9.19	9.22	8.92	9.96	10.30	10.31	10.15	10.30	10.28
Na_2O	5.18	5.37	5.37	5.45	5.26	5.26	5.70	5.08	5.70	5.62	5.19	5.45	5.36	5.37	4.92
K_2O	0.21	0.27	0.25	0.22	0.23	0.23	0.26	0.22	0.27	0.17	0.25	0.23	0.25	0.24	0.21
Total	97.64	98.15	98.34	98.99	98.19	98.06	98.17	96.88	97.26	99.01	98.49	98.73	98.81	97.30	97.62
Si	2.51	2.52	2.52	2.54	2.50	2.50	2.57	2.57	2.59	2.55	2.53	2.55	2.56	2.50	2.53
Al(IV)	0.00	0.00	0.00	0.00	0.00	0.00	0.00	0.00	0.00	0.00	0.00	0.00	0.00	0.00	0.00
Al	1.49	1.47	1.46	1.45	1.52	1.52	1.42	1.45	1.40	1.44	1.45	1.43	1.43	1.49	1.47
Ti	0.00	0.00	0.00	0.00	0.00	0.00	0.00	0.00	0.00	0.00	0.00	0.00	0.00	0.00	0.00
Cr	0.00	0.00	0.00	0.00	0.00	0.00	0.00	0.00	0.00	0.00	0.00	0.00	0.00	0.00	0.00
Fe^{2+}	0.00	0.01	0.01	0.00	0.00	0.01	0.00	0.00	0.00	0.00	0.01	0.00	0.00	0.01	0.00
Fe^{3+}	0.00	0.00	0.00	0.00	0.00	0.00	0.00	0.00	0.00	0.00	0.00	0.00	0.00	0.00	0.00
Mg	0.00	0.00	0.00	0.00	0.00	0.00	0.01	0.00	0.00	0.00	0.00	0.00	0.00	0.00	0.01
Mn	0.00	0.00	0.00	0.00	0.00	0.00	0.00	0.00	0.00	0.00	0.00	0.00	0.00	0.00	0.00
Ca	0.50	0.49	0.50	0.49	0.47	0.48	0.45	0.46	0.44	0.48	0.50	0.50	0.49	0.51	0.51
Na	0.46	0.48	0.48	0.48	0.47	0.47	0.50	0.45	0.51	0.49	0.46	0.48	0.47	0.48	0.44
K	0.01	0.02	0.01	0.01	0.01	0.01	0.02	0.01	0.02	0.01	0.01	0.01	0.01	0.01	0.01
Ab	0.513	0.499	0.505	0.498	0.496	0.497	0.464	0.494	0.456	0.490	0.515	0.504	0.504	0.507	0.529
An	0.474	0.485	0.479	0.489	0.490	0.489	0.521	0.492	0.528	0.500	0.470	0.482	0.481	0.479	0.458
Or	0.013	0.016	0.016	0.013	0.014	0.014	0.015	0.014	0.016	0.010	0.015	0.014	0.015	0.014	0.013

Appendix B

Thermodynamics of Reaction

The coefficients in the formula for heat capacity and standard state properties of the minerals and gases involved in reaction 1 and 2 are taken from Berman (1988). The temperature and pressure dependency of molar volumes of minerals is also taken from Berman (1988). The Gibbs free energy calculation (Eq. B1) was used to determine the reaction in p-T-V-x space.

$$\Delta_R G \;=\; \sum_i v_i G_i \;=\; 0 \tag{B1a}$$

$$\Delta_R G \;=\; G_{prl} \;+\; G_{pg} \;+\; 2G_{cal} \;-\; G_{ab} \;-\; G_{an} \;-\; 2G_{H_2O} \;-\; 2G_{CO_2} \;=\; 0 \tag{B1b}$$

where v and G are the stoichiometric coefficient and the molar Gibbs free energy of the indicated phase, respectively. For each phase the change of Gibbs free energy with temperature, pressure and composition is expressed according to equation (B2).

$$dG \;=\; \left(\frac{\partial G}{\partial T}\right)_{P,n_i} dT \;+\; \left(\frac{\partial G}{\partial P}\right)_{T,n_i} dP \;+\; \sum_i \left(\frac{\partial G}{\partial n_i}\right)_{T,P,n_j} dn_i \tag{B2a}$$

$$\left(\frac{\partial G}{\partial n_i}\right)_{T,P,n_j} \;=\; \mu_i \tag{B2b}$$

where T, P, and n are temperature, pressure and the amount of component i given in moles, respectively. μ_i is the chemical potential of component i. The reaction (1) involves a fluid mixture and a plagioclase mixture, whereas the reaction products pyrophyllite, paragonite and calcite are pure phases. Although, paragonite may include a calcium component and calcite may include a sodium component, the mass balance easily indicates that both margarite and sodium carbonate can not be obtained from the specific reactants in reaction (1), which is confirmed by Raman microspectrometry. The chemical potential of a component i in a mixture is calculated according to equation (B3).

$$\mu_i(T,P,x) \;=\; \mu_i^{pure}(T,P) \;+\; RT\ln\!\left(a_i\right) \tag{B3}$$

where x and a are the mole fraction and the activity of component i, respectively. This equation is also valid for pure phases, where the activity equals unity. The standard state condition for the fluid mixture is the thermodynamic properties of the pure components at the given temperature and 0.1 MPa, whereas properties of the

pure components at the given temperature and pressure is the standard condition for the plagioclase. The chemical potential at standard conditions is obtained from the integration of the temperature and pressure dependent parameters in equation (B2a) (eq. B4),

$$\int_{T_0}^{T}\left(\frac{\partial G}{\partial T}\right)_{P_0,n_i}dT \;=\; \int_{T_0}^{T}(Cp)_{P_0,n_i}\,dT \;-\; S^0\cdot(T-T_0) \;-\; T\cdot\int_{T_0}^{T}\left(\frac{Cp}{T}\right)_{P_0,n_i}dT \tag{B4a}$$

$$\int_{P_0}^{P}\left(\frac{\partial G}{\partial P}\right)_{T,n_i}dP \;=\; \int_{P_0}^{P}(V)_{T,n_i}\,dP \tag{B4b}$$

where S^0 is the standard state entropy, Cp is the heat capacity at constant pressure, V is the molar volume, and T_0 and P_0 are the standard conditions, respectively.

The activity of fluid components is defined by the fugacities (f) of H_2O and CO_2 (eq.B5),

$$a_i \;=\; \frac{f_i(T,P)}{f_i^{pure}(T,P)} \tag{B5}$$

where i is either H_2O or CO_2. The fugacity of H_2O and CO_2 in gas mixtures was calculated with the modified Redlich-Kwong equation of state according to Holloway (1977, 1981) and Flowers (1979). This equation is the most accurate available thermodynamic model representing experimental fugacities of CO_2-H_2O fluids within the temperature and pressure limits of the reaction. The fugacity of fluid components in the ternary H_2O-CO_2-NaCl system are calculated with the equation of state from Anderko & Pitzer (1993) and Duan *et al.* (1995). The boundaries of the immiscibility field of CO_2-rich fluid mixtures are highly inaccurately estimated by this equation. Therefore, it is only applied to homogeneous mixtures.

The activities of albite and anorthite in the plagioclase are obtained from a non-ideal mixing model for ternary feldspar according to Elkins & Grove (1990). This model is an empirical fit to experimental data on the feldspar composition at temperatures between 600 and 900 °C, and at pure H_2O pressures between 100 MPa and 300 MPa. Although reaction (1) occurs at temperatures well below this fit, it is assumed that the estimated ternary Margules expression is also valid at lower temperatures.

The effect of several mixing models on the fluid and the plagioclase of reaction (1) is illustrated in Fig. B1.
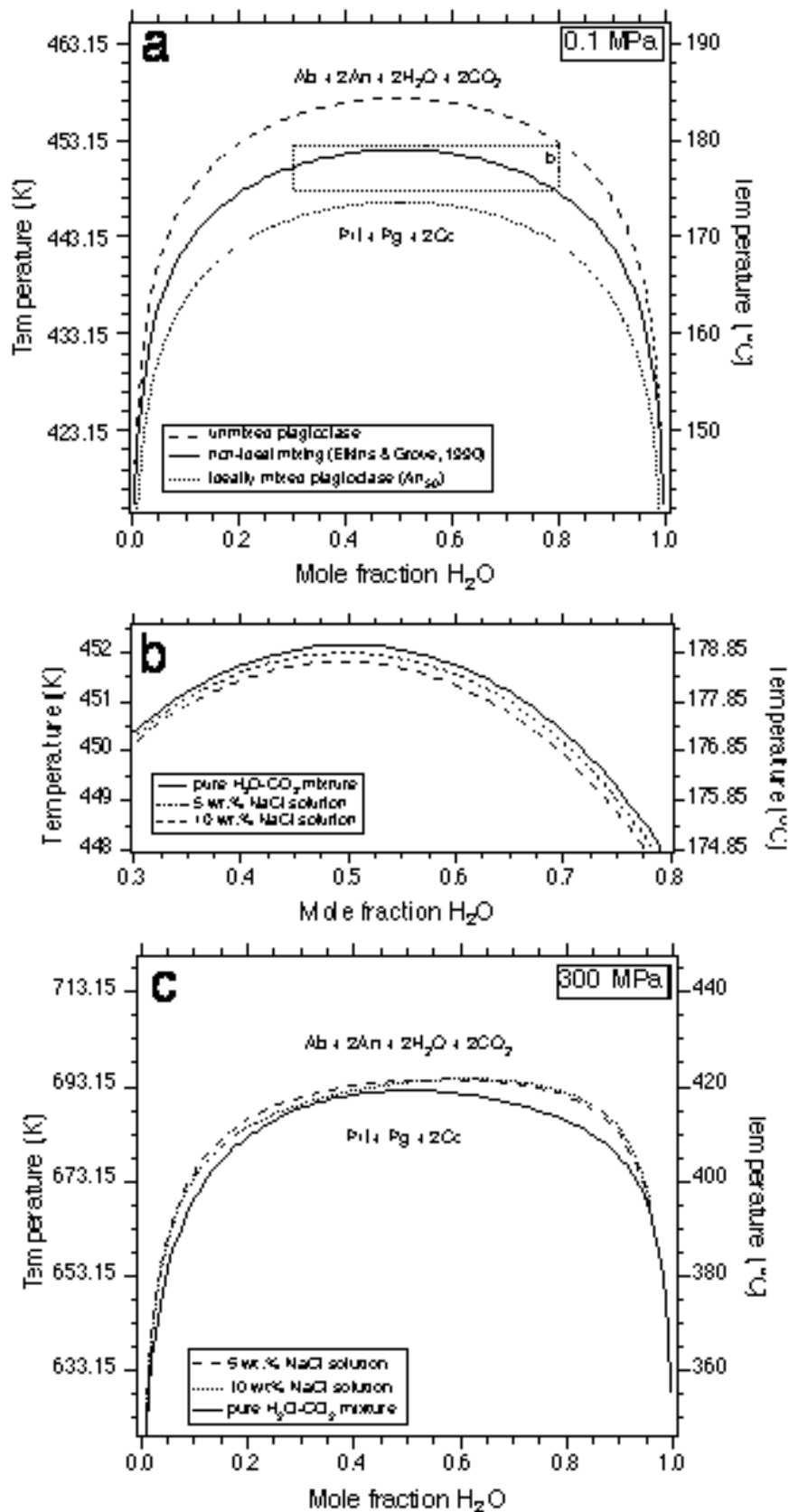
Fig. B1: *Fluid composition (CO₂-H₂O) - temperature diagrams with reaction (1) according to different mixing models for the plagioclase at 0.1 MPa (**a**), the influence of 5 and 10 wt% NaCl solution at 0.1 MPa (**b**), and the reaction curve at 300 MPa with 5 and 10 wt% NaCl solution (**c**). The salinity is expressed relative to the amount of H₂O.*

For any pressure, the maximum reaction temperature is defined at a fluid composition of approximately 50 mol% CO_2 and 50 mol% H_2O. The ideal mixing model for plagioclase causes a decrease of about 10 °C of the reaction temperature for any fluid composition compared to a model with unmixed plagioclase (Fig. B1a). The non-ideal mixing model of plagioclase according to Elkins & Grove (1990) puts the reaction curve about 5 °C higher than the ideal mixing model. Addition of small amounts of NaCl to the fluid mixture has a minor effect on the reaction temperature (Fig. B1b). In H_2O-rich fluids the reaction temperature is decreased by 0.2 and 0.5 ° for a 5 wt% and a 10 wt% NaCl solution, respectively. Additional NaCl in CO_2-rich fluids is a negligible factor. At higher pressures (Fig. B1c), the reaction curve is asymmetrical in a T-x diagram due to differences in the activities of H_2O and CO_2. The immiscibility field of H_2O-CO_2 mixtures is elevated to higher pressures and temperatures if certain amounts of NaCl are added to the system (Fig. B2).
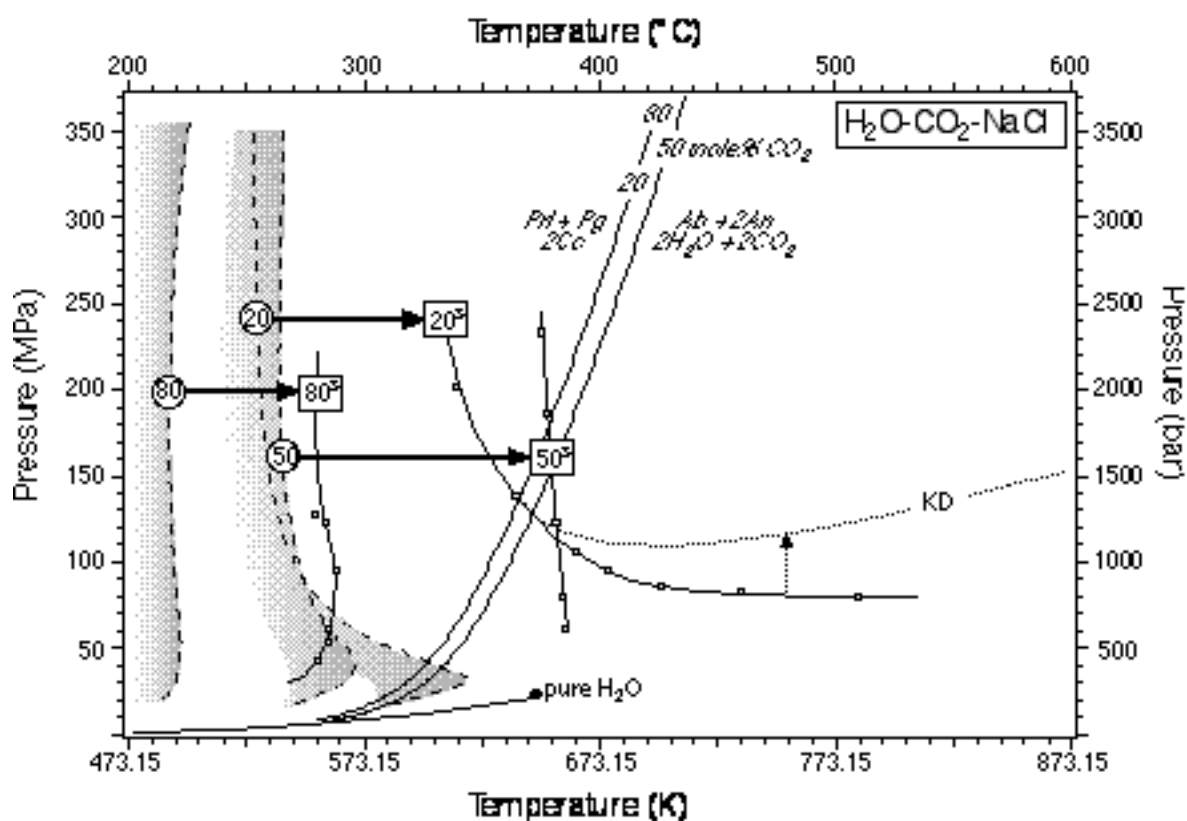
Fig. B2: *Temperature - pressure diagram with the solvi of H_2O-CO_2 fluid mixtures (dashed curves) and the solvi of H_2O-CO_2 fluid mixtures with 6 wt% NaCl (solid curves). The numbers 80, 50, and 20 denote the mole percentage of CO_2. The superscript [S] indicates the addition of 6 wt% NaCl to the corresponding fluid. The open circles are experimental data from Gehrig (1984). KD marks the corrected solvus of a 21.01 mol% CO_2, 77.47 mol% H_2O and 1.52 mol% NaCl fluid mixture (i.e. 6 wt% NaCl) according to Krüger & Diamond (2001). The reaction is illustrated for a 20, 50 and 80 mol% CO_2 fluid mixture.*

Experimental data from Tödheide & Franck (1963) and Gehrig (1980) illustrate, that the addition of 6 wt% NaCl to a fluid mixture of 50 mol% H_2O and 50 mol% CO_2 raises its solvus about 100 °C at variable pressures. A H_2O-rich fluid mixture has a large expansion of its immiscibility field to low pressures and higher temperatures (see also Krüger & Diamond, 2001), whereas the effect of the addition of NaCl diminishes with higher CO_2 contents. The reaction (1) between the entrapped fluids and the plagioclase appears to proceed mainly outside the immiscibility fields of salt-free systems. In a 6 wt% NaCl solution, only H_2O-rich fluids, i.e. > 50mol% H_2O, interfere with the reaction at about 380 °C, whereas CO_2-rich fluids remain homogeneous at reaction conditions. Within fluid inclusions in quartz salinities of < 6 wt% NaCl have been measured. Therefore, it can be concluded that there is no interference between the reaction and the immiscibility field at any conditions.

References

Anderko, A. & Pitzer, K.J., 1993. Equation of state representation of phase equilibria and volumetric properties of the system NaCl-H_2O above 573 K. *Geochimica et Cosmochimica Acta*, **57**, 1657-1680.

Andersen, T., O' Reilly, S. Y. & Griffin, W. L., 1984. The trapped fluid phase in upper mantle xenoliths from Victoria, Australia; implications for mantle metasomatism. *Contributions to Mineralogy and Petrology*, **88,** 72-85.

Bakker, R. J. & Jansen, J. H. B., 1991. Experimental post-entrapment water loss from synthetic CO_2-H_2O inclusions in natural quartz. *Geochimica et Cosmochimica Acta*, **55,** 2215-2230.

Bakker, R. J., 1997. Clathrates: Computer Programs to calculate fluid inclusion V-X properties using clathrate melting temperatures. *Computers & Geosciences*, **23**, 1-18.

Bakker, R. J., in press. Package *Fluids*1 Computer programs for the analysis of fluid inclusion data and general fluid properties research. *Chemical Geology*.

Bauer, W., Jacobs, J. & Paech, H.-J., in press. Structural evolution of the Crystalline Basement of central Dronning Maud Land, East Antarctica. *Geologisches Jahrbuch, 96.*

Berman, R. G., 1988. Internally-consistent thermodynamic data for minerals in the system Na_2O-K_2O-CaO-MgO-FeO-Fe_2O_3-Al_2O_3-SiO_2-TiO_2-H_2O-CO_2. *Journal of Petrology*, **29**, 445-522.

Bischoff, W. D., Sharma, S. K. & Mackenzie, F. T., 1985. carbonate disorder in synthetic and biogenetic magnesian calcites: a Raman spectral study. *American Mineralogist*, **70**, 581-589.

Davis, D. W., Lowenstein, T. K. & Spencer, R. J., 1990. Melting behaviour of fluid inclusions in laboratory grown halite crystals in the systems NaCl-H_2O, NaCl-KCl-H_2O, NaCl-$MgCl_2$-H_2O and NaCl-$CaCl_2$-H_2O. *Geochimica et Cosmochimica Acta*, **54,** 591-601.

Duschek, W., Kleinrahm, R. & Wagner, W., 1990. Measurement and correlation of the (pressure, density, temperature) relation of carbon dioxide. II. Saturated-liquid and saturated-vapour density and the vapour pressure along the entire coexistence curve. *Journal of Chemical Thermodynamics*, **22**, 841-864.

Duan, Z., Moller, N. & Weare, J.H., 1995. Equation of state for the NaCl-H_2O-CO_2 system: Prediction of phase equilibria and volumetric properties. *Geochimica et Cosmochimica Acta*, **59**, 2869-2882.

Elkins, L.T. & Grove, T.L., 1990. Ternary feldspar experiments and thermodynamic models. *American Mineralogist*, **75**, 544-559.

Flowers, G. C., 1979. Correction of Holloway's (1977) adaption of the modified Redlich-Kwong equation of state for calculation of fugacities of molecular species in supercritical fluids of geological interest. *Contributions to Mineralogy and Petrology*, **69**, 315-318.

Gehrig, M., 1980. Phasengleichgewichte und PVT-daten ternärer Mischungen aus Wasser, Kohlendioxid und Natriumchlorid bis 3 kbar und 550 °C. PhD Thesis, University Karlsruhe, Hochschulverlag, Freiburg.

Heinrich, W. & Gottschalk, M., 1995. Metamorphic reactions between fluid inclusions and mineral hosts; I, Progress of the reaction calcite+quartz = wollastonite+CO_2 in natural wollastonite-hosted fluid inclusions. *Contributions to Mineralogy and Petrology*, **122,** 51-61.

Holloway, J. R., 1977. Fugacity and activity of molecular species in supercritical fluids. In: Fraser D. G. (ed.), Thermodynamics in geology. NATO ASI, Series D. Reidel, Dordrecht, pp 161-182.

Holloway, J. R., 1981. Compositions and volumes of supercritical fluids in the earth's crust. In: Hollister, L. S. & Crawford, M. L. (ed.), Short Course in Fluid inclusions: Application to Petrology, pp 13-38.

Jacobs, J., Fanning, C. M., Henjes, K. F., Olesch, M. & Paech, H. J., 1998. Continuation of the Mozambique Belt into East Antarctica; Grenville-age metamorphism and polyphase Pan-African high-grade events in central Dronning Maud Land. *Journal of Geology*, **106**, 385-406.

Jacobs, J., Klemd, R., Fanning, C.M., Bauer, W. & Colombo, F, (in press). Extensional collapse of the Late Neoproterozoic/Early Palaeozoic East African/Antarctic Orogen in central Dronning Maud Land. *Journal of the Geological Society of London. Special Publications.*

Johannes, W., 1978. Melting of plagioclase in the system Ab-An-H_2O and Qz-Ab-An-H_2O at P_{H2O} = 5 kbars, an equilibrium problem. *Contributions to Mineralogy and Petrology*, **66**, 295-303.

Johannes, W., 1989. Melting of plagioclase-quartz assemblages at 2 kbar water pressure. *Contributions to Mineralogy and Petrology*, **103**, 270-276.

Krüger, Y. & Diamond, L. W., 2001. P-V-T-X properties of two H_2O-CO_2-NaCl mixtures up to 850 °C and 500 MPa: A synthetic fluid inclusion study. XVI ECROFI, *Faculdade de Ciências do Porto, Departamiento de Geologia, Memória*, **7**, 241-244.

Markl, G. & Piazolo, S., 1998. Halogen-bearing minerals in syenites and high-grade marbles of Dronning Maud Land, Antarctica; monitors of fluid compositional changes during late-magmatic rock-rock interaction processes. *Contributions to Mineralogy and Petrology*, **132**, 246-268.

Mikhalsky, E. V., Beliatsky, B. V., Savva, E. V., Wetzel, H. U., Federov, L. V., Weiser, T. & Hahne, K., 1997. Reconnaissance Geochronologic Data on Polymetamorphic and Igneous rocks of the Humboldt Mountains, central Queen Maud Land, East Antarctica. In: *The Antarctic Region: Geological Evolution and Processes* (ed. Ricci, C. A.), pp. 45-53, Terra Antarctica Publication, Siena, Italy.

Passchier, C. W. & Trouw, R. A. J., 1996. Microtectonics. Springer-Verlag, Berlin.

Schulze, D. J., 1985. Evidence for primary kimberlite liquids in megacrysts from kimberlites in Kentucky, USA. *Journal of Geology*, **93**, 75-80.

Svensen, H., Jamtveit, B., Yardley, B., Engvik, A. K., Austrheim, H. & Broman, C., 1999. Lead and bromine enrichment in eclogite-facies fluids: Extreme fractionation during lower crustal hydration. *Geology*, **27,** 467-470.

Svensen, H., Jamtveit, B., Banks, D. A. & Austrheim, H., 2001. Halogen contents of eclogite facies fluid inclusions and minerals; Caledonides, western Norway. *Journal of Metamorphic Geology*, **19,** 165-178.

Span, R. & Wagner, W., 1996. A new equation of state for carbon dioxide covering the fluid region from the triple point temperature to 1100 K at pressures up to 800 MPa. *Journal of Physical Chemistry Reference Data*, **25**, 1509-1596.

Sterner, S. M. & Bodnar, R. J., 1989. Synthetic fluid inclusion; VII, Re-equilibration of fluid inclusions in quartz during laboratory simulated metamorphic burial and uplift. *Journal of Metamorphic Geology*, **7,** 243-260.

Tödheide, K. & Franck, E. U., 1963. Das Zweiphasengebiet und die kritische Kurve im System Kohlendioxid-Wasser bis zu Drucken von 3500 bar. *Zeitschrift Physikalische Chemie. Neue Folge*, **37,** 387-401.

9. Conclusions

The results of this study are discussed at the end of the respective chapters.

Chapter 6: The petrography and fluid imprint of the basement lithologies exposed in the central Petermannketten, and the resulting implications for secondary charnockitisation, leaching processes, and the retrograde P-T-path

Chapter 7: The petrography of the O.-v.-Gruber anorthosite body, the assessment of the actual fluid content in context of possible secondary modification of the original fluid composition

Chapter 8: The possible post peak-metamorphic and retrograde P-T-path, and the modelling of micro-chemical reactions of a CO_2-H_2O fluid with its plagioclase host under formation of "step-daughter" phases, to evaluate the resulting volumetrical and compositional change and its implications for isochore calculations.

In the following, the results of the preceding chapters are summarised.

The nature of rocks exposed in central Dronning Maud Land

It has been shown that the granulite-facies basement of the central Petermannketten, and Otto-von-Gruber-Gebirge is largely composed of lithologies belonging to the charnockite-anorthosite suite of rocks. Gneisses that were locally transformed into arrested-type charnockites represent the (relatively) more superficial part, and the anorthosite body the more igneous, intrusive deeper part of late Neoproterozoic/early Palaeozoic granulitic continental crust.

Subsequent to charnockite formation, gneisses were subjected to alteration processes leading to partial or complete orthopyroxene breakdown. This was accompanied by the formation of hydrous mineral assemblages and severe leaching of the previously darkish/greenish rocks. However, the complete orthopyroxene decomposition was not necessarily connected to intense leaching. Some gneisses that still display the typical charnockite colouring do not contain orthopyroxene any more, and can thus not be included in a classification of charnockitic rocks in the narrowest sense. This implies that declarations of the occurrence of charnockites, given by field observations of "typical" rock colouring, have to be carefully reviewed and attested on the basis of further scientific investigations. Magmatic bodies of charnockitic and syenitic compositions remained nearly undeformed and unaltered. Their intrusion could not unequivocal be linked with large scale alteration mechanisms (e.g., invasion of a fluid phase responsible for leaching).

The anorthosite body reveals features typical of Precambrian massif-type anorthosite complexes. It is composed of >90 vol% plagioclase, and the homogeneous rock composition exhibits major changes only in discrete mylonitic shear zones. The latter are characterised by secondary garnet growth and noritic or tonalitic

composition. The norites belong to the group of charnockitic rocks. Thus a further example of "arrested-type" charnockitisation, connected with shear zone formation, is shown to occur in central Dronning Maud Land. Additionally, iron-enrichment of pyroxenes and the local concentration of opaque mineral phases most probably hint at shear zone formation under the influence of an iron-rich fluid phase.

The fluids preserved in gneissic and anorthositic rocks

All fluid inclusions under investigation in this study reveal textural evidence of primary (metamorphic) origin. No indication of secondary fluid influx or the presence of various fluid generations is given. The most abundant type of fluids enclosed in all samples under investigation is comprised of a $CO_2 \pm N_2$ mixture. The nitrogen content generally ranges between 2 - 5 mol%. This "dry" character of fluid inclusions hosted either by plagioclase, quartz or garnet is in accordance with fluid inclusion studies that have been performed on rocks from Precambrian granulite facies terranes worldwide.

For the anorthosite complex and shear zones, carbonic inclusions are the only type of fluids present, and no conspicuous difference with regard to the fluid composition can be detected. It is concluded that the preserved fluid has its origin in the magmatic source of the "anorthositic" melts. Inclusion shapes and crystal microstructures imply that the fluid inclusions and host minerals have undergone post-peak metamorphic changes through reequilibration and recrystallisation processes. Furthermore, a detailed examination of microsolids enclosed in some fluid inclusions has led to the assertion that inclusions were also modified by back-reactions of the enclosed fluid with its mineral host. Thus, the present-day $CO_2 \pm N_2$ fluid only represents the residual proportion of a more complex $CO_2 \pm H_2O \pm N_2$ fluid.

A CO_2-H_2O fluid that is trapped in minerals crystallising from an ascending magma, or during prograde metamorphism (mechanisms accompanied by dehydration and decarbonation) will most likely react with its host during retrogression, provided, that the host is a reactive mineral. This results in the formation of microcrystals, which may be detected as solid inclusions in fluid inclusions, and the partial or complete consumption of the fluid components. In the O.-v.-Gruber anorthosite body the enclosed solids are carbonates and sheet silicates. As it can be precluded that the crystals were accidentally trapped they are presumed to have formed by "back-reactions". They can only have formed if an aqueous phase had been present in the inclusion at some stage in the past.

A detailed examination of fluid inclusion densities exhibits that plagioclase and garnet from the shear zones have preserved the highest inclusion densities, whereas lowest density values were found to be evenly distributed throughout all samples and host minerals. High density isochores are in accordance with independent P-T-constraints on peak-metamorphic conditions. Consequently, metamorphic minerals are

able to preserve the original metamorphic fluid, even though the influence of post-entrapment changes are severe. The statement that $CO_2\pm N_2$ inclusions have preserved the original fluid density is only seemingly contradictory to the argument that the original fluid must have had a H_2O component. Fluid compositions can vary on a small local scale as each inclusion reacts individually on applied modification processes. The fact that high densities were exclusively found in shear zone samples support this observation, as the destruction and tapping of inclusions generally leads to a preferred loss of H_2O and N_2.

In the light and dark coloured gneissic/charnockitic lithologies of the central Petermannketten the overall fluid imprint is more complex. Besides inclusions that contain a $CO_2\pm N_2$ mixture, H_2O-salt inclusions and CO_2-$H_2O\pm N_2$-salt fluids have been detected. As they all give textural prove of primary (metamorphic) origin it is concluded that none of the preserved fluids is connected with the late, structurally controlled leaching processes. Salinities of the aqueous inclusions do not exceed 6.74 wt% NaCleq. Nevertheless, the occurrence of nahcolite as a real daughter mineral indicates that high alkaline brines have at least locally been present at an earlier stage in geologic evolution. This is in good agreement with studies from different granulite terranes where rather recent findings of highly saline fluid phases are interpreted to play an important role in charnockite formation, and questions the widely accepted model that granulitisation is mainly governed by CO_2-dominated fluids. The aqueous phase was most probably captured during the prograde path, whereas the carbonic fluid is suggested to originate from influx of external fluids during peak metamorphism. However a more precise explanation of the origin of the fluid cannot be given on the base of the available data.

The fluid inclusions which are predominantly hosted by quartz have been subjected to substantial retrograde reequilibration processes, and no densities reflecting Pan African high-grade metamorphism were found. The position of isochores only correlates with the rough P-T estimates on retrograde conditions available from independent P-T data.

Implications for a possible retrograde P-T-path

A selection of representative isochores from the different basement lithologies have been correlated with P-T constraints based on mineral-equilibria data available from other studies. Taking into account the evidence of reequilibration processes prevailing during the retrograde evolution, the gradual decrease in fluid densities best fits a clockwise P-T path and mineral-fluid equilibration during near isothermal decompression.
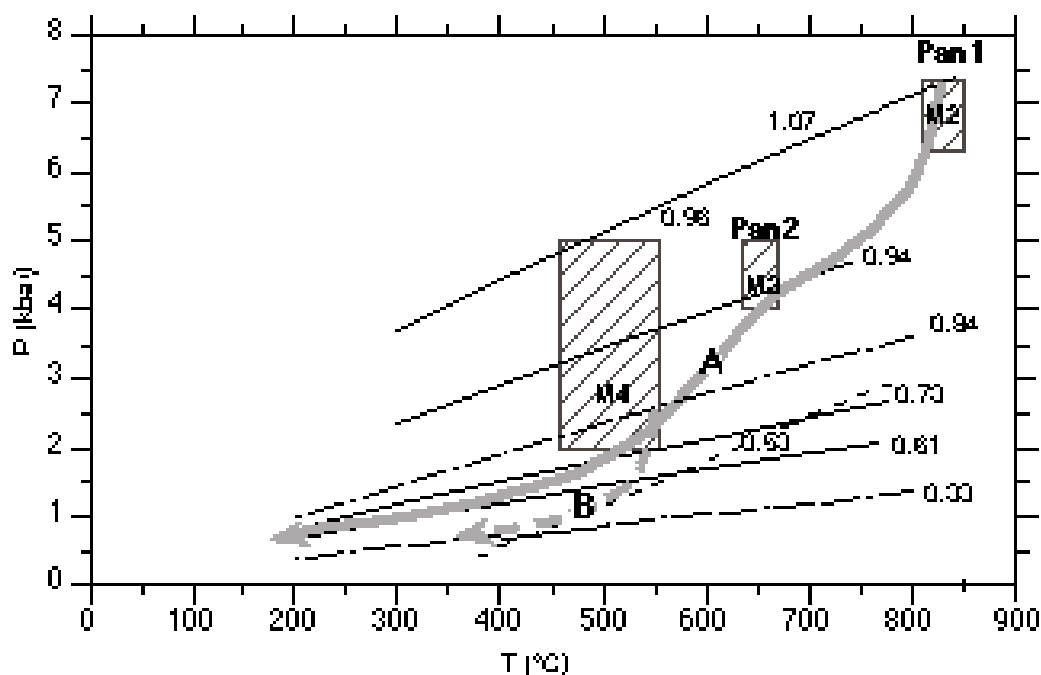
*Fig. 9.1: P-T-paths as derived from isochore data from the varying lithologies investigated during this study. Path **A** is based on data from the O.-v.-Gruber anorthosite body and associated shear zones. Path **B** is based upon fluid inclusion data gathered from gneissic and charnockitic samples from the central Petermannketten. Boxes indicate P-T conditions of the successive metamorphic stages as proposed by Markl & Piazolo (1998). Numbers indicate densities (in gcm^{-3}) of fluids used for isochore calculations. Dashed lines: H_2O-salt inclusions; dash-dot-line: qtz-hosted CO_2-N_2 inclusions from Petermannketten; solid lines: pl-hosted CO_2-N_2 inclusions from anorthosite and shear zones.*

A compilation of the two independent P-T-paths (Fig. 9.1) described and favoured in chapters 6.3 and 7.3 illustrates that the mode and P-T-conditions of retrogression are in good accordance for both sample localities as to be expected from data gathered in a close spatial relationship. Additionally, pressure estimates of c. 2.5 kbar for the beginning of M4 are depicted, which argue for the low pressure range proposed by Markl & Piazolo (1998). A similar P-T-path has been postulated from the Lützow Holm Bay region, East Antarctica by Santosh & Yoshida (1992). The tendency of isochores from the Petermannketten towards lower densities and the absence of high density isochores from that region also illustrates the different potential of varying host minerals to preserve peak metamorphic fluids. The higher resistance of plagioclase to the application of stress seems to be reflected in the better ability of rocks that nearly completely consist out of plagioclase to preserve metamorphic fluids. In the gneissic basement lithologies, mechanically less stable quartz is much more abundant and modification of fluid inclusions is much more profound.

References

Andersen, T., O'Reilly, S. Y. & Griffin, W. L., 1984. The trapped fluid phase in upper mantle xenoliths from Vicotria, Australia: implications for mantle metasomatism. *Contributions to Mineralogy and Petrology*, 88, 72-85.

Andersen, T., Burke, E. A. J., Austrheim, H., 1989. Nitrogen-bearing, aqueous fluid inclusions in some eclogites from the Western Gneiss Region of the Norwegian Caledonides. *Contributions to Mineralogy and Petrology*, 103, 153-165.

Aranovich, L. Y. & Newton, R. C., 1998. H_2O activity in concentrated KCl and KCl-NaCl solutions at high temperatures and pressures measured by the brucite-periclase equilibrium. *Contributions to Mineralogy and Petrology*, 127, 261-271.

Ashwal, L. D., 1993. *Anorthosites*. Springer, Berlin, Heidelberg, New York, 422 pp.

Audétat, A. & Günher, D., 1999. Mobility and H_2O loss from fluid inclusions in natural quartz crystals. *Contributions to Mineralogy and Petrology*, 137, 1-14.

Bakker, R. J., & Jansen, J. B. H., 1994. Preferential water leakage from fluid inclusions by means of mobile dislocations. *Nature*, 345, 58-60.

Bakker, R. J., 1997. Clathrates: Computer Programs to calculate fluid inclusion V-X properties using clathrate melting temperatures. *Computers & Geosciences*, **23**, 1-18.

Bakker, R. J., 1998. Improvements in clathrate modelling; II, The H_2O-CO_2-CH_4-N_2-C_2H_6 fluid system. In: *Gas hydrates; relevance to world margin stability and climate change.* (eds. Henriet, J.-P. & Mienert, J.) *Geological Society Special Publications*, pp. 75-105, Geological Society of London, London, United Kingdom.

Bakker, R.J., 1999. Adaption of the Bowers & Helgeson (1983) equation of state to the H_2O-CO_2-CH_4-N_2-NaCl system. *Chemical Geology*, 154, 225-236.

Bakker, R. J. & Mamtani, M. A., 2000. Fluid inclusions as metamorphic process indicators in the Southern Aravali Mountain Belt (India). *Contributions to Mineralogy and Petrology*, 139, 163-179.

Bakker, R. J., in press. Package *Fluids*1 Computer programs for the analysis of fluid inclusion data and general fluid properties research. *Chemical Geology*.

Bauer, W., Jacobs, J. & Paech, H. J., 1996. Structural evolution of polyphase metamorphosed basement rocks in central Dronning Maud Land, East Antarctica. In: *Proceedings of the UNESCO-IUGS-IGCP-368 international field workshop on the Proterozoic continental crust of southern India.* (eds. Santosh & M ; Yoshida) *Gondwana Research Group Miscellaneous Publication*, 4-6, Osaka City University, Department of Geosciences, Faculty of Science, Gondwana Research Group, Osaka, Japan.

Bauer, W., Jacobs, J. & Paech, H.-J., 2003. Structural evolution of the Crystalline Basement of central Dronning Maud Land, East Antarctica. *Geologisches Jahrbuch*, B 96.

Becke, F, 1903. Über Mineralbestand und Struktur der kristallinen Schiefer. *IX. Session du Congres geologique internationaux*, Compte rendu. Part 2, 553-570.

Berman, R. G., 1988. Internally consistent thermodynamic dataset for minerals in the system Na_2O-K_2O-CaO-MgO-FeO-Fe_2O_3-Al_2O_3-SiO_2-TiO_2-H_2O-CO_2. *Journal of Petrology*, 29, 445-552.

Bhattacharya, A. & Sen, S. K., 1986. Granulite metamorphism, fluid buffering, and dehydration melting in the Madras charnockites and metapelites. *Journal of Petrology*, 27, 1119-1141.

Black, R. & Liegeois, J. P., 1993. Cratons, mobile belts, alkaline rocks and continental lithospheric mantle; the Pan-African testimony. *Journal of the Geological Society of London*, 150 (Part 1), 89-98.

Blom, K. A., 1988. Fluid inclusions from the Suosmujarvi area, Southwest Finland. *Lithos*, 21, 263-278.

Bodnar, R. J. Binns, P. R. & Hall, D. L., 1989. Synthetic fluid inclusions; VI, Quantitative evaluation of the decrepitation behaviour of fluid inclusions in quartz at one atmosphere confining pressure. *Journal of Metamorphic Geology.* 7; 2, Pages 229-242.

Bodnar, R. J., 1993. Revised equation and table for determining the freezing point depression of H_2O-NaCl solutions. *Geochimica et Cosmochimica Acta*, 57, 683-684.

Bodnar, R. J. & Vityk, M. O., 1994. Applications of fluid inclusions in tectonic reconstruction; microthermometric analysis. In: *Fifth biennial Pan-American conference on Research on fluid inclusions.* (eds. Izquierdo M. G., Suarez-A. M. C., Guevara G. M., Vanko D., Viggiano G.J.C.), Program and Abstracts; Biennial Pan-American Conference on Research on Fluid Inclusions, 5, 10.

Bond, G. C., Nickeson, P. A. & Kominz, M. A., 1984. Breakup of a supercontinent between 625 Ma and 555 Ma; new evidence and implications for continental histories. *Earth and Planetary Science Letters*, 70(2), 325-345.

Borg, S. G. & DePaolo, D. J., 1994. Laurentia, Australia, and Antarctica as a late Proterozoic supercontinent; constraints from isotopic mapping. *Geology* 22, 307-310.

Bowers, T. S. & Helgeson, H. C., 1983. Calculation of the thermodynamic and geochemical consequences of nonideal mixing in the system H_2O-CO_2-NaCl on phase relations in geologic systems; equation of state for H_2O-CO_2-NaCl fluids at high pressures and temperatures. *Geochimica et Cosmochimica Acta*, 47, 1247-1275.

Brewster , D., 1823. Notice respecting the existence of the new fluid in a large cavity in a specimen of sapphire. *Edinburgh Journal of Science*, 6, 155-156.

Bruce, R. M., Nelson, E. P. & Weaver, S. G., 1989. Effects of synchronous uplift and intrusion during magmatic arc construction. In: *Growth of the continental crust.* (eds. Ashwal & Lewis) *Tectonophysics*, 317-329, Elsevier, Amsterdam, Netherlands.

Bucher, K. & Frey, 1994. *Petrogenesis of metamorphic rocks.* Springer, Berlin, 318 pp.

Burke, E. A. J., 2001. Raman microspectrometry of fluid inclusions. In: *Fluid inclusions; phase relationships-methods-applications; special volume in honour of Jacques Touret.* (eds. Andersen, T.; Frezzotti, M. L.; Burke E.), 139-158, Elsevier. Amsterdam.

Burruss, R. C. 1981. Analysis of phase equilibria in C-O-H-S fluid inclusions. In: *Short Course in Fluid inclusions: Application to Petrology*, (eds. Hollister, L. S. & Crawford, M. L.), pp 39-74.

Burton, K. W. & O'Nions, R. K., 1990. The timescale and mechanism of granulite formation at Kurunegala, Sri Lanka. *Contributions to Mineralogy and Petrology*, 106, 66-89.

Collins, P., L., F., 1979. Gas hydrates in CO_2-bearing fluid inclusions and the use of freezing data for estimation of salinity. *Economic Geology*, 74, 1435-1444.

References

Colombo, F. & Talarico, F., 2003. Regional metamorphism in the high grade basement of central Dronning Maud Land, East Antarctica. *Geologisches Jahrbuch*, B 96.

Dalziel, I. W. D., 1991. Pacific margins of Laurentia and East Antarctica-Australia as a conjugate rift pair; evidence and implications for an Eocambrian supercontinent. *Geology,* 19, 598-601.

De Waard, D., 1968a. Annotated bibliography of anorthosite petrogeneses. In: *Origin of anorthosite and related rocks* (ed. Isachsen, Y. W.), 1-11, New York State Museum Science Service Memoir, Albany, N.Y.

De Waard, D., 1968b. The Anorthosite Problem: The problem of the anorthosite-charnockite suite of rocks. In: *Origin of anorthosite and related rocks* (ed. Isachsen, Y. W.), 71-91, N.Y. State Museum Science Service Memoir, Albany, N.Y.

Demaiffe, D., Moreau, C. & Brown, W. L., 1991a. Ring-complexes of Ofoud-type in Aïr, Niger: a new anorogenic-type anorthosite association. In: *Magmatism in extensional structural settings.* (eds. Kampunzu, A. B. & Lubala, R. T.), 353-376, Springer, Berlin, Heidelberg, New York.

Demaiffe, D., Moreau, C., Brown, W. L. & Weis, D., 1991b. Geochemical and isotopic composition (Sr, Nd and Pb) and the origin of the anorthosite-bearing anorogenic complexes of the Aïr Province, Niger. *Earth and Planetary Science Letters*, 105, 28-46.

Diamond, L. W., 1992. Stability of CO_2 clathrate hydrate $+CO_2$ liquid $+ CO_2$ vapour $+$ aqueous KCl-NaCl solutions.: Experimental determination and application to salinity estimates of fluid inclusions. *Geochimica et Cosmochimica Acta*, 56, 19-41.

Diamond, L. W., 2001. Review of the systematics of CO_2-H_2O fluid inclusions. *Lithos*, 55, 69-99.

Dirks, P. H. G. M. & Wilson, C. J. L., 1995. Crustal evolution of the East Antarctic mobile belt in Prydz Bay; continental collision at 500 Ma? In: *Tectonics of East Antarctica. Precambrian Research*, 75, 209-230.

Dobmeier, C. & Raith, M. M., 2000. On the origin of "arrested" charnockitization in the Chilka Lake area, Eastern Ghats Belt, India; a reappraisal. *Geological Magazine*, 137, 27-37.

Duan, Z. H.; Moller, N. & Weare, J. H., 1992. An equation of state for the CH_4-CO_2-H_2O system: 2. Mixtures from 50°C to 1000°C and 0 to 1000 bar. *Geochimica Cosmochimica Acta*, 56, 2619-2631.

Duan, Z. H., Moller, N. & Weare, J. H., 1996. A general equation of state for supercritical fluid mixtures and molecular dynamics simulation of mixture PVTX properties. *Geochimica Cosmochimica Acta*, 60, 1209-1216.

Dubessy, J., Poty, B. & Ramboz, C., 1989. Advances in C-O-H-N-S fluid geochemistry based on micro-Raman spectrometric analysis of fluid inclusions. *European Journal of Mineralogy*, 1, 517-534.

Duchesne, J. C., Liégeois, J. P., Van der Auwera, J. & Longhi, J., 1999. The crustal tongue melting model and the origin of massive anorthosites. *Terra Nova*, 11, 100-105.

Duschek, W., Kleinrahm, R. & Wagner, W., 1990. Measurement and correlation of the (pressure, density, temperature) relation of carbon dioxide. II. Saturated-liquid and saturated-vapour density and the vapour pressure along the entire coexistence curve. *Journal of Chemical Thermodynamics*, 22, 841-864.

Emslie, R. F., 1985. The deep Proterozoic crust in the north atlantic provinces (eds. Tobi, A. C. & Touret, J. L. R.), 39-60, Reidel, Dordrecht.

Emslie, R. F., Hamilton, M. A. & Théiault, R. J., 1994. Petrogenesis of a Mid-Proterozoic Anorthosite-Mangerite-Charnockite-Granite- (AMCG) complex: Isotopic and chemical evidence from the Nain Plutonic Suite. *Journal of Geology*, 102, 539-558.

Fyfe, W. S., 1973. Dehydration Reactions. *The American Association of Petroleum Geologists Bulletin*, 57, 190-197.

Glassley, W. E., 1983. The role of CO_2 in the chemical modification of deep continental crust. *Geochimica et Cosmochimica Acta*, 47, 597-616.

Goldschmidt, V. M., 1916. *Geologisch-petrographische Studien im Hochgebirge des südlichen Norwegens. IV. Übersicht der Eruptivgesteine im kaledonischen Gebirge zwischen Stavanger und Trondhjem.* Vidensk.-Selsk. Kristiania Skrifter. I. Mat.-Naturvidenskaften.

Goldstein, R. H. & Reynolds, T. J., 1994. *Systematics of Fluid Inclusions in Diagenetic Minerals.* SEPM Short course, 31, 198 pp.

Grunow, A. M., Hanson, R. & Wilson, T. J., 1996. Were aspects of Pan-African deformation linked to Iapetus opening? *Geology* , 24, 1063-1066.

Grunow, A. M., 1999. Gondwana events and palaeogeography; a palaeomagnetic review. In: *Alex du Toit special issue; Gondwana 10; event stratigraphy of Gondwana; keynote presentations.* (eds. De Wit & Maarten) *Journal of African Earth Sciences*, 53-69, Pergamon, London-New York.

Hall, D. L. & Sterner, S. M. 1993. Preferential water loss from synthetic fluid inclusions. *Contributions to Mineralogy and Petrology*, 114, 489-500.

Hansen, E. C., Janardhan, A. S., Newton, R. C., Prame, W. K. B. N. & Ravindra, K. G. R., 1987. Arrested charnockite formation in southern India and Sri Lanka. *Contributions to Mineralogy and Petrology*, 96, 225-244.

Heinrich, W. & Gottschalk, M., 1995. Metamorphic reactions between fluid inclusions and mineral hosts; I, Progress of the reaction calcite+quartz = wollastonite+CO_2 in natural wollastonite-hosted fluid inclusions. *Contributions to Mineralogy and Petrology*, 122**,** 51-61.

Hoffman, P. F., 1991. Did the breakout of Laurentia turn Gondwanaland inside-out? *Science*, 252, 1409-1412.

Holland, T. H., 1900. The charnockite series, a group of Archean hyperstenic rocks in peninsular India. *Geological Survey of India Memorandum*, 28, 119-249.

Holloway, J. R., 1977. Fugacity and activity of molecular species in supercritical fluids. In: Fraser D. G. (ed.), Thermodynamics in geology. NATO ASI, Series D. Reidel, Dordrecht, pp. 161-182.

Holness, M. B., 1993. Temperature and pressure dependence of quartz-aqueous fluid dihedral angles; the control of adsorbed H_2O on the permeability of quartzites. *Earth and Planetary Science Letters*, 117, 363-377.

Hosieni, K. R., Howald, R. A. & Scanlon, M. W., 1985. Thermodynamics of the lambda transition and the equation of state of quartz. *American Mineralogist*, 70, 782-793.

Isachsen, Y. W., 1968. Origin of anorthosites and related rocks; a summarization. *Memoir - New York State Museum and Science Service*, 18, 435-445.

References

Jacobs, J., Ahrendt, H., Kreutzer, H. & Weber, K., 1995. K-Ar, ^{40}Ar-^{39}Ar and apatite fission-track evidence for Neoproterozoic and Mesozoic basement rejuvenation events in the Heimefrontfjella and Mannefallknausane (East Antarctica). In: *Tectonics of East Antarctica.* (eds. Dirks, P. H. G. M., Passchier, C. W. & Hoek, J. D.) *Precambrian Research*, 251-262, Elsevier, Amsterdam, International.

Jacobs, J., Fanning, C. M., Henjes, K. F., Olesch, M. & Paech, H. J., 1998. Continuation of the Mozambique Belt into East Antarctica; Grenville-age metamorphism and polyphase Pan-African high-grade events in central Dronning Maud Land. *Journal of Geology*, 106, 385-406.

Jacobs, J. & Thomas, R. J., in press. The Mozambique Belt from an East Antarctic perspective. *Proceedings of the VIII International Symposium on Antarctic Earth Sciences.*

Janardhan, A. S., Newton, R. C. & Smith, J. V., 1979. Ancient crustal metamorphism at low pH$_2$O; charnockite formation at Kabbaldurga, South India. *Nature*, 278, 511-514.

Joshi, A., Pant, N. C. & Parimoo, M. L., 1991. Granites of Petermann Ranges, East Antarctica, and implications on their genesis. *Journal of the Geological Society of India*, 38, 169-181.

Kämpf, H & Stackebrandt, W., 1985. Geologic investigations in the Eliseev Anorthosite Massif, Central Dronning Maud Land, East Antarctica. Zeitschrift der Geologischen Wissenschaft, 13, 321-333.

Kolker, A. & Lindsley, D. H., 1989. Geochemical evolution of the Maloin Ranch pluton, Laramie Anorthosite Complex, Wyoming: petrology and mixing relations. *American Mineralogist*, 74, 307-324.

Krause, O., Dobmeier, C., Raith, M. M. & Mezger, K., 2001. Age of emplacement of massif-type anorthosites in the Eastern Ghats Belt, India; constraints from U-Pb zircon dating and structural studies. *Precambrian Research*, 109, 25-38.

Kröner, A., Sacchi, R., Jaeckel, P. & Costa, M., 1997. Kibaran magmatism and Pan-African granulite metamorphism in northern Mozambique; single zircon ages and regional implications. *Journal of African Earth Sciences*, 25, 467-484.

Küster, M. & Stöckhert, B., 1997. Density changes of fluid inclusions in high-pressure low-temperature metamorphic rocks from Crete: A thermobarometric approach based on the creep strength of the host mineral. *Lithos*, 41, 151-167.

Lafrance, B.; John, B. E. & Scoates, J. S., 1996. Syn-emplacement recrystallization and deformation microstructures in the Poe Mountain Anorthosite, Wyoming. *Contributions to Mineralogy and Petrology*, 122, 431-440.

Lamb, W. M. & Valley, J. W., 1984. Metamorphism of reduced granulites in low-CO$_2$ vapour-free environment. *Nature*, 312, 56-58.

Lamb, W. M., Valley, J. W. & Brown, P. E. 1987. Post-metamorphic CO$_2$ inclusions in granulites. *Contributions to Mineralogy and Petrology*, 96, 485-495.

Lamb, W. M., 1990. Fluid inclusions in granulites: peak versus retrograde formation. In: *Granulites and crustal evolution.* (eds. Vielzeuf, D. & Vidal, P.) *NATO ASI Series. Series C: Mathematical and Physical Sciences*, 419-433, D. Reidel Publishing Company, Dordrecht-Boston.

Lamb, W. M. & Morrison, J., 1997. Retrograde fluids in the Archean Shawmere anorthosite, Kapuskasing Structural Zone, Ontario, Canada. *Contributions to Mineralogy and Petrology*, 129, 105-119.

Lawver, L. A. & Scotese, C. R. 1987. A revised reconstruction of Gondwanaland. In: *Gondwana six: Structure, Tectonics, and Geophysics* (ed. G.D. McKenzie), 40, 17-20. American Geophysical Union Geophysical Monographs.

Le Maitre, R. W., 1989. *A classification of igneous rocks and glossary of terms.* Blackwell Science Publications, Oxford, 139 pp.

Lee, B. I. & Kesler, M. G., 1975. A generalized thermodynamic correlation based on three-parameter corresponding states. *American Institute of Chemical Engeneering Journal*, 21, 510-527.

Li, Z. X. & Powell, C. M., 1993. Late Proterozoic to early Paleozoic paleomagnetism and the formation of Gondwanaland. In: *Assembly, evolution and dispersal; proceedings of the Gondwana eight symposium.* (eds. Findlay, H. ; Unrug, R. ; Banks, D. & Veevers, R.) *International Gondwana Symposium*, 9-21, International Gondwana Symposium.

LINKAM, Scientific Instruments, Ltd., 1993. *Stage Reference Manual (Geology Version).* 18 pp.

LINKAM, Scientific Instruments, Ltd., 1993. *TP 92 Reference Manual.* 9 pp.

Longhi, J., Van der Auwera, J., Fram, M. S. & Duchesne, J. C., 1999. Some phase equilibrium constraints on the origin of Proterozoic (massif) type anorthosites and related rocks. *Journal of Petrology*, 40, 339-362.

Markl, G. & Piazolo, S., 1998. Halogen-bearing minerals in syenites and high-grade marbles of Dronning Maud Land, Antarctica; monitors of fluid compositional changes during late-magmatic rock-rock interaction processes. *Contributions to Mineralogy and Petrology*, 132, 246-268.

Markl, G., Piazolo, S., Bauer, W., Paech, H. J., Krauß, U. & Mikhalsky, E. V., 2003. Panafrican massif-type anorthosites from central Dronning Maud Land, Antarctica. *Geologisches Jahrbuch*, B 96, in press.

Martignole, J. & Nantel, S., 1982. Geothermobarometry of cordierite-bearing metapelites near the Morin anorthosite complex, Grenville Province, Quebec. *The Canadian Mineralogist*, 20, 307-318.

McLelland, J. M., 1989. Crustal growth associated with anorogenic, mid-Proterozoic anorthosite massifs in northeastern North America. In: *Growth of the continental crust,* (ed. Ashwal, L. D.), *Tectonophysics*, 3-4, 331-341, Elsevier, Amsterdam, Netherlands.

McMenamin, M. A. S. & McMenamin, D. L. S., 1990. *The emergence of animals; the Cambrian breakthrough.* Columbia Univ. Press, New York, NY, United States.

Meert, J. G., Van, d. V. R., Pisarevsky, S. A., Komissarova, R. A. & Khramov, A. N., 2001. New palaeomagnetic results from Vendian red sediments in Cisbaikalia and the problem of the relationship of Siberia and Laurentia in the Vendian; discussion and reply. *Geophysical Journal International*, 146, 867-873.

Mikhalsky, E. V., Beliatsky, B. V., Savva, E. V., Wetzel, H.-U., Federov, L. V., Weiser, T. & Hahne, K., 1997. Reconnaissance Geochronologic Data on Polymetamorphic and Igneous Rocks of the Humboldt Mountains, Central Queen Maud Land, East Antarctica. In: *The Antarctic Region:*

Geological Evolution and Processes. Proceedings of the VII International Symposium on Antarctic Earth Sciences, Siena, 1995 (ed. Alberto, R. C.), 45-54, Terra Antarctica Publication, Siena.

Milisenda, C., Liew, T. C., Hofmann, A. W. & Kroener, A., 1991. Isotopes, element mobility and mineral stability during charnockite formation in Sri Lanka. In: *Sixth meeting of the European Union of Geosciences.* (ed. Anonymous) *Terra Abstracts*, 437, Blackwell Scientific Publications, Oxford, International.

Moores, E. M., 1991. Southwest U.S.-East Antarctic (SWEAT) connection; a hypothesis. *Geology*, 19, 425-428.

Morimoto, N., 1988. Nomenclature of pyroxenes; Subcommitee on Pyroxenes, Commission on New Minerals and Mineral Names (CNMMN), International Mineral Association (IMA). *Schweizerische Mineralogische und Petrographische Mitteilungen = Bulletin Suisse de Mineralogie et Petrographie*, 68, 95-111.

Newton, R. C., Smith, J. V. & Windley, B. F., 1980. Carbonic metamorphism, granulites and crustal growth. *Nature*, 288, 45-50.

Newton, R. C., Aranovich, L. Y., Hansen, E. C. & Vandenheuvel, B. A., 1998. Hypersaline fluids in Precambrian deep-crustal metamorphism. In: *Earth's evolution through the Precambrian.* (eds. Percival, J. & Ludden, A.) *Precambrian Research*, 41-63, Elsevier, Amsterdam.

Olesch, M., 1991. Metamorphism of basement rocks from the southern Shackleton Range. In: *Sixth international symposium on Antarctic earth sciences.* (ed. Anonymous), International Symposium on Antarctic Earth Sciences, 6, 456.

Paech, H. J., 1997. Central Dronning Maud Land; its history from amalgamation to fragmentation of Gondwana. In: *European Union of Geoscience; EUG 9, symposium on Antarctic Earth sciences.* (eds. Kleinschmidt, G., Ricci, C. A., Storey, B. C., Tessensohn, F. & van, d. W. F. M.) *Terra Antartica*, 41-49, Universita di Siena. Dipartimento di Scienze della Terra, Siena, Italy.

Parimoo, M. L., Joshi, A. & Pant, N. C., 1988. Petrogenesis of the anorthosite suite of central Dronning Maud Land, East Antarctica. In: *Penrose Conference on the origin and evolution of anorthosite and associated rocks*, 38, Wyoming, U.S.

Passchier, C. W. & Trouw, R. A. J., 1996. *Microtectonics*. Springer-Verlag, Berlin, 289 pp.

Pelechaty, S. M., Grotzinger, J. P., Kashirtsev, V. A. & Zhernovsky, V. P., 1996. Chemostratigraphic and sequence stratigraphic constraints on Vendian-Cambrian basin dynamics, Northeast Siberian Craton. *Journal of Geology*, 104, 543-563.

Perchuk, L., Gerya, T. & Nozhkin, A., 1989. Petrology and retrograde P-T path in granulites of the Kanskaya Formation, Yenisey Range, eastern Siberia. *Journal of Metamorphic Geology*, 7, 599-617.

Perchuk, L. L. v. & Gerya, T. V., 1992. The fluid regime of metamorphism and the charnockite reaction in granulites; a review. *International Geology Review*, 34, 1-58.

Perchuk, L. L. & Gerya, T. V., 1993. Fluid control of charnockitization. In: *Fluid-rock interaction in the deeper continental lithosphere.* (eds. Touret, J., R. & Thompson, A.) *Chemical Geology*, 175-186, Elsevier, Amsterdam, Netherlands.

Perchuk, L. L., Safonov, O. G., Gerya, T. V., Fu, B. & Harlov, D. E., 2000. Mobility of components in metasomatic transformation and partial melting of gneisses; an example from Sri Lanka. *Contributions to Mineralogy and Petrology*, 140, 212-232.

Phillipot, P. & Selverstone, J., 1991. Trace-element-rich brines in eclogite veins: Implications for fluid composition and and transport during subduction. *Contributions to Mineralogy and Petrology*, 106, 417-430.

Piazolo, S. & Markl, G., 1999. Humite- and scapolite-bearing assemblages in marbles and calcsilicates of Dronning Maud Land, Antarctica; new data for Gondwana reconstructions. *Journal of Metamorphic Geology*, 17, 91-107.

Pichamuthu, C. S., 1960. Charnockite in the making. *Nature,* 188(4745), 135-136.

Pineau, F., Javoy, M. Behar, F. & Touret, J., 1981. La géochimie isotopique du facies granulite du Bamble (Norvège) et l'origine des fluides carbonés dans la crote profonde. *Bulletin de Mineralogie*, 104, 630-641.

Pinna, P., Jourde, G., Calvez, J. Y., Mroz, J. P. & Marques, J. M., 1993. The Mozambique Belt in northern Mozambique; Neoproterozoic (1100-850 Ma) crustal growth and tectogenesis, and superimposed Pan-African (800-550 Ma) tectonism. *Precambrian Research*, 62, 1-59.

Powell, C. M., Li, Z. X., McElhinny, M. W., Meert, J. G. & Park, J. K., 1993. Paleomagnetic constraints on timing of the Neoproterozoic breakup of Rodinia and the Cambrian formation of Gondwana; with Suppl. Data 9335. *Geology*, 21, 889-892.

Raith, M., Hoernes, S., Klatt, E. & Staehle, H. J., 1989. Contrasting mechanisms of charnockite formation in the amphibolite to granulite grade transition zones of southern India. In: *Fluid movements; element transport and the composition of the deep crust.* (eds. Bridgwater & David) *NATO ASI Series. Series C: Mathematical and Physical Sciences*, 29-38, D. Reidel Publishing Company, Dordrecht-Boston, International.

Raith, M., Srikantappa, C., Ashamanjari, K. G. & Spiering, B., 1990. The granulite terrane of the Nilgiri Hills (southern India); characterization of high-grade metamorphism. In: *Granulites and crustal evolution.* (eds. Vielzeuf, D. & Vidal, P.) *NATO ASI Series. Series C: Mathematical and Physical Sciences*, 339-365, D. Reidel Publishing Company, Dordrecht-Boston.

Raith, M. & Srikantappa, C., 1993. Arrested charnockite formation at Kottavattam, southern India. In: *Special issue on South Indian granulites.* (ed. Mohan, A.) *Journal of Metamorphic Geology*, 815-832, Blackwell, Oxford, United Kingdom.

Ravich, M. G. & Kamenev, E. N., 1975. *Crystalline basement of the Antarctic platform.* Wiley, New York.

Ravindra-Kumar, G. R., Srikantappa, C. & Hansen, E., 1985. Charnockite formation at Ponmudi in southern India. *Nature*, 313, 207-209.

Roedder, E., 1984. *Fluid inclusions.* Mineralogical Society of America.

Rogers, J. J. W., Miller, J. S. & Clements, A. S., 1995a. A Pan-African zone linking East and West Gondwana. In: *India and Antarctica during the Precambrian.* (eds. Yoshida & M ; Santosh) *Memoir - Geological Society of India*, 11-23, Geological Society of India, Bangalore, India.

Rogers, J. J. W., Unrug, R. & Sultan, M., 1995b. Tectonic assembly of Gondwana. *Journal of Geodynamics*, 19, 1-34.

Santosh, M., Harris, N. B. W., Jackson, D. H. & Mattey, D. P., 1990. Dehydration and incipient charnockite formation; a phase equilibria and fluid inclusion study from South India. *Journal of Geology*, 98, 915-926.

Santosh, M. & Yoshida, M., 1991. Trapped carbon dioxide in East Antarctic granulites: Evidence from fluid inclusions. *Proceedings of the NIPR Symposium on Antarctc Geosciences*, 5, 136-145.

Santosh, M. & Yoshida, M., 1992. A petrologic and fluid inclusion study of charnockites from the Lützow-Holm Bay region, East Antarctica; evidence for fluid-rich metamorphism in the lower crust. *Lithos*, 29, 107-126.

Schiellerup, H., Lambert, D. D., Prestvik, T., Robins, B., McBride, J. S. & Larsen, R. B., 2000. Re-Os isotopic evidence for a lower crustal origin of massif-type anorthosites. *Nature*, 405, 781-784.

Scientific Committee on Antarctic Research (SCAR) - Working Group on Geodesy and Geographic Information. Composite Gazetteer of Antarctica" (www.pnra.it/SCAR_GAZE).

Scoates, J. S., 2000. The plagioclase-magma density paradox re-examined and the crystallisation of Proterozoic anorthosites. *Journal of Petrology*, 41, 627-649.

Shackleton, R. M., 1996. The final collision zone between East and West Gondwana; where is it? In: *IGCP 348 (Mozambique and related belts).* (eds. Thomas, J, Shackleton R. M. & Muhongo, A.) *Journal of African Earth Sciences*, 271-287, Pergamon, London-New York.

Shelley, D., 1993. *Igneous and metamorphic rocks under the microscope*. Chapman & Hall, London.

Sheperd, T. J., Rankin, A. H. & Alderton, D. H. M., 1985. *A practical guide to fluid inclusion studies*. Blackie & Son, London and Glasgow.

Shiraishi, K., Ellis, D. J., Hiroi, C., Fanning, C. M., Motoyoshi, Y. & Nakai, Y., 1994.Cambrian Orogenic Belt in East Antarctica and Sri Lanka: Implications for Gondwana Assembly. *The Journal of Geology*, 102, 47-65.

Shmulovich, K. & Graham, C. M., 1996. Melting of albite and dehydration of brucite in H_2O-NaCl fluids to 9 kbars and 700-900 °C; implications for partial melting and water activities during high pressure metamorphism. *Contributions to Mineralogy and Petrology*, 124, 370-382.

Soave, G., 1972. Equilibrium constants from a modified Redlich-Kwong equation of state. *Chemistry in English Science*, 27, 1197-1203.

Sorby, H. C., 1858. On the microscopical structure of crystals, indicating the origin of minerals and rocks. *Journal of the Geological Society of London*, 14, 453-500.

Span, R. & Wagner, W., 1996. A new equation of state for carbon dioxide covering the fluid region from the triple point temperature to 1100 K at pressures up to 800 MPa. *Journal of Physical Chemistry Reference Data*, 25, 1509-1596.

Spear, F. S., Rumble, D., III & Ferry, J. M., 1982. Linear algebraic manipulation of n-dimensional composition space. In: *Characterization of metamorphism through mineral equilibria.* (eds. Ferry & John) *Reviews in Mineralogy*, 53-104, Mineralogical Society of America, Washington, DC, United States.

Spear, F. S., 1993. *Metamorphic phase equilibria and pressure-temperature-time paths*. Mineralogical Society of America, Washington, D. C., 799 pp.

Srikantappa, C., Raith, M. & Spiering, B., 1985. Progressive charnockitization of a leptynite-khondalite suite in southern Kerala, India; evidence for formation of charnockites through decrease in fluid pressure? *Journal of the Geological Society of India*, 26, 849-872.

Stähle, H. J., Raith, M., Hoernes, S. & Delfs, A., 1987. Element mobility during incipient granulite formation at Kabbaldurga, southern India. *Journal of Petrology*, 28, 803-834.

Stern, R. J., 1994. Arc-assembly and continental collision in the Neoproterozoic East African Orogen; implications for the consolidation of Gondwanaland. *Annual Review of Earth and Planetary Sciences*, 22, 319-351.

Sterner, S. M. & Bodnar, R. J., 1989. Synthetic fluid inclusion; VII, Re-equilibration of fluid inclusions in quartz during laboratory simulated metamorphic burial and uplift. *Journal of Metamorphic Geology*, 7, 243-260.

Streckeisen, 1976. To each plutonic rock its proper name. *Earth Science Review*, 12, 1-33.

Svensen, H., Jamtveit, B., Yardley, B., Engvik, A. K., Austrheim, H. & Broman, C., 1999. Lead and bromine enrichment in eclogite-facies fluids: Extreme fractionation during lower crustal hydration. *Geology*, 19, 165-178.

Svensen, H., Jamtveit, B., Banks, D. A. & Austrheim, H., 2001. Halogen contents of eclogite facies flued inclusions and minerals; Caledonites, western Norway. *Journal of Metamorphic Geology*, 19, 165-178.

Swanenberg, H. E. C., 1980. Fluid inclusions in high-grade metamorphic rocks from Southern Norway. Geologia Ultraiectina, 25, 147 pp.

Thiery, R., van den Kerkhof, A. M. & Dubessy, J., 1994. VX properties of CH_4-CO_2 and CO_2-N_2 fluid inclusions; modelling for T<31 degrees C and P<400 bars. *European Journal of Mineralogy*, 6, 753-771.

Torsvik, T. H., Smethurst, M. A., Meert, J. G., Van, d. V. R., McKerrow, W. S., Brasier, M. D., Sturt, B. A. & Walderhaug, H. J., 1996. Continental break-up and collision in the Neoproterozoic and Palaeozoic; a tale of Baltica and Laurentia. *Earth-Science Reviews*, 40, 229-258.

Touret, J. L. R., 1971. Controle du facies granulite dans le Bamble par le CO_2 de la phase fluide. *Bulletin de la Societe Geologique de France*, 3, 143-145.

Touret, J. L. R. 1995. The role and nature of fluids in the continental lower crust. In: *India and Anatarctic during the precambrian*, (eds. Yoshida, M. & Santosh, M.), 143-160, Memoir 35, Geological Society of India, Bangalore.

Touret, J. L. R. & Huizenga, J. M., 1999. Precambrian intraplate magmatism: high temparture, low pressure crustal granulites. *Journal of African Earth Sciences*, 28, 367-382.

Touret, J. L. R., 2001. Fluids in metamorphic rocks. *Lithos*, 55, 1-25.

United States Geological Survey (U.S.G.S), 1988. *Fluid Inclusion Instruction Manual*. U.S.G.S., USA, 34 pp.

Unrug, R., 1996. The assembly of Gondwanaland; Scientific results of IGCP Project 288; Gondwanaland sutures and mobile belts. *Episodes*, 19, 11-20.

van den Kerkhof, A. M., 1988. The system CO_2-CH_4-N_2 in fluid inclusions: theoretical modelling and geological applications. Ph. D. thesis, Amsterdam (Free University), pp 206.

van den Kerkhof, A. M. & Grantham, G. H., 1999. Metamorphic charnockite in contact aureoles around intrusive enderbite from Natal, South Africa. *Contributions to Mineralogy and Petrology*, 137, 115-132.

Vityk, M. O. & Bodnar, R. J., 1998. Statistical microthermometry of synthetic fluid inclusions in quartz during decompression reequilibration. *Contributions to Mineralogy and Petrology*, 132, 149-162.

Vry, J. K. & Brown, P.E., 1991. Texturally-early fluid inclusions in garnets: evidence of the prograde metamorphic path? *Contributions to Mineralogy and Petrology*, 108, 271-282.

Waters, D. J., 1988. Partial melting and the formation of granulite facies assemblages in Namaqualand, South Africa. In: *Studies in the genesis and deformation of migmatites.* (eds. Tracy, Robert, J ; Day & Howard) *Journal of Metamorphic Geology*, 387-404, Blackwell, Oxford, United Kingdom.

Weil, A. B., Van der Voo R., MacNiocall, C. & Meert, J. G., 1998. The Proterozoic supercontinent Rodinia; paleomagnetically derived reconstructions for 1100 to 800 Ma. *Earth and Planetary Science Letters*, 154, 13-24.

Wilson, T. J., Grunow, A. M. & Hanson, R. E., 1997. Gondwana assembly: The view from southern Africa and East Gondwana. Journal of Geodynamics, 23, 263-286.

Zhang, Y. G. & Frantz, J. D. 1987. Determination of the homogenisation temperatures and densities of supercritical fluids in the system NaCl-KCl-$CaCl_2$-H_2O using synthetic fluid inclusions. *Chemical Geology*, 64. 335-350.

Acknowledgements